View metadata, citation and similar papers at core.ac.uk
brought to you by CORE
provided by Infoscience - École polytechnique fédérale de Lausanne

ATOM CENTERED POTENTIALS FOR THE DESCRIPTION AND THE DESIGN OF CHEMICAL COMPOUNDS WITHIN DENSITY FUNCTIONAL THEORY

THÈSE N^{O} 3240 (2005)

PRÉSENTÉE À LA FACULTÉ SCIENCES DE BASE

Institut des sciences et ingénierie chimiques

PROGRAMME DOCTORAL EN CHIMIE ET GÉNIE CHIMIQUE

ÉCOLE POLYTECHNIQUE FÉDERALE DE LAUSANNE

POUR L'OBTENTION DU GRADE DE DOCTEUR ÈS SCIENCES

PAR

Otto Anatole VON LILIENFELD-TOAL

Chimiste diplômé EPF
et de nationalité allemande

acceptée sur proposition du jury:

Prof. U. Röthlisberger, directeur de thèse
Prof. A. Pasquarello, rapporteur
Dr A. Seitsonen, rapporteur
Dr T. Wesolowski, rapporteur

Lausanne, EPFL
2005

PREAMBLE

"Chemistry provides not only a mental discipline but an adventure and an aesthetic experience. Its followers seek to know the hidden causes which underlie the transformations of our changing world, to learn the essence of the rose's color, the lilac's fragrance, and the oak's tenacity, and to understand the secret paths by which the sunlight and the air create these wonders.

And to this knowledge they attach an absolute value, that of truth and beauty. The Vision of Nature yields the secret of power and wealth, and for this it may be sought by many. But it is revealed only to those who seek it for itself. Its pursuit has united the predecessors whom we commemorate: it will unite our successors for as long as the spirit of man endures."

Cyril N. Hinshelwood, Oxford
Closing Remarks of the 100 years celebration of the British Chemical Society
J. Chem. Soc., 1277 (1947).

Mr. L.: A fundamental motivation to do science is to enhance personal freedom, *i.e.* to contribute to the enlargement of conscience. And it is deeply human then to express yourself *via* the combination of the freely chosen actions. It is in this respect that scientists and artists resemble each other.

Mss. B.: But enlarging conscience leads to an increase in wealth as well as it implies new opportunities to abuse the gained power.

Mr. L.: This is the theme of Adam and Eve. Conscience and responsibility must not be considered as separable. Since human beings are capable of being conscious they also have to accept their responsibility. Many legal systems even force their citizens to accept responsibility independently on the degree of their conscience. Hence, the messenger of conscience is not to be blamed for the increase in responsibility.

Mss. B.: What if someone refuses to act in a responsible manner?

Mr. L.: It is a pretentious illusion that mankind has a right to succeed in its conservation. There is a practically infinite amount of scenarios which constitute a threat to mankind, and only the maximization of conscience will allow to minimize the danger. However, there is no guarantee for success. All an individual can do for mankind is to fight for enlightenment.

Zusammenfassung

Im ursprünglichen Sinne der elektronischen Schrödingergleichung beinflusst das durch die *nuclei* generierte externe Potential die Erwartungswerte während des iterativen Selbstkonsistenzcyclus. Mit Hilfe von Dichtefunktionaltheorie wird in dieser Arbeit die Optimierung und der Nutzen von kernzentrierten Potentialen für eine Verbesserung der Beschreibung und des Designs von Molekülen untersucht. Zum einen wird gezeigt, wie die atomzentrierten Potentiale die Genauigkeit in der Beschreibung von Eigenschaften von Molekülen erhöhen können. Zum anderen können sie für eine allgemein rationale Erforschung des chemischen Raumes genutzt werden, um jene Strukturen zu identifizieren, die bestimmte Eigenschaften haben.

Der Grad, in dem Anwendungen mit diesem Ansatz möglich sind, wird anhand mehrerer Beispiele erläutert. Erstens wird ein automatisierbares Vorgehen beschrieben, um optimale Verknüpfungsatome für quantenmechanische/molekularmechanische Studien zu erhalten. Zweitens wird gezeigt, wie man atomzentrierte Potentiale variationell verändert, sodass die Abweichung der Elektronendichte von einer willkürlichen Referenzdichte minimiert wird. Für diese Studie wurde eine Referenzdichte genommen, die durch das Benutzen eines anderen Austauschskorrelationsfunktionals entsteht. Drittens können London Dispersionskräfte imitiert werden. Viertens wird die Transferabilität dieses Ansatzes für die Dispersionskräfte korrigierenden atomzentrierten Potentiale untersucht. Fünftens wird, im Rahmen der konzeptuellen Dichtefunktionaltheorie, ein Ausdruck für das molekulare nukleare chemische Potential hergeleitet. Letzteres ermöglicht, in Verbindung mit dem elektronischen chemischen Potential, eine generelle Formulierung des rationalen Strukturdesigns mit einer Gradient-basierten Minimierung eines Eigenschaftpenaltyfunktionales im chemischen Raum.

Summary

Within the Born-Oppenheimer picture of the electronic Schrödinger equation the external potential due to the nuclei influences the resulting expectation values during the self consistent field procedure. In this thesis, the optimization and the benefit of atom centered potentials for an improved description and design of molecules is studied using density functional theory (DFT). It is shown that atom centered potentials can be used to increase the accuracy of the description of molecular properties as well as to generally explore chemical space rationally for structures which exhibit desired properties.

The wide range of possible applications is illustrated by addressing several issues. First, an automated procedure is proposed for the design of optimal link pseudopotentials for quantum mechanics/molecular mechanics calculations. Secondly, it is shown how to tune variationally atom centered potentials within density functional perturbation theory in order to minimize the deviation in electron density from an arbitrary reference density. Here, a reference density has been chosen which results from the use of a different exchange-correlation potential. Thirdly, London dispersion interactions are mimicked with dispersion corrected atom centered potentials. Fourthly, the transferability of these dispersion corrected atom centered potentials is assessed. Fifthly, an expression for the molecular nuclear chemical potential is derived within the context of conceptual DFT. It offers the possibility to develop a general formulation for rational compound design *via* gradient based minimization of a property-penalty functional in chemical space.

Contents

1 Introduction **3**
1.1 Remarks on computational chemistry 3
1.2 Motivation 7
1.3 Overview 9

2 Theory **11**
2.1 Density Functional Theory 11
2.1.1 Motivation 11
2.1.2 Exchange-correlation functionals 14
2.2 Pseudopotentials and plane waves 16
2.3 Density functional perturbation theory 18
2.4 *Ab-initio* molecular dynamics 20
2.4.1 Born-Oppenheimer molecular dynamics 21
2.4.2 Car-Parrinello molecular dynamics 21
2.5 QM/MM 22

3 Optimization of molecular properties **25**
3.1 Introduction 26
3.2 Methods and computational details 29
3.3 Results and discussion 32
3.3.1 QM/MM link atom optimization 32
3.3.2 B3LYP density reconstruction using BLYP 34
3.4 Conclusions 38

4 London dispersion forces in DFT **41**
4.1 Introduction 42
4.2 Methods and computational details 43
4.3 Results and discussion 46
4.3.1 Calibration 46
4.3.2 Assessing transferability 47
4.4 Conclusions 52

5 Transferability of DCACPs 55
- 5.1 Introduction 56
- 5.2 Methods and computational details 61
  - 5.2.1 Rare gas atoms 63
  - 5.2.2 Cyclooctatetraene 64
  - 5.2.3 Bromine compounds 64
- 5.3 Results and discussion 65
  - 5.3.1 Rare gas atoms 65
  - 5.3.2 Cyclooctatetraene 66
  - 5.3.3 Bromine compounds 69
- 5.4 Conclusions 71

6 General rational compound design 73
- 6.1 Introduction 74
- 6.2 Methods and computational details 76
- 6.3 Results and discussion 80
  - 6.3.1 Atoms 80
  - 6.3.2 Molecules 81
  - 6.3.3 Compound design 83
  - 6.3.4 A non-peptidic inhibitor for XIAP 85
- 6.4 Conclusions 89

7 Conclusions 91

Appendix: Perturbation Hamiltonian 115

Publications 117

Acknowledgment 119

Curriculum Vitae 123

Chapter 1

Introduction

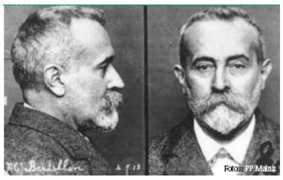

One can only see what one observes, and one observes only things which are already in the mind.
Alphonse Bertillon (1853-1914).

1.1 Remarks on computational chemistry

History

Among the many computational models being used in theoretical chemistry, quantum mechanical methods are of special interest. Apart from the fact that quantum mechanics is more realistic than classical mechanics, this is mainly because only quantum mechanics is able to properly describe the electronic rearrangements as they are ubiquitous in chemical reactions and all molecular processes. Quantum chemistry (the quantum mechanics dealing with molecules) has a long tradition reaching back to the beginnings of last century when the German physicist Hans Hellmann applied the preceding most fascinating quantum mechanical results in physics from Planck, Bohr, Pauli, Dirac and Heisenberg to chemical problems. His studies have been followed by the subsequent work of Schrödinger, Hund, Heitler, London, Herzberg, Mulliken, Slater, Pauling, and many others [1]. Using quantum mechanics to solve the problems of theoretical chemistry, Hellmann was among the first who used the term ’Quantum Chemistry’ within the scientific community when he chose it as a title for his textbook in 1937 [2]. However, only recently the interest in theoretical models has reached a broad scale because it is only now that for a larger scientific community computational solutions of relevant problems are becoming tractable.

Variety

Quantum chemical problems are as diverse as chemistry can be. They range from fundamental quantum theory problems up to pharmacy, from material design up to interstellar chemistry. On the one hand, for instance, problems are addressed such as the determination of rovibrational spectra with an accuracy superior to experiment [3], the investigation of fundamental physical laws such as the importance of electroweak interactions to account for the violation of parity [4], the computational advantages of non-equilibrium dynamics in free energy calculations (Jarzynski’s equality) [5], or defining and predicting chemical reactivity [6, 7]. On the other hand, in conjunction with classical and statistical mechanics, theoretical chemistry allows already nowadays to tackle chemical problems dealing with hundreds or thousands of atoms on a picosecond timescale and often with sufficient accuracy [8].

Advantages

With respect to experimental techniques aiming at a deeper understanding of matter, the fundamental advantage inherent to atomistic computational simulations is that they allow insights into all molecular processes. Some of them might be just difficult to observe experimentally because no analytical techniques are at disposal which are accurate enough. However, even more important, through computation properties become accessible which are generally impossible to measure because the perturbation of the observable due to the measurement would be of the same order of magnitude (or even larger) than the observable itself. Hence, through the virtual character of simulation, a detailed observation of matter is possible which in return allows to monitor *all* possible observables (such as for example the flux of electron density during a catalyzed peptide hydrolysis in the active site of an enzyme) without any perturbation at all. However, the fundamental problem of computational chemistry which needs to be faced when doing simulations is the issue of accuracy [9].

Accuracy

In computational chemistry inaccuracy has two very distinct sources. It can be either due to fundamental theorems on which the framework of physics is built (famous examples include the hypothesis of ergodicity, axioms in Euclidean geometry, the fundamental laws of thermodynamics, and the postulates of quantum mechanics) or due to the errors which are introduced by the approximations which represent the applied model. While the first source of inaccuracy is subject to philosophical scientific studies, the latter is subject to the field of theoretical physics which is greatly enhanced by nowadays increased computational power.

Even though being well defined, these inaccuracies can eventually lead to qualitatively different results. In analogy to experimental procedures it is thus quite common to compute and compare the same properties for a large set of molecules in order to assess the performance of a model. As an example see Ref. [10] for a recent assessment of the accuracy of generalized gradient approximation density functionals in predicting energy barriers for hydrogen abstraction reactions. However, since there is likewise an accuracy issue for experimental studies due to the measurement concept, the experimental apparatus and the execution, computational inaccuracy does not represent a fundamental disadvantage with respect to experiment. In fact, already nowadays there are many systems for which calculations are assumed to be more accurate than measurements. This is always the case when the observable is either impossible to be measured experimentally or when the experimental imprecision is larger than the theoretical inaccuracy. An example for the latter is the determination of the relative energies of low-energy conformers of carbon clusters such as C_{20} where quantum Monte Carlo methods predict the bowl form to be more stable than the ring which is more stable than the cage [11].

It appears that the question of accuracy, which is always measured with respect to a reference, is fundamental for any kind of observation. Thus, the establishment of precise and accurate reference data sets is crucial for the benchmark assessment of all new models as well as of new experiments.

Status quo

The power to predict reliably important properties in condensed phase as for example binding affinities of potential drug candidates in quantitative structure activity relationship (QSAR) studies [12], to carry out material design studies [13], or to compute rate constants for organometallic compounds in homogeneous catalysis [14] renders computational chemistry such an important and general tool that it has become virtually equivalent to the classical (experimental) disciplines in chemistry: inorganic, organic, analytical, medicinal, and physical chemistry. As an illustration for the impressive emergence of this ’new’ discipline of chemistry a survey over the number of scientific publications containing ’density functional theory’ in their title is given in Fig. 1.1.

Outlook

This success story of computational chemistry is mostly due to the still ongoing impressive increase of computational power. Being in principle limited in its accuracy and the size of the investigated problem only by the performance of the latest processor generation [16] and having Moore’s law in mind (which is expected to be valid at least until the year 2013 - referring to the standard silicon chip technology only [17]) the future of computational chemistry looks very bright.[1]

---

[1] Moore’s law states that processor performance doubles every 18 months. This has had and still will have considerable impact on the size and length scales computational chemistry can deal with.

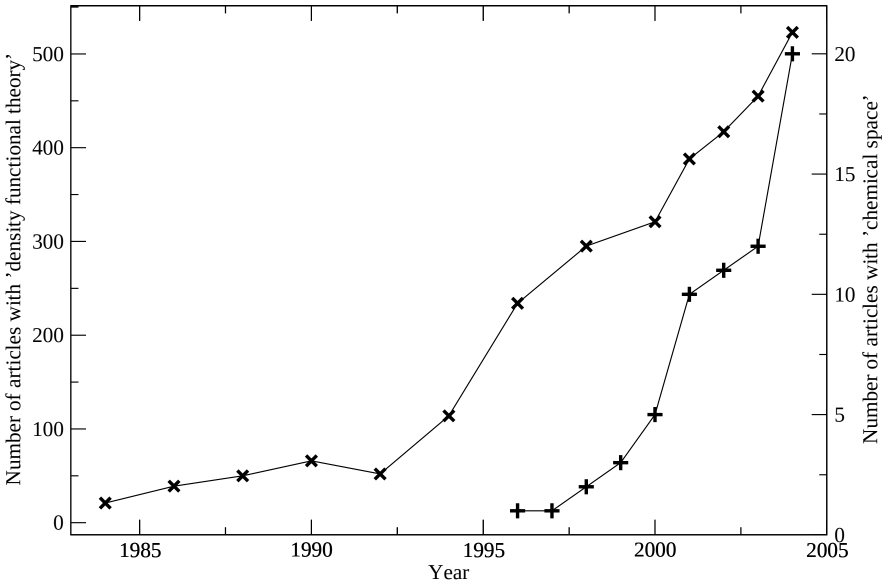

Figure 1.1: A survey over the number of scientific publications containing 'density functional theory' (cross) in their title or 'chemical space' (plus) in their text [15].

1.2 Motivation

There are two principal limits why computational chemistry is still unable to tackle all kinds of chemical problems: Firstly, the time and size scales which can be treated with the help of currently available computers are still too small for a large number of problems. Secondly, computational chemistry is such a young and interdisciplinary field that simply not all possibilities to tackle even very important questions have been explored yet.

The easiest way out of the first limitation is to wait. In view of the good correlation between the evident increase in computational power (Moore's law) and the growing relevance of computational chemistry (see e.g. Fig. 1.1) waiting is not the worst approach. In fact, the world's first supercomputer (the Cray Research-CRAY I vector architecture designed by Seymour Cray [18] shown in Fig. 1.2) was only built in 1976 - the year of birth of the author of this thesis.

Figure 1.2: Cray Research-CRAY I vector architecture designed in 1976 by Seymour Cray [18]

However, the scientifically and intellectually more interesting approach to address the first limitation is the optimization of not only all mathematical algorithms but also of all physical approximations used to solve the time dependent Schrödinger equation without exceeding the relevant accuracy of a given chemical problem. Linear scaling methods seem to do a very promising job with respect to rendering already established approximations computationally cheaper and tackling already macromolecular systems at a quantum mechanical level. See Ref. [19] as an example for semi-empirical quantum chemical calculations of the solvation energy of DNA. Alternatively, the accuracy of cheap methods can be improved by finding more appropriate physical approximations or corrections.

The second limitation is subject to intense efforts worldwide trying to evaluate and exploit all implications due to the increasing computer power and depth of knowledge on algorithms for the computation of molecular systems. It was only in 1964 that the seminal work of Hohenberg and Kohn [20] has laid the foundations for density functional theory (DFT). And the number of applications of DFT to more and more problems is increasing ever since [Fig. 1.1]. The article by Runge and Gross introducing time-dependent density functional theory, as well as the fundamental paper by Car and Parrinello, initiating the development of *ab initio* molecular dynamics, were published only as recently as 20 years ago [21, 22]. And it was only in 1992 that the optimized effective potential (OEP) method for accurate Kohn-Sham exchange functionals was devised for the purposes of numerical evaluation [23].

As it has been outlined recently by *Nature* editors Kirkpatrick and Ellis [24], and as a survey on literature would suggest [Fig. 1.1], also the concept of chemical space seems to be at the dawn of becoming an important topic in chemistry. Chemical space standing for the space being spanned by all stable stoichiometries and isomers will be addressed in chapter 6 .

1.3 Overview

The purpose of this thesis is twofold. First, the limit of inaccuracy is addressed for the computationally relatively cheap electronic structure method DFT. Specifically, the chapters 3-5 deal with an improvement of accuracy over the standard methods for the description of molecular properties. Secondly, the question of how to explore chemical space from first principles is introduced in chapter 6.

Chapter 2 introduces shortly the theoretical background. Since all the other chapters are rather theoretically oriented, only a rough overview for the methods being used in this thesis is given in the beginning. Chapter 3 discusses how atom centered potentials can be generally used to improve the description of molecular properties. The feasibility is illustrated for the design of special linking atoms which minimize the error at the boundary of quantum mechanical/molecular mechanical calculations, and for a minimization of differences in electron density. Chapter 4 studies the performance of atom centered potentials when used to remedy the lack of London dispersion forces in generalized gradient approximation DFT. Chapter 5 assesses the transferability for dispersion corrected atom centered potentials to a selected number of points in phase and chemical space. Chapter 6 considers the suitability of atom centered potentials for general compound design schemes. Chapter 7 overviews the achievements of this thesis and draws the conclusions. The appendix gives the explicit expression for the perturbation Hamiltonian which is the fundamental quantity being used for all the gradient based property or structure optimizations which are performed in this thesis.

Chapter 2

Theory

What we observe is not nature itself, but nature exposed to our method of questioning.
Werner Heisenberg (1901-1976)

2.1 Density Functional Theory

2.1.1 Motivation

Density functional theory (DFT) is a general theory being used in many different fields of science [25]. For the purpose of electronic quantum chemistry, an electron density approach is especially attractive because the central variable, *i.e.* the electron density, depends only on the 3 spatial coordinates, and - for spin polarized systems - also on the spin. This concept is hence more condensed than the electronic many particle wave function ($\Psi(\mathbf{x}_1, \mathbf{x}_2, \ldots, \mathbf{x}_N)$) approach in which Ψ depends on all coordinates of all particles $\{\mathbf{x}_i\}$, *i.e.* for N_e electrons, it depends on $3N_e$ variables (or 4 N_e if the spin is counted).

$$\Psi(\mathbf{x}_1, \mathbf{x}_2, \ldots, \mathbf{x}_{N_e})$$

$$\downarrow$$

$$n(\mathbf{x}_1) = M \int d\mathbf{x}_2 \ldots d\mathbf{x}_{N_e}\, \Psi(\mathbf{x}_1, \mathbf{x}_2, \ldots, \mathbf{x}_{N_e}) \Psi^*(\mathbf{x}_1, \mathbf{x}_2, \ldots, \mathbf{x}_{N_e}) \tag{2.1}$$

where M is a normalization factor.

Modern DFT is not only computationally very efficient, it also provides conceptual insights:

A great strength of DFT language is its appropriateness for defining and elucidating important universal concepts of molecular structure and molecular reactivity. In traditional quantum chemistry this has, of course, also been a major goal, but it is tortuous to try to conceptualize how many-body wavefunctions are related to structure and behavior. In DFT not only is the electron density itself very easy to visualize, but there is the big advantage that the electron number N_e has a central place in the theory. After all, much of the chemistry is about transfer of electrons from one place to another ... DFT thus promises relief from the old curse of needing to difference large numbers in making chemical predictions. (from Kohn et al. [26]).

Concepts like the *chemical potential* or *electronegativity*, *hardness*, *polarizability*, *response functions* and *reactivity functions (Fukui functions)* emerge naturally from the DFT energy functional, $E[\rho]$, and its derivatives, and their quantitative computation becomes possible within the accuracy of the chosen exchange-correlation functional. Furthermore, DFT can be easily combined with classical molecular dynamics schemes for the nuclei as discussed in chapter 2.4 '*Ab initio* molecular dynamics'. The classical forces on the ions are then computed from the electron density and using the Hellmann-Feynman theorem. As illustrated in chapter 1, the use of DFT has skyrocketed in the last decades.

Fundamentals

The fundamentals of DFT will be sketched only very briefly in this thesis. The reader is referred to the extensive and recent literature [26–29]. In all what follows we always limit ourselves to the simplest cases, *i.e.* non-relativistic, interacting electrons (fermions) in a closed shell ground state system with integer occupation numbers for which the Born-Oppenheimer approximation is valid. The famous first Hohenberg-Kohn (HK) theorem specifies that the external potential v is uniquely determined by the ground state density n up to a constant [20]:

$$n(\mathbf{r}) \mapsto v(\mathbf{r}) \tag{2.2}$$

Since also the number of electrons (N_e) is uniquely defined by the electron density, $N_e = \int d^3r\, n(\mathbf{r})$, n determines the full Hamiltonian and therefore implicitly all properties of the system. Defining for a fixed v the energy as a functional of n, a minimal variational principle exists for the true ground state energy E_0 as stated by the second HK theorem [20].

$$\begin{aligned} E[n] &= \int d^3r\, vn + F[n], && (2.3)\\ &= E_{ext} + F[n], && (2.4)\\ &\geq E[n_0] = E_0. && (2.5) \end{aligned}$$

Here, $F[n]$ is the universal functional introduced within the Kohn-Sham (KS) formalism [30] as

$$F[n] = T_s[n] + J[n] + E_{\mathrm{xc}}[n]. \tag{2.6}$$

It consists of an expression for the kinetic energy in terms of noninteracting KS-orbitals ($\{\phi_i\}$) which minimize the following expectation value

$$T_s[n] = -\frac{1}{2}\sum_i^{N_e}\langle\phi_i|\nabla^2|\phi_i\rangle, \;\; n = \sum_i^{N_e}|\phi_i|^2. \tag{2.7}$$

Furthermore, the universal energy functional consists of the classical Coulomb repulsion for a negative charge distribution,

$$J[n] = \frac{1}{2}\int d^3r d^3r'\, \frac{n(\mathbf{r})n(\mathbf{r}')}{|\mathbf{r}-\mathbf{r}'|}, \tag{2.8}$$

and an exchange-correlation term E_{xc} containing all the remainder - yet undefined - contributions to the energy.

In analogy to the Hartree-Fock scheme, the KS-orbitals must minimize the energy under the constraint that $\langle \phi_i | \phi_j \rangle = \delta_{ij}$. This results into the KS-equations,

$$\left(-\frac{1}{2}\nabla^2 + v + \int d^3r' \, \frac{n(\mathbf{r}')}{|\mathbf{r}-\mathbf{r}'|} + \frac{\delta E_{\mathrm{xc}}}{\delta n} \right) \phi_i = \varepsilon_i \phi_i, \tag{2.9}$$

which differ from the Hartree equations only by the xc-contribution and which have to be solved until self-consistency. Apart from the kinetic term, all other terms in the bracket of Eq. (2.9) constitute the so called KS-potential, $\hat{v}^{\mathrm{KS}}$.

If only the correct expression for the exchange-correlation potential,

$$\hat{v}_{xc} = \frac{\delta E_{\mathrm{xc}}}{\delta n}, \tag{2.10}$$

was known, solving Eq. (2.9) would be the equivalent of solving the exact Schrödinger equation within the Born-Oppenheimer approximation. Unfortunately, the exact exchange-correlation potential is unknown and much effort has been and is being devoted to find good approximations to $\hat{v}_{xc}$.

2.1.2 Exchange-correlation functionals

To make DFT a theory of practical use, many approximations to the xc-potential $\hat{v}_{xc}$ have been proposed [29]. Here, only three of these functional are presented: LDA (because of its simplicity), BLYP (because it has been used for all the research in this thesis), and B3LYP (because it has been used as a reference for some studies in this thesis).

LDA The local density approximation (LDA) is

$$E_{\mathrm{xc}}^{\mathrm{LDA}} = \int d^3r \, \hat{v}_{xc}^{\mathrm{LDA}}(n) n, \tag{2.11}$$

where $\hat{v}_{xc}^{\mathrm{LDA}}(n)$ is the exchange-correlation potential per particle of a uniform interacting electron gas of density n:

$$\hat{v}_{xc}^{\mathrm{LDA}}(n) = \hat{v}_{x}^{\mathrm{LDA}}(n) + \hat{v}_{c}^{\mathrm{LDA}}(n). \tag{2.12}$$

Where the exchange part $\hat{v}_x^{\mathrm{LDA}}$ was derived analytically by Slater [31] and could be shown to be identical with an expression obtained by Bloch and Dirac in the late 1920's [32, 33]. The correlation part is usually approximated by comparison to accurate Monte Carlo simulations of the homogeneous electron gas by Ceperley and Alder [34].

BLYP The Becke Lee Yang Parr (BLYP) exchange correlation functional belongs to the group of generalized gradient approximation (GGA) functionals. GGAs are not only functionals of the local density but also of its local gradient. In addition some of them are also forced to satisfy additional important constraints due to the exchange and correlation holes. GGAs are sometimes called 'semi'-local, however, in a purely mathematical sense they are local too.

A general form of a GGA exchange functional is

$$\begin{aligned} E_{\mathrm{x}}^{\mathrm{GGA}} &= \int d^3r \, v_x^{\mathrm{GGA}}(n, \nabla n) n, && (2.13) \\ &= \int d^3r \, [v_x^{\mathrm{LDA}} - F(s) n^{1/3}] n, && (2.14) \\ &= E_{\mathrm{x}}^{\mathrm{LDA}} - \int d^3r \, F(s) n^{4/3}, && (2.15) \end{aligned}$$

where s is the *reduced density gradient*: $s = |\nabla n| / n^{4/3}$ and is considered to be an inhomogeneity parameter. To be dimensionless s is normalized by the density to the 4/3rd power. Becke presented in 1988 the ultimately used form of F in the BLYP functional [35]:

$$F = \frac{\beta s^2}{1 + 6\beta \, s \sinh^{-1}(s)}. \qquad (2.16)$$

The parameter β = 0.0042 a.u. is a best-fit value which yields a relative root mean square deviation of only 0.11 % from the exact exchange energies of the rare gas atoms He up to Rn.

The LYP correlation functional [36] has a lengthy, yet analytical, form which is not based on the uniform electron gas but on a correlated wavefunction expression for He presented by Colle and Salvetti already in 1975 [37].

B3LYP The B3LYP uses Becke's exchange functional [35], together with LYP [36] for the correlation. It contains 3 empirical parameters a, b, and c which had actually been fitted for another correlation functional to reproduce best atomization, ionization, and proton affinities coming from a G2 data base. However, Stephens et al. [38] used the same parameters with the LYP correlation,

$$E_{\mathrm{xc}}^{\mathrm{B3LYP}} = (1-a)E_{\mathrm{x}}^{\mathrm{LDA}} + aE_{\mathrm{x}}^{\mathrm{HF}} + bE_{\mathrm{x}}^{\mathrm{B88}} + cE_{\mathrm{c}}^{\mathrm{LYP}} + (1-c)E_{\mathrm{c}}^{\mathrm{LDA}}, \tag{2.17}$$

a, b, and c turn out to be 0.20, 0.72, and 0.81, respectively. $E_{\mathrm{x}}^{\mathrm{HF}}$ is the Hartree-Fock exchange integral using KS-orbitals.

2.2 Pseudopotentials and plane waves

The Kohn Sham orbitals can be obtained from an expansion in a complete set of known basis functions and solving the KS equations self-consistently. There are several basis sets introduced in computational chemistry. However, since for this thesis, mostly plane waves have been used, we will refer to them as basis. Apart for their intuitive concept, the use of plane waves is numerically very efficient. They allow a simple integration of the Poisson equation for the determination of the electronic Coulomb repulsion and for the kinetic energy contribution. However, there are considerable oscillations of the atomic core electrons in the closer region around the ion, implying that a very high density of plane waves would be needed if the core electrons were to be included into the calculations. Fortunately, chemical transformations involve mostly variations in the valence electronic structure which have less stronger oscillations in the core regions.

Hence, the effect of the core electrons on the valence electrons can be seen as a constant and can therefore be mimicked by a ’pseudopotential’ or effective core potential (ECP), allowing not only to decrease the density (and hence the number) of plane waves, but also to limit the number of KS-states to the valence electrons only. Both of these facts allow for a substantial gain in computational efficiency.

In general of course, the pseudopotential will contain a dominant attractive short-ranged term for the atomic number, corresponding to the number of atomic valence electrons. In addition, there are terms which shall mimic the presence of the core electrons. Hence, they shall obey orthogonality for the core-valence interaction as well as Coulomb repulsion, or exchange and correlation interaction. Usually ECPs are norm-conserving meaning that - apart from the fact that the pseudized wavefunction outside a certain cutoff core radius has to be the same as the full-electron wavefunction - also the integrated charge of the core region has to be in agreement with the all-electron case. To this end, non-local pseudopotentials are being used which usually have the form

$$V_{\mathbf{I}}^{PP}(\mathbf{r},\mathbf{r}') = V_{\mathbf{I}}^{loc}(\mathbf{r})\delta(\mathbf{r}-\mathbf{r}') + \sum_{l}\sum_{m=-l}^{m=+l} |l,m\rangle V_{l,\mathbf{I}}^{nl}(\mathbf{r},\mathbf{r}')\langle l,m|. \tag{2.18}$$

Where $|l,m\rangle$ represents the spherical harmonics with the angular moment eigenfunctions l and m. Generating a pseudopotential means hence to identify the local V^{loc} and non-local V^{nl} that respect best the above mentioned criteria. See Ref. [39, 40] for recent reviews.

Having ensured the use of transferable ECPs, the numerical advantages of the plane wave basis set can be fully acknowledged. Furthermore, they offer the advantage with respect to localized atomic orbitals that they are not attached to the ions. This implies, that the Hellmann-Feynman forces can be directly used for the computation of the nuclear forces, and no Pulay forces do occur [41]. Also, no basis set superposition error must be taken into account when relative energies are determined. For the orbitals or the density to be used in real space (as in the case of the computation of the contribution of the external potential), the plane wave expansion can be efficiently transformed from Fourier space using Fast Fourier Transformation techniques [42]. Nevertheless, one of the major drawbacks of using plane waves for DFT calculations, namely the increase in computational cost for the Hartree-Fock exchange integral within commonly used hybrid functionals such as B3LYP, remains. This question will also be addressed in chapter 3.

Hence, because of the user-friendly and modular nature of the plane waves, all the quantities needed for the implementations performed in this work could be transformed to real space before using them and back to Fourier space after wards. For this thesis, ensuring that the plane wave density, *i.e.* the basis set size, is large enough by testing for convergence, has been sufficient.

2.3 Density functional perturbation theory

Some of the work in this thesis has been obtained from the implementation of a variational density functional perturbation theory module [43] in the program CPMD [44]. Here, a short outline of this approach is given, for more details the reader is referred to Ref. [43].

Starting from the Kohn-Sham energy functional of the density, Eq. 2.3 may be rewritten in terms of the density matrix defined by

$$\rho(\mathbf{r},\mathbf{r}') = \sum_{i,j} \phi_i^*(\mathbf{r}) S_{ij}^{-1} \phi_j(\mathbf{r}'), \tag{2.19}$$

where S_{ij}^{-1} is the inverse of the overlap matrix $S_{ij} = \langle\phi_i|\phi_j\rangle$. The energy functional becomes then:

$$\begin{aligned} E_{\mathrm{KS}}[\rho(\mathbf{r},\mathbf{r}')] &= \frac{1}{2}\int d^3r\, d^3r'\ \delta(\mathbf{r}-\mathbf{r}')\nabla^2\rho(\mathbf{r},\mathbf{r}') \\ &+\frac{1}{2}\int d^3r\, d^3r'\ \frac{|\rho(\mathbf{r},\mathbf{r}')|^2}{|\mathbf{r}-\mathbf{r}'|} + E_{xc}[n] + E_{ext}[n]. \end{aligned} \tag{2.20}$$

where the density n simply equals $\rho(\mathbf{r},\mathbf{r})$, and E_{ext} corresponds to the contribution due to the interaction of the electrons with an external potential, $E_{ext}[n] = \int d^3r\ nv_{ext}$.

For an external perturbation, a perturbation functional of arbitrary form is added to E:

$$E_{\mathrm{tot}}[\{|\phi_i\rangle\}] = E_{\mathrm{KS}}[\{|\phi_i\rangle\}] + \lambda E_{\mathrm{p}}[\{|\phi_i\rangle\}]. \tag{2.21}$$

Here, λ is a small perturbing parameter and represents the strength of the interaction with the static, but otherwise arbitrarily complex external field contribution E_{p}.

The total functional Eq. (2.21) will have a minimum which is expanded perturbatively in powers of λ,

$$E = E^{(0)} + \lambda E^{(1)} + \lambda^2 E^{(2)} + \ldots \tag{2.22}$$

Likewise, the KS-orbitals that minimize E_{tot} can be expanded in λ,

$$\phi_i = \phi_i^{(0)} + \lambda\phi_i^{(1)} + \lambda^2\phi_i^{(2)} + \ldots, \tag{2.23}$$

and up to first order the electronic density reads

$$n(\mathbf{r}) \quad = \quad n^{(0)}(\mathbf{r}) + \lambda n^{(1)}(\mathbf{r}) + \ldots \tag{2.24}$$

Where

$$n^{(1)}(\mathbf{r}) = \sum_{i=1}^{N} [\phi_i^{*(0)}(\mathbf{r})\phi_i^{(1)}(\mathbf{r}) + \phi_i^{*(1)}(\mathbf{r})\phi_i^{(0)}(\mathbf{r})]. \tag{2.25}$$

While the first order energy is simply the ground state expectation value of the perturbation Hamiltonian, the second-order energy of the system - which is variational in the first order perturbation wavefunctions $\phi^{(1)}$ - can be obtained by expanding Eq. (2.21) up to the second power in λ. The calculation [43] yields

$$\begin{aligned} E^{(2)} \quad = \quad & \sum_k \left[\left\langle \phi_k^{(1)} \middle| \partial_{\langle \phi_k |} E_{\text{tot}}[\{|\phi_i^{(0)}\rangle\}] + \partial_{|\phi_k\rangle} E_{\text{tot}}[\{|\phi_i^{(0)}\rangle\}] \middle| \phi_k^{(1)} \right\rangle \right] \\ & + \sum_{kl} \left\langle \phi_k^{(1)} \middle| H^{(0)} \delta_{kl} - \lambda_{kl} \middle| \phi_k^{(1)} \right\rangle \\ & + \frac{1}{2} \int d^3r \, d^3r' \, \frac{\delta^2 E_{Cxc}[n^{(0)}]}{\delta n(\mathbf{r}) \delta n(\mathbf{r}')} n^{(1)}(\mathbf{r}) n^{(1)}(\mathbf{r}'). \end{aligned} \tag{2.26}$$

Where the functional $E_{Cxc}[n^{(0)}]$ represents the sum of the Coulomb and the exchange-correlation energy functionals. The Lagrange multipliers λ_{kl} are the matrix elements of the KS-Hamiltonian $H^{(0)}$

$$H^{(0)} \quad = \quad H_{\text{KS}}, \tag{2.27}$$

$$\lambda_{kl} \quad = \quad \langle \phi_k^{(0)} | H^{(0)} | \phi_l^{(0)} \rangle. \tag{2.28}$$

The orthonormality constraint of the total wavefunctions, expanded to first order in the perturbation, yields

$$\langle \phi_k^{(0)} | \phi_k^{(1)} \rangle + \langle \phi_k^{(1)} | \phi_k^{(0)} \rangle = 0 \ \ \forall \ k. \tag{2.29}$$

This is achieved by imposing a general orthogonality condition on the first order perturbation wavefunctions,

$$\langle \phi_k^{(0)} | \phi_l^{(1)} \rangle = 0 \ \ \forall \ k, l. \tag{2.30}$$

This automatically implies the conservation of the total charge of the system, by enforcing the integrated perturbation charge $q^{(1)}$ to vanish,

$$q^{(1)} = \int d^3r \, n^{(1)}(\mathbf{r}) = 0. \tag{2.31}$$

Usually, the perturbation functional E_p [Eq. (2.21)] can be written as the expectation value of a perturbation Hamiltonian $H^{(1)}$,

$$E_\mathrm{p}[\{|\phi_i\rangle\}] = \sum_k \langle\phi_k^{(0)}|H^{(1)}|\phi_k^{(0)}\rangle. \tag{2.32}$$

However, the formulation through an arbitrary perturbation functional, Eq. (2.21), also allows to include orbital dependent perturbations in the scheme, *i.e.* a perturbation Hamiltonian specific for each k,

$$E_\mathrm{p}[\{|\phi_i\rangle\}] = \sum_k \langle\phi_k^{(0)}|H_k^{(1)}|\phi_k^{(0)}\rangle. \tag{2.33}$$

In summary, the second order energy, Eq. (2.26), is variational in the first order perturbation wavefunctions, satisfying the stationarity condition that

$$\frac{\delta E^{(2)}}{\delta\phi^{(1)}} = 0, \tag{2.34}$$

under the orthogonality constraint of Eq. (2.30).

2.4 *Ab-initio* molecular dynamics

Ab initio molecular dynamics (AIMD) schemes overcome the limitation of classical force fields to be restricted to very small regions in chemical space. They offer a pragmatic definition of *ab initio* namely transferability to all regions of chemical space. So far, mainly Kohn-Sham DFT formulations have been devised for AIMD schemes. Usually AIMD schemes use a classical propagation of the ions according to the laws of Newton, while the electronic contribution to the sampling of phase space is computed with quantum chemistry methods. Hence, atomic quantum effects, like for instance the tunneling of the lighter atoms or relativistic effects for heavier elements are usually neglected and have to be included using more sophisticated methods like for instance path integrals or relativistic pseudopotentials, respectively. Furthermore, the most widely used AIMD-schemes, namely Born-Oppenheimer MD (BOMD) and Car-Parrinello MD (CPMD), both rely heavily on the Born-Oppenheimer approximation that ionic and electronic degrees of freedom can be adiabatically separated at all points in phase space. This is, especially for situations when surfaces cross - as it is often the case in reactions for which for instance frontier orbital theory has been devised - a crude approximation and must be remedied by more advanced AIMD schemes, such as for instance Ehrenfest dynamics.

However, for the purpose of this thesis, a short introduction to BOMD and CPMD is considered to be sufficient. For more details see Ref. [45].

2.4.1 Born-Oppenheimer molecular dynamics

BOMD is based on the idea that the potential energy at any moment in time, *i.e.* at any geometry, is calculated from an electronic-structure calculation. For a given set of nuclear coordinates, the electronic contribution to the forces acting on the ions is calculated *via* the Hellmann-Feynman theorem, which is equivalent to the first order perturbation of the Hamiltonian due to small variation of the ionic positions.

$$\mathbf{F_I} = \langle \Psi_0 | H' | \Psi_0 \rangle, \tag{2.35}$$

$$H' = -\nabla_{\mathbf{I}} H\,. \tag{2.36}$$

The forces are used to move the nuclei according to the laws of classical mechanics. Since the accuracy of the forces in BOMD depends linearly on the accuracy of the minimization of the KS energy, the wave function has to be tightly converged at each MD time step.

2.4.2 Car-Parrinello molecular dynamics

The Car-Parrinello approach [22] is closely related to BOMD in so far as the ions are also propagated classically according to the forces obtained from the Hellmann-Feynman theorem. The fundamental difference is that the orbitals are no longer optimized at every time step but treated and propagated like classical objects, correspondingly being assigned a fictitious mass (μ) and temperature. It could be shown that also for this approach, the adiabatic separation of the BO-approximation is conserved [45]. Hence, the computational bottleneck of BOMD, *i.e.* the wavefunction optimization, can be circumvented within CPMD and usually speed ups of up to one order of magnitude can be obtained.

The Car-Parrinello Lagrangian,

$$\begin{aligned} L_{CP}(\mathbf{R},\dot{\mathbf{R}},[\{\phi_i\}],[\{\dot{\phi}_i\}]) &= \frac{1}{2}\sum_{\mathbf{I}} m_{\mathbf{I}}\,\dot{\mathbf{R}}_{\mathbf{I}}^2 + \frac{1}{2}\sum_i \mu\langle\dot{\phi}_i \mid \dot{\phi}_i\rangle - \langle\Psi_0|H\,|\Psi_0\rangle \\ &+ \sum_{i,j}\Lambda_{ij}(\langle\phi_i \mid \phi_j\rangle - \delta_{ij}), \end{aligned} \tag{2.37}$$

contains the kinetic energy of the nuclei and of the electrons (fictitious), the potential energy, and the constraints ensuring that the classical orbital objects remain orthonormal. A fictitious mass (or inertia parameter) μ is assigned to the orbital degrees of freedom and must be tuned in order to maintain the adiabatic separation. The Newtonian equations of motion are obtained from the associated Euler-Lagrange equations

$$\frac{d}{dt}\frac{\partial L_{CP}}{\partial\,\dot{\mathbf{R}}} = \frac{\partial L_{CP}}{\partial\,\mathbf{R}}, \tag{2.38}$$

$$\frac{d}{dt}\frac{\delta L_{CP}}{\delta\,\langle\dot{\phi}_i|} = \frac{d}{dt}\frac{\delta L_{CP}}{\delta\,\langle\phi_i|}. \tag{2.39}$$

The corresponding Car-Parrinello equations are found to be of the form:

$$m_{\mathbf{I}}\,\ddot{\mathbf{R}}_{\mathbf{I}} = -\frac{\partial E_{\mathrm{KS}}}{\partial\mathbf{R}_{\mathbf{I}}} + \sum_{ij}\Lambda_{ij}\frac{\partial\langle\phi_i \mid \phi_j\rangle}{\partial\mathbf{R}_{\mathbf{I}}}, \tag{2.40}$$

$$\mu\,|\ddot{\phi}_i\rangle = -\frac{\delta E_{\mathrm{KS}}}{\partial\langle\phi_i|} + \sum_{ij}\Lambda_{ij}|\phi_i\rangle. \tag{2.41}$$

The constant of motion is then

$$E_{const} = \frac{1}{2}\sum_{\mathbf{I}} m_{\mathbf{I}}\,\dot{\mathbf{R}}^2 + \sum_i \mu\langle\dot{\phi}_i \mid \dot{\phi}_i\rangle + E_{\mathrm{KS}}. \tag{2.42}$$

2.5 QM/MM

The total energy of a quantum mechanical/molecular mechanical (QM/MM) system is an eigenvalue of the Hamiltonian

$$H = H_{QM} + H_{MM} + H_{QM/MM}. \tag{2.43}$$

Here, $H_{QM/MM}$ describes the interaction between the QM ad the MM part of the system which have to be suitably chosen. $H_{QM/MM}$ can be divided into a bonded term, if covalent bonds exist between the QM and the MM subsystems, and a non-bonded term

$$H_{QM/MM}^{\text{non-bonded}} = \sum_{\mathbf{I}\in MM} Q_{\mathbf{I}}\int d^3r\,\frac{n(\mathbf{r})}{|\mathbf{r}-\mathbf{R}_{\mathbf{I}}|} + \sum_{\mathbf{I}\in MM,\mathbf{J}\in QM} V_{vdW}(|\mathbf{R}_{\mathbf{J}}-\mathbf{R}_{\mathbf{I}}|). \tag{2.44}$$

$\mathbf{R_I}$ is the position of the MM atom **I** with the point charge $Q_{\mathbf{I}}$, $n(\mathbf{r})$ is the total (*i.e.* ionic and electronic) charge density of the quantum system, and V_{vdW} is the van der Waals interaction between atoms **I** and **J**. In the employed QM/MM scheme, the van der Waals interaction term is simply taken from the classical force field.

The implementation of the Coulomb term in Eq. (2.44) is non trivial due to (i) the 'electron spill-out problem' (the Pauli repulsion term between the electrons and positively charged nearby MM atoms is missing) and (ii) the high computational cost due to the - in principle - continuous electron density. The first problem is usually handled by replacing for those MM atoms close to the QM region the short ranged Coulomb $1/r$ interaction by a damped attraction which goes to a finite value for small r. The computational problem is tackled by modeling the long-range electrostatics with a Hamiltonian that couples the multipole moments of the quantum charge distribution with the classical point charges. More details of the implementation are described in Ref. [46].

If the QM/MM boundary cuts through a covalent bond, care has to be taken to saturate the valence orbitals. This issue is subject to the QM/MM boundary study in chapter 3.

Chapter 3

Optimization of molecular properties

All you need is ignorance and confidence; then success is sure.
Samuel Langhorne Clemens (Mark Twain) (1835-1910)

Abstract

In plane wave based electronic structure calculations the interaction of core and valence electrons is usually represented by atomic effective core potentials. They are constructed in such a way that the shape of the atomic valence orbitals outside a certain core radius is reproduced correctly with respect to the corresponding all-electron calculations and that the integrated atomic charge of the core is conserved. Here, a

novel method in conjunction with density functional perturbation theory is used to optimize effective core potentials in order to reproduce ground-state molecular properties from arbitrarily accurate reference calculations within standard density functional calculations. The wide range of possible applications of such optimized atom centered potentials (OACPs) is demonstrated by means of two examples. First OACPs are used to tackle the link atom problem in QM/MM schemes proposing a fully automatized procedure for the generation of link OACPs which are designed in such a way that they minimally perturb the electronic density structure in the QM region. In the second application, OACPs are used for two example molecules (water and acetic acid) in such a way as to reproduce electronic densities and derived molecular properties of hybrid (B3LYP) quality within GGA (BLYP) density functional calculations.

3.1 Introduction

Many *ab initio* electronic structure calculations, especially when dealing with large systems or heavy atoms, exploit the frozen-core approximation: only the chemically relevant valence electrons are treated explicitly while an effective core potential (ECP) or pseudopotential accounts for the effects of the core electrons [47–49]. Within the field of condensed matter physics the use of pseudopotentials is particularly crucial for plane wave based calculations. Atomic pseudopotentials were introduced and have been used since 1959 [50–55]. ECPs for heavy atoms, molecules and condensed phase calculations have been subject to improvement ever since. See Ref. [39, 40] for reviews. In 1996, analytic (Gaussian-based) norm conserving separable dual-space pseudopotentials were introduced by Goedecker et al. for all first, second and third row elements [56] and extended to all atoms up to Radon including relativistic effects in 1998 [57]. The parameters of these ECPs are generated for each atom by iteratively minimizing an atomic penalty functional, which expresses the deviations of ECP-generated Kohn-Sham (KS) valence orbitals from their (relativistic) all-electron counterparts. Here, a method is proposed which exploits an analogous procedure in such a way that not only atomic but also molecular properties are included as a reference. Specifically, complex molecular properties are considered as target quantities in the penalty functional. In turn, the transferability requirements of the atomic pseudopotential are generally relaxed in favor of ECPs optimized for specific molecular properties. In principle, this atom-based potential optimization approach can be seen in analogy to the optimized effective potential (OEP) method in density functional theory (DFT) [23, 58–62] where usually an orbital dependent external effective potential is optimized. However, while the OEP scheme exploits the variational principle, here it is suggested to consider the atom centered ECPs as tunable and to directly vary them in such a way as to reproduce some molecular reference property. So far, only properties as (interaction) energies, nuclear forces, and electron densities have been studied, optimized, or successfully included in the penalty functional. For instance, reproducing forces and binding energies at the equilibrium geometry, it could be shown that extended and calibrated optimized atom centered potentials (OACPs) can cure the lack of dispersion forces in commonly used exchange-correlation (xc-) functionals [63, 64]. In this chapter, the generality of OACPs is illustrated by addressing electron densities as molecular property. Zhao et al. [65–67] have already shown for single atoms that a density penalty allows to compute KS-orbitals, energies, and in principle also to extract the exact exchange-correlation potential - if the reference density was exact and differencing large numbers was not a problem. Here, the same scheme is applied to molecules but instead of obtaining orbitals and energies its usefulness is demonstrated by tackling other kinds of problems within DFT based electronic structure theory. First, the approach is used for the design of special link atoms for binding quantum to classical fragments in QM/MM applications. Secondly, by the means of OACPs a given reference electronic density computed with a certain amount of nonlocal exact exchange, using the B3LYP hybrid functional [36, 68], is reconstructed within a standard local general gradient approximated (GGA) xc-potential calculation, using BLYP [35, 36].

Hybrid quantum mechanics/molecular mechanics (QM/MM) calculations have attracted a lot of attention in recent years because of their ability to accurately treat at the quantum level (QM-part) molecules or molecular fragments (containing hundreds of atoms) embedded in a large environment (many thousands of atoms) which is described classically (MM-part) [69, 70]. However, when the classical surrounding is covalently bound to the quantum region, the problem of how to link the QM part to the

MM region is encountered. A popular choice is to cap all boundary atoms by hydrogens, however, this often leads to a distortion of the electronic density [71]. Several research groups proposed to design special capping effective potentials to reduce this effect [72–75]. Recently, a general scheme to fit pseudopotential parameters in order to reproduce model system properties such as bond lengths or charges has also been introduced [76]. Alternatively, the frontier orbitals of the link atom which point into the direction of the MM-region can be considered to be frozen [77, 78]. In this context, it should be mentioned that there are also frozen density approaches avoiding the linking atom problem by construction [79]. Here, it is proposed to optimize systematically the capping ECPs at the QM/MM boundary using density functional perturbation theory. Specifically, using perturbed electron densities it will be shown how to iteratively minimize differences in electron density between the QM region and an all-atom QM reference calculation.

In the second application the performance of GGA based DFT functionals using OACPs is attempted to be improved. Often, hybrid functionals like B3LYP are able to yield a more accurate description of molecular systems [80] and reaction profiles [81] than calculations using the GGA such as e.g. BLYP. Especially transition states are described significantly better when exact exchange is included in the xc-functional [29]. Unfortunately, the inclusion of exact exchange, such as it is necessary for B3LYP DFT calculations, into the wavefunction optimization algorithm increases the computational cost for plane wave calculations typically by one order of magnitude. As a solution to this problem it is proposed to use specially designed OACPs within the BLYP DFT level of theory in order to rebuild the electronic density from a corresponding B3LYP reference calculation of the same molecular system. Therefore, it is investigated how the OACP-method responds to the question of how the external potential has to be modified in order yield an electron density maximally close to an unmodified external potential plus the nonlocal B3LYP xc-potential. As molecular test systems for this application, water and acetic acid, which are two ubiquitous solvent molecules and which can act simultaneously as hydrogen bond acceptors and donors, have been chosen.

3.2 Methods and computational details

The basic idea of the approach has been introduced in Ref. [63] and is outlined here in more detail. The method employs the iterative minimization of a penalty functional $\mathcal{P}$ by variational tuning of a certain number of ECP parameters. The way the penalty functional is designed determines which molecular property will be optimized. Usually it represents the difference of selected physical properties, e.g. the electronic density and its higher moments, computed with a given set of values for the ECP parameters (which is denoted by σ_i), with respect to a reference system which can be computed at any level of theory. Thus, the minimization of $\mathcal{P}(\{\sigma_i\})$ (which may depend on all quantities that can be expressed *via* the KS-orbitals of the system) allows to approach as much as possible an arbitrary reference - within the limits of the chosen functional form of the ECP approach. In principle, this approach can be applied to any molecular property such as the electronic density $n(\mathbf{r})$, its multipole moments, ionic forces, as well as the total energy. For the applications of this chapter, $\mathcal{P}(\{\sigma_i\})$ is chosen to depend only indirectly on the set of parameters $\{\sigma_i\}$ through the electronic density.

Without any loss of generality, the procedure is illustrated supposing a simple functional form only dependent on the electronic density $n(\mathbf{r}) = \sum_{k=1}^{N} |\phi_k(\mathbf{r})|^2$, where N is the number of occupied KS-orbitals ϕ_k,

$$\mathcal{P}\left[n(\mathbf{r},\{\sigma_i\})\right] = \int d^3r\, w(\mathbf{r})\, \mathcal{F}\,\left(n(\mathbf{r})\right), \tag{3.1}$$

where $\mathcal{F}$ is a simple function of the density. The weighting function $w(\mathbf{r})$ can be used to restrict the integration to a certain volume or to certain atoms only. The minimization of Eq. (3.1) is performed by following the gradient of $\mathcal{P}$ with respect to the ECP parameters σ_j:

$$\frac{d\mathcal{P}}{d\sigma_j} = \int d^3r\, w(\mathbf{r})\, \frac{\partial \mathcal{F}}{\partial n}(\mathbf{r})\, \frac{dn}{d\sigma_j}(\mathbf{r}). \tag{3.2}$$

The derivatives $dn(\mathbf{r})/d\sigma_j$, which will be denoted $n_j^{(1)}(\mathbf{r})$, represent the linear change in the electronic structure of the system which is induced by a variation of one of the ECP parameters $\sigma_j \mapsto \sigma_j + d\sigma_j$:

$$n_j^{(1)}(\mathbf{r}) = \sum_{i=1}^{N} [\phi_i^{*(0)}(\mathbf{r})\phi_{ij}^{(1)}(\mathbf{r}) + \phi_{ij}^{*(1)}(\mathbf{r})\phi_i^{(0)}(\mathbf{r})]. \tag{3.3}$$

Here, the perturbed orbitals $\phi_{ij}^{(1)}$ denote the linear change of orbital i due to a small variation of parameter σ_j. This linear density response can be computed through density functional perturbation theory, where the perturbation Hamiltonian is given by the change in the ECP due to the variation of σ_j,

$$\hat{H}'_j = \frac{\partial \hat{V}^{\mathrm{ECP}}(\{\sigma_i\})}{\partial \sigma_j}. \tag{3.4}$$

Eq. (3.4) has been implemented into the program CPMD [82]. Eq. (3.4) is applied to each orbital within the implementation of a general variational density functional perturbation theory module [43] in order to determine the vector of response densities $\left\{ n_j^{(1)}(\mathbf{r}) \right\}$. Following the gradients of Eq. (3.2) until convergence of the penalty P [Eq. (3.1)] that set of ECP parameters $\{\sigma_i\}$ is determined which represents best the OACP corresponding to the chosen penalty. To implement Eq. (3.4) analytical ECPs as the one introduced by Goedecker et al. [56] are used. The latter consist of a local $V^{\mathrm{loc}}(\mathbf{r})$ and of a sum of nonlocal parts $V_l^{\mathrm{nl}}(\{\sigma_i\}, \mathbf{r}, \mathbf{r}')$ with specific projectors for each angular momentum channel l:

$$\begin{aligned} V_{\mathrm{I}}^{\mathrm{ECP}}(\mathbf{r},\mathbf{r}') &= V^{(\mathrm{loc})}(\mathbf{r})\delta(\mathbf{r}-\mathbf{r}') + \sum_l V_l^{(\mathrm{nl})}(\mathbf{r},\mathbf{r}'). && (3.5)\\ V^{(\mathrm{loc})}(\mathbf{r}) &= \frac{-Z_{\mathrm{ion}}}{r}\mathrm{erf}\left[\frac{r}{r_{\mathrm{loc}}\sqrt{2}}\right] + \exp\left[-\frac{r^2}{2r_{\mathrm{loc}}^2}\right] \times \\ &\quad \left(C_1 + C_2\left(\frac{r}{r_{\mathrm{loc}}}\right)^2 + C_3\left(\frac{r}{r_{\mathrm{loc}}}\right)^4 + C_4\left(\frac{r}{r_{\mathrm{loc}}}\right)^6\right). && (3.6)\\ V_l^{(\mathrm{nl})}(\mathbf{r},\mathbf{r}') &= \sum_{m=-l}^{+l} Y_{lm}(\hat{\mathbf{r}}) \sum_{j,h=1}^{3} p_{lh}(r) h_{hj}^{(l)} p_{lj}(r') Y_{lm}^*(\hat{\mathbf{r}}'). && (3.7) \end{aligned}$$

where $p_{lh}(r) \propto r^{l+2(h-1)}\exp(-r^2/(2r_l^2))$, $r = |\mathbf{r} - \mathbf{R}_{\mathrm{I}}|$ on the position $\mathbf{R}_{\mathrm{I}}$ of nucleus I, $\hat{\mathbf{r}}$ is the unit vector in the direction of $\mathbf{r}$, and Y_{lm} denotes a spherical harmonic. The parameters $\{r_{\mathrm{loc}}, C_1, C_2, C_3, C_4, h_{hj}^{(l)}, r_l, ...\}$ span the parameter space $\{\sigma_i\}$, its dimensionality being determined by the largest angular momentum component of the ECP. One could also have investigated the effect of optimizing additional larger angular momentum channels, not included in the conventional ECP. For example for carbon or oxygen the ECP series can be safely truncated at the first l-term not contained in the core. However, in this chapter the optimization of the ECPs is restricted in all cases to the already existing parameters defining an ECP of a second row atom such as carbon or oxygen. In contrast, in the dispersion forces related study of chapter 4, the optimization uses only parameters defining an additional angular momentum channel, being introduced solely for the purpose of the optimization. The explicit form of Eq. (3.4) for all first and second row elements is presented in the appendix at the end of this thesis.

For the first two applications described in detail in the next section, it was chosen to optimize electron densities as molecular properties. In full analogy to Eq. (22) in Ref. [66] the following penalty functional - being closely related to the accuracy of a description - has been used

$$P\left[n(\mathbf{r})\right] \quad = \quad \int d^3r\, w(\mathbf{r})\, \left|n^{\text{ref}}(\mathbf{r}) - n(\mathbf{r})\right|^2, \tag{3.8}$$

with individual weighting functions $w(\mathbf{r})$ and appropriate reference densities $n^{\text{ref}}(\mathbf{r})$. According to Eq. (3.2) the gradient of Eq. (3.8) with respect to an ECP parameter σ_j is given by

$$\frac{\mathrm{d}P\left[n(\mathbf{r})\right]}{\mathrm{d}\sigma_j} = 2\int d^3r\, w(\mathbf{r})\, n_j^{(1)}(\mathbf{r})\left(n(\mathbf{r}) - n^{\text{ref}}(\mathbf{r})\right). \tag{3.9}$$

All calculations have been carried out using CPMD [82] at an orbital plane wave cutoff of 100 Ry with the isolated system Poisson solver according to Ref. [83]. As pseudopotentials the BLYP ECPs from Goedecker et al. [56] have been used for all calculations in this chapter, including the B3LYP reference calculations. B3LYP ECPs have not been used because first of all the choice of the reference is purely arbitrary - any reference can be used. Furthermore, it is the intention of this study to measure if the OACPs can account for the isolated impact on the electron density due to a change in the xc-functional. Therefore, if B3LYP ECPs had been used, the OACPs would have to account for both, the difference in the functional and the difference in the ECPs.

However, by doing so the B3LYP calculations can not be compared to 'pure' B3LYP calculations from literature. For the purpose of this thesis, the absolute accuracy of the reference is of minor importance.

3.3 Results and discussion

3.3.1 QM/MM link atom optimization

As a first application, it is addressed how to design optimal intramolecular link atoms between quantum and classical regions in QM/MM simulations where typically a C-C bond is cut. The substitution of a real carbon atom within a macromolecule by a so-called link atom, designed to saturate the open valence, inherently leads to a distortion of the electronic density in the QM neighborhood of the link atom. The aim is to investigate if one can minimize this perturbing effect of the artificial QM/MM bond cleavage on the electronic density in the QM region by applying this scheme to identify an OACP for the link atom.

As a model system for the link atom optimization acetic acid has been chosen where the methyl group is replaced by a link OACP, and the weighting function $w(\mathbf{r})$ is chosen such as to restrict the integration volume in Eq. (3.8) to the union of spheres of radius of 1.5 Å (corresponding roughly to a C-C bond length) centered on each atom, while on the linking nucleus the corresponding radius is only 0.7 Å. By doing so, from the penalty functional P^{link} the necessarily different electron density of the methyl group is excluded while the rest of the QM region is part of the integration volume.

Table 3.1: Calculated total permanent dipole moments $|\mu|$ for geometrically fixed R-CO_2H. R = CH_3 corresponds to full QM acetic acid, D^{opt} is a link OACP replacing the CH_3 group, H indicates hydrogen capping, D^{con} is an empirically optimized monovalent link carbon atom which reproduces a H_3C-CH_3 bond length [75], and F corresponds to fluorine capping. All values are in Debye.

R	CH_3	D^{opt}	H	D^{con}	F
$\|\mu\|$	1.70	1.32	0.69	3.10	2.31

Using a gradient based optimization technique, P^{link} has been minimized in the space of all ECP parameters of the capping atom to identify the OACP. The results for calculated total permanent dipole moments are presented in table 3.1. Acetic acid has been investigated using four different replacements for the methyl group: an optimized heptavalent ECP, hydrogen capping, an empirically modified monovalent link atom [75] based on a carbon ECP, and fluorine capping. In comparison to the full QM calculation of acetic acid, the OACP D^{opt} closely reproduces the total dipole moment, while all alternatives yield rather unsatisfying results. The small dipole moment in the case of hydrogen saturation reflects the fact that the hydrogen 1s electron is less polarizable by the electron attracting $-CO_2H$ group than the methyl group. In contrast to that, when using a conventional empirically adjusted monovalent linking carbon atom or fluorine capping the dipole moment is overestimated and inverted. Especially a wrong dipole moment often constitutes one of the major sources of errors at the boundary of QM/MM calculations. Furthermore, an accurate description of the QM/MM boundary makes it possible to reduce the size of the QM region, thereby allowing a decrease in computational cost. The scheme presented here can easily be implemented into an automatic procedure for the generation of optimal link ECPs for arbitrary chosen reference situations.

Figure 3.1: LEFT to RIGHT: Isosurfaces of some occupied KS-orbitals of the full acetic acid (lower row) and of the link atom acetic acid (upper row).

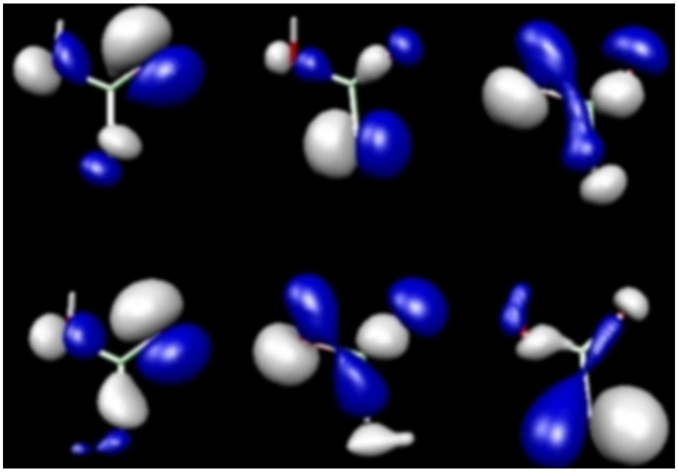

In Fig. 3.1, KS-orbitals are depicted for acetic acid with and without the linking atom. While in the first column the regions of the orbital which is located on the acidic group still resemble each other significantly, it becomes clear that for the other columns, the parts located on the carboxy group differs substantially. This indicates significant changes in the electronic structure. These results suggest that also other properties, such as orbitals and eigenvalues, should be considered to be taken into account. A way out of the specific problem illustrated in Fig. 3.1 would hence be provided by an extended penalty functional which includes explicitly differences in a set of chosen orbitals $\{\phi_i\}$ (intuitively the frontier orbitals):

$$P^{\text{extended}} = P[n] + P[\{\phi_i\}] \tag{3.10}$$

It becomes also clear, that mimicking a whole methyl group by a single atom centered potential is not straightforward and has - even if the electron density is optimized - still a substantial potential to perturb the electronic structure, and hence reactivity for instance, significantly.

3.3.2 B3LYP density reconstruction using BLYP

Using the same approach, OACP parameters have been determined for all heavy atoms in water and acetic acid which yield a density as close as possible to the reference electron density within a pure DFT BLYP functional calculation. I.e. the OACPs are able to reproduce the chosen reference electronic density with the smallest least square error. In principle, one could have taken as a reference an electron density originating from any level of theory, such as Møller-Plesset or coupled cluster calculations. However, for the reason of simplicity, we have chosen a B3LYP electron density. Instead of a reference electron density one could also use other molecular properties, e.g. ionic forces (geometry) or KS-eigenvalues for the construction of the penalty functional. Here, the simplest form of a penalty functional is used, Eq. (3.8), which imposes an approximate reconstruction of the electron density obtained from a B3LYP calculation, namely $n^{\text{ref}} = n_{B3LYP}$. The ECP parameters of all oxygen and carbon atoms have been taken as variables and have been used to minimize Eq. (3.8) at the original B3LYP-optimized geometry.

For the oxygen and carbon ECPs in water and acetic acid, the progressive minimization of the penalty in its high dimensional parameter space is shown as a function of only σ_1 [r_{loc} in Eq. (3.6)] in Fig. 3.2. σ_1 represents approximatively the core radius of the ECP. It is interesting to note that there seems to be a general trend to decrease σ_1

Figure 3.2: History of the minimization of the density penalty as a function of σ_1 of oxygen in water and acetic acid and of carbon in acetic acid.

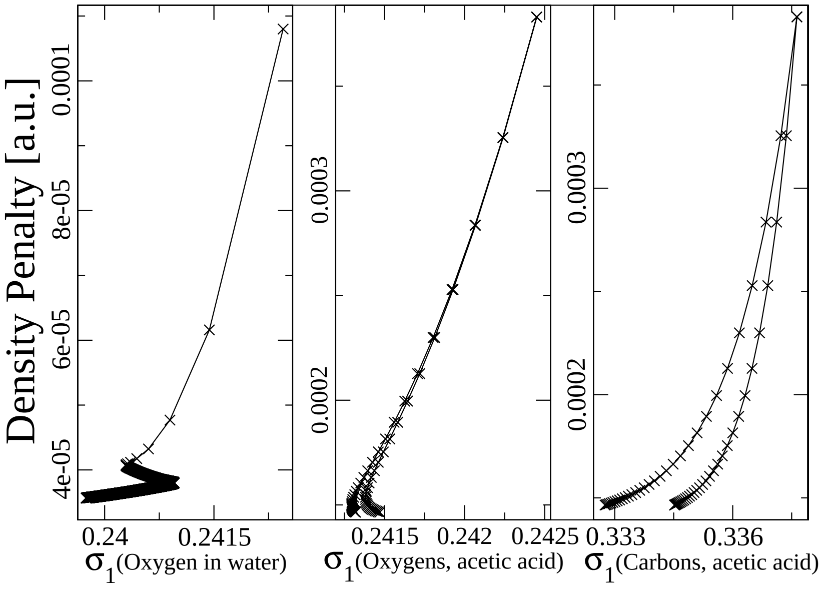

in order to reproduce the B3LYP xc-functional better, independently of the atom type or the molecule. This seems to be in consistence with the common experience that the repulsive potential for B3LYP is steeper than for BLYP. Throughout the minimization, while also all the other ECP parameters (not shown in Fig. 3.2) vary only by a few percents, P decreases to roughly one third of its initial value.

The penalty functional in Fig. 3.2 decreases to only a third of its initial value. This indicates that the flexibility in parameter space is not yet exhausted and that inclusion of more parameters might even still improve the minimization.

Furthermore, one should note that - as one would expect - the optimized parameters of the same atom type in different chemical environments adapt in a slightly different manner, relaxing thereby the criterion of transferability. For example, the OACP of a carbon atom in a carboxy group or in a methyl group differ slightly. However, as presented in Fig. 3.2, the final core radii σ_1 of the two carbon or oxygen atoms in acetic acid differ only by less than 1%. This suggests a certain transferability of a common atom type B3LYP-OACP to different hybridization states.

Table 3.2: Deviation Δ with respect to the B3LYP results for calculated total dipole moments $|\mu|$, RESP charges q^{RESP}, bond lengths $d_{\mathrm{O\text{-}H}}$ and angles for water. Dipole moments are in Debye, charges are in atomic units, and angles are in degrees.

Method	$\Delta\ |\mu|$	$\Delta\ q_{\mathrm{O}}^{\mathrm{RES}}$	$\Delta\ q_{\mathrm{H}}^{\mathrm{RES}}$	$\Delta\ d_{\mathrm{O\text{-}H}}$	$\Delta\ \angle_{\mathrm{HOH}}$
BLYP	0.038	0.022	0.011	0.018	0.9
BLYP+OACP	0.010	0.009	0.004	0.016	0.3

In Tables 3.2, 3.3, and 3.4, the deviations of several quantities which are derived from the electronic density with respect to the corresponding B3LYP results are presented for comparison. Dipole moments, atomic restrained electrostatic potential derived charges (RESP [84]) and geometries of water and acetic acid have been computed.

Figure 3.3: The labeling of the atoms in acetic acid for table 3.3.

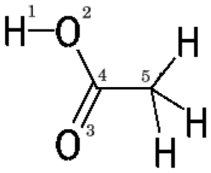

Table 3.3: Deviation Δ with respect to the B3LYP results for calculated RESP charges q^{RESP} for acetic acid: $H_3C^{(5)}C^{(4)}O^{(3)}O^{(2)}H^{(1)}$ (precise labeling in Fig. 3.3). All values are in atomic units.

Method	$\Delta\ q_{\mathrm{C}^{(5)}}^{\mathrm{RESP}}$	$\Delta\ q_{\mathrm{C}^{(4)}}^{\mathrm{RESP}}$	$\Delta\ q_{\mathrm{O}^{(3)}}^{\mathrm{RESP}}$	$\Delta\ q_{\mathrm{O}^{(2)}}^{\mathrm{RESP}}$	$\Delta\ q_{\mathrm{H}^{(1)}}^{\mathrm{RESP}}$
BLYP	0.011	0.016	0.011	0.016	0.011
BLYP+OACP	0.001	0.017	0.006	0.005	0.000

A systematic tendency is observed for all considered properties to approach the B3LYP values. With respect to the B3LYP results, static electronic properties such as dipole moments and RESP charges improve in general by an order of magnitude. Interestingly, the RESP charge on the carboxy carbon atom does not change. It is suspected that this exclusive behavior is due to the somewhat more complex electronic structure surrounding this carbon atom having three σ- and one π-bond.

Table 3.4: Deviation Δ with respect to the B3LYP results for calculated dipole moment along the molecular axis (μ_z) and the O-H bond length $d_{\text{O-H}}$ for acetic acid. Dipole moments are in Debye, distances are in atomic units.

Method	$\Delta\ \mu_z$	$\Delta\ d_{\text{O-H}}$
BLYP	0.016	0.017
BLYP+OACP	0.002	0.012

Here, one should point out that due to the significant improvement in the description of the charge distribution obtained using OACPs together with a GGA xc-functional, also a more accurate description of hydrogen bonds should be possible. Therefore the interaction energy (E^{int} = E^{Dimer} - 2*$E^{Monomer}$) of the water and of the acetic acid dimers has been computed. The deviation with respect to the B3LYP results decreases in the case of the water dimer from 0.38 to 0.20 kcal/mol and in the case of the acetic acid dimer even from 0.97 to 0.03 kcal/mol.

But to account fully for properties other than those which are directly derived from the electron density, a more suitable penalty needs to be defined which includes properties such as energies or ionic forces explicitly. This statement is illustrated by table 3.5 where bond lengths after and before the optimization are shown. Upon inclusion of the OACPs, the bond lengths change remain practically unchanged. Also, proton affinities have been determined for water and acetic acid. They are given in table 3.6. Upon inclusion of the OACPs, also in the case of the proton affinities the values change only very slightly. Interestingly, they change in the opposite direction with respect to the reference results.

The great advantage of the use of the OACP-BLYP scheme instead of the ECP-

Table 3.5: Bond lengths d for acetic acid $H_3C^{(5)}C^{(4)}O^{(3)}O^{(2)}H^{(1)}$ (precise labeling in Fig. 3.3) in Å.

Method	$d_{O^{(2)}-C^{(3)}}$	$d_{O^{(3)}-C^{(3)}}$	$d_{C^{(4)}-C^{(3)}}$	$d_{C^{(4)}-H}$
B3LYP	1.265	1.260	1.561	1.095
BLYP	1.276	1.275	1.574	1.099
BLYP+OACP	1.277	1.271	1.574	1.100

Table 3.6: Proton affinities for water (wat) and acetic acid (acac) at fixed geometry being optimized for the protonated species. For acetic acid, also the deprotonated species has been optimized (acac-geo). All values are in a.u..

Method	wat	acac	acac-geo
B3LYP	-0.6279	-0.5803	-0.5647
BLYP	-0.6212	-0.5758	-0.5612
BLYP+OACP	-0.6218	-0.5761	-0.5761

B3LYP scheme lies in the decrease of the computational cost, which within plane wave calculations is one order of magnitude when BLYP is used instead of B3LYP. Using CPMD [44] on one CPU of an AMD OPTERON (244 1.8 GHz 4GB Memory) workstation an average wavefunction optimization step of acetic acid in a 8*8*9 Å ^{3} box at a wavefunction cutoff of 100 Ry took $\approx$ 80 s using B3LYP and $\approx$ 7.8 s using BLYP.

3.4 Conclusions

A novel iterative method has been presented for tuning on a molecular level parameters of analytic ECPs in electronic structure calculations by means of minimizing a suitably defined penalty functional. The penalty consists of an appropriate and differentiable function of the electronic density, and is constructed in such a way as to penalize deviations from a given reference calculation. This approach has been implemented in the plane wave pseudopotential code CPMD [82].

The potential of the method has been illustrated by means of two applications.

First, an OACP has been constructed for a link atom for bond cuts in QM/MM schemes which minimizes the perturbation of the QM region using an electron density penalty to quantify the differences between a full QM calculation and a QM/MM calculation. The error on the quantum region introduced by the use of link atoms can thus be generally minimized within this scheme. The minimization of the error has been demonstrated by obtaining a correct dipole moment even when the QM/MM boundary is included. The approach is general enough to be used in order to automatically obtain the optimal capping OACP for any kind of bond by minimizing the above mentioned penalty inside the quantum region. Therefore, using OACPs, the polarity of the QM/MM boundary can be conserved, which is important for the accuracy of the QM/MM approach. Furthermore, it is conceivable to reduce the size of the QM region because of the increased accuracy of the description of the QM/MM bond, thus allowing for a decrease in computational cost. Hence, the scheme presented here can be used for an automatic procedure to generate optimal link ECPs.

As a second application an electronic density computed with the B3LYP functional has been reconstructed within an OACP-BLYP calculation. Significant improvements for electrostatic properties such as dipole moments, RESP charges, and dimer interactions could been demonstrated. The results suggest that any kind of electron density corresponding to a given potential of arbitrary complexity can be approximately reconstructed by using the suggested scheme of tuning the external atom centered nonlocal potential represented by the OACPs. This is of interest for the well known quest for better approximations to the unknown yet existing exact exchange-correlation potential. Further calculations of this kind are being pursued - with more accurate reference methods, such as explicitly correlated approaches. Considering the decrease of computational cost, in the special case of B3LYP the use of OACPs seems to be very promising to carry out more accurate ’B3LYP-emulating’ condensed phase plane wave calculations. However, while the assessment of the transferability of these OACPs with respect to other atoms or dynamical effects is beyond the scope of this study, the limit of the density penalty has been illustrated. Molecular properties, such as nuclear forces or hydrogen affinities, which depend only implicitly on the electron density can not necessarily be expected to be improved upon inclusion of OACPs which have been calibrated within the context of a density penalty minimization. A density penalty using an exact (from experiment or from most accurate quantum chemical calculations) reference density should allow the construction of a fitted approximating atom centered xc potential with minimal deviation from the exact xc potential.

We conclude that with the use of OACPs in molecules the external potential can be tailored to special purposes. The inherent technical advantage of this approach consists in the fact that the computational cost is not increased because the standard pseudopotential machinery as it is implemented in most plane wave electronic structure codes can be used. Since molecules consist of atoms, it is also legitimate to use series of atom based optimized potentials as a correction to the external potential to meet additional requirements for the description of molecular systems. It has been shown that the question of transferability has to be treated with caution and it is clear that transferability is not guaranteed by default.

This general scheme can also be applied to other purposes by using other references, more complex tailor-made penalty functionals, and extended functional forms of the OACPs.

Chapter 4

London dispersion forces

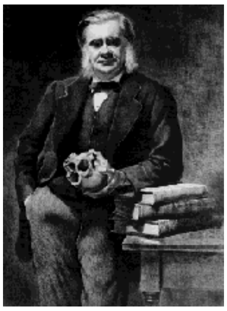

The great tragedy of science is the slaying of a beautiful hypothesis by an ugly fact.

Thomas Henry Huxley (1825-1895)

Abstract

An effective atom-centered nonlocal term is introduced in the Hamiltonian as a correction to the exchange-correlation potential in order to cure the lack of London dispersion forces in standard local Density Functional Theory (DFT) calculations. Calibration of this long-range correction is performed using Density Functional Perturbation Theory and an arbitrary reference. Without any prior assignment of types and structures

of molecular fragments, corrected generalized gradient approximation DFT calculations yield correct equilibrium geometries and dissociation energies of argon-argon, benzene-benzene, graphite-graphite, argon-benzene, and H_2-benzene complexes.

4.1 Introduction

London dispersion forces are crucial for many fundamental molecular processes such as the interactions between rare gas atoms, the formation of tertiary and quaternary structures of biomolecules, the packing of molecular crystals, and the intercalation of drugs into DNA, to name only a few. These forces belong to the group of weak long range van der Waals (vdW) forces: they represent the attractive interaction between self induced instantaneous multipole moments of ground state electron distributions [85]. Despite their obvious importance, it is not yet generally possible to correctly describe these nonlocal correlation effects within DFT calculations with purely local exchange-correlation functionals [86–89]. Introduction of non-locality into a “vdW-functional” as proposed in Ref. [90, 91] or by electron density partitioning [92] can abolish this deficiency but usually implies the artificial assignment of molecular fragments. Alternatively, Kohn et al. [89] or Misquitta et al. [93] proposed a general scheme for the explicit perturbation calculation of dispersion forces in DFT but only at prohibitive computational costs. As a consequence, empirical atom-atom based correction terms of the C_6/R^6-type are frequently used instead [88, 94]. Though very successful in many cases [95], preliminary calculations and validations are necessary to determine the values of these C_6 coefficients. In addition, for each pair of fragments or atom types individual damping functions have to be identified to account for the correct repulsive short-range behavior; rendering this approach somewhat cumbersome. Furthermore, empirical atom-atom potentials solely act on the ionic cores and do not influence the electronic structure, *i.e.* they do not correct any electronic properties.

Here, it is proposed to construct an effective potential consisting of optimized non-local higher angular momentum dependent terms for all atoms in the system in order to compensate for the absence of dispersion forces in the generalized gradient approximation (GGA) functional. Thus, instead of approximating the attractive long range electron density correlation by an atom-atom interaction, vdW forces are modeled by an atom-electron interaction, mediated by appropriate nonlocal atom centered potential projectors which are obtained from the optimization scheme. This additional atom centered contribution is grouped together with the employed exchange-correlation potential to form an extended exchange-correlation potential, $\hat{v}_{\text{xc}}^{\text{extended}} = \hat{v}_{\text{xc}}^{\text{GGA}} + \sum_{\mathbf{I}} \hat{v}_{\mathbf{I}}^{\text{correct}}$. Where the correcting term sums over all atoms **I**. For the calibration of the atom-centered effective potentials, accurate large basis set MP2 results for typical weakly bonded systems are used as a reference. To this purpose, molecular complexes have been chosen which are well known to be bonded solely due to dispersion forces. The GGA functional BLYP [35, 36] is used, and MP2 as a reference. This is an arbitrary choice, the approach could equally well be applied in the context of any other exchange-correlation functional and any other arbitrarily exact reference. In this chapter, references at the MP2 level of theory are considered to be a reasonable compromise between accuracy and computational cost. High accuracy methods like coupled cluster theory or SCF response methods (e.g. coupled perturbed Hartree-Fock) are desirable as benchmarks, but unfortunately, for larger systems, theoretical treatments beyond MP2 rapidly become computationally intractable.

Specifically, the dispersion interaction between benzene dimers, graphene sheets, rare gases, rare gas plus benzene, and hydrogen plus benzene have been studied. These systems have been chosen because they constitute well known vdW complexes which have been difficult to describe from first principles.

4.2 Methods and computational details

In electronic structure theory atomic effective core potentials (ECPs) represent the potential of nuclei and their core electrons [47, 49]. In particular, DFT calculations using plane wave basis sets are unfeasible without this technique. Initially introduced in an empirical form 1970 [52] and later in a first-principles formulation [54], ECPs have been subject to continuous development ever since [39]. Recently, Goedecker et al. [57] published a library of analytic, separable, norm conserving *ab initio* pseudopotentials, which contain local and nonlocal, angular momentum l dependent, terms of the form $V^{\mathrm{ECP}}(\mathbf{r},\mathbf{r}') = V^{(\mathrm{loc})}(\mathbf{r})\delta(\mathbf{r}-\mathbf{r}') + \sum_l V_l^{(\mathrm{nl})}(\mathbf{r},\mathbf{r}')$. Their local part consists of an errorfunction and a Gaussian while the nonlocal terms consist of Gaussian-type radial projectors p for each angular momentum channel l,

$$V_l^{(\mathrm{nl})}(\mathbf{r},\mathbf{r}') = \sum_{m=-l}^{+l} Y_{lm}(\hat{\mathbf{r}}) \sum_{j,k=1}^{3} p_{lk}(r) h_{kj}^{(l)} p_{lj}(r') Y_{lm}^{*}(\hat{\mathbf{r}}'). \tag{4.1}$$

where $p_{lh}(r) \propto r^{l+2(h-1)} \exp(-r^2/(2r_l^2))$, $r = |\mathbf{r}-\mathbf{R}_{\mathrm{I}}|$ on the position $\mathbf{R}$ of nucleus I, $\hat{\mathbf{r}}$ is the unit vector in the direction of $\mathbf{r}$, and Y_{lm} denotes a spherical harmonic. The parameters $\{..., h_{kj}^{(l)}, r_l, ...\}$ of these pseudopotentials (called $\{\sigma_i\}$ in the following) are generated by iteratively minimizing a penalty functional which expresses the deviations of the Kohn-Sham (KS) pseudoorbitals from their all-electron counterparts.

The spirit of this generation procedure has motivated us to design optimized atom-centered potentials (OACPs) by considering not only atomic but also complex molecular electronic properties as target quantities in the penalty functional. Here, an analogous iterative minimization of a penalty functional (P) is performed, where P is designed in such a way that it penalizes deviations from molecular properties (e.g. the electronic density) with respect to experimental or theoretical references.

The penalty functional $P(\{\sigma_i\})$ may depend on all quantities that can be expressed in terms of the KS-orbitals. It can thus describe any arbitrary molecular property such as electronic densities $n(\mathbf{r})$ and multipole moments as well as ionic forces $\mathbf{F}_{\mathrm{Ions}}$ or energies. Therefore, P depends only indirectly (*i.e. via* the KS-orbitals) on the ECP parameters $\{\sigma_i\}$.

In this way an additional atom centered potential can be introduced that has formally the same form as the ion-electron interaction potential, *i.e.* a linear combination of atom centered *nonlocal* potentials. It can thus be treated with the usual computational machinery at negligible additional cost. However, the number and magnitude of all the parameters of this nonlocal OACP potential are freely tunable; the potential can e.g. be chosen to act on a different characteristic length scale than the localized electron-core interaction. This approach is therefore in close analogy to the optimized effective potential (OEP) method in DFT [23, 58–62] where an orbital dependent external effective potential is optimized. In the case that P is designed to minimize the total energy of the system the scheme introduced here can be reduced to OEP.

The procedure is illustrated using a functional form only dependent on the electronic density $n(\mathbf{r}) = \sum_{k=1}^{N} |\phi_k(\mathbf{r})|^2$, N being the number of the occupied KS orbitals ϕ_k.

$$P\left[n(\mathbf{r},\{\sigma_i\})\right] = \int d^3r\, w(\mathbf{r})\, F\,\left(n(\mathbf{r})\right), \tag{4.2}$$

with a weighting function w and a penalty function F. Eq. (4.2) is minimized by following the gradient of P with respect to the parameters σ_j:

$$\frac{dP}{d\sigma_j} = \int d^3r\, w(\mathbf{r})\, \frac{\partial F}{\partial n}(\mathbf{r})\, \frac{dn}{d\sigma_j}(\mathbf{r}). \tag{4.3}$$

The derivatives $dn(\mathbf{r})/d\sigma_j$, which are denoted $n_j^{(1)}(\mathbf{r})$, represent the linear response of the density induced by the parameter variation $\sigma_j \mapsto \sigma_j + d\sigma_j$. This density response can be computed through first order perturbation theory, where the perturbation Hamiltonian is given by the change in the effective potential due to the variation in σ_j: $\hat{H}_j^{(1)} = \partial\hat{V}^{\mathrm{ECP}}(\{\sigma_i\})/\partial\sigma_j$. The density functional perturbation theory module [43] of the program CPMD [82] can be used to determine the vector of response densities $\{n_i^{(1)}(\mathbf{r})\}$. The penalty functional P in Eq. (4.2) has to be chosen specifically for each application. To obtain an attractive London dispersion interaction, the penalty functional in Eq. (4.2) is chosen to be a sum of energy dependent and ionic force dependent terms (both functionals of the electron density):

$$P^{\mathrm{disp}}(\mathbf{R}^{\mathrm{ref}}) = |E^{\mathrm{ref}}(\mathbf{R}^{\mathrm{ref}}) - E(\mathbf{R}^{\mathrm{ref}})|^2 + \sum_{\mathrm{I}}^{N_{\mathrm{ions}}} w_{\mathrm{I}}\, |\mathbf{F}_{\mathrm{I}}(\mathbf{R}^{\mathrm{ref}})|^2, \tag{4.4}$$

where $w(\mathbf{r})$ of Eq. (4.2) becomes $\sum_I w_{\mathrm{I}}\delta(\mathbf{r}-\mathbf{R}_{\mathrm{I}})$, $w_{\mathrm{I}} = 0$ or $w_{\mathrm{I}} = 1$ select specific atoms for the optimization process, and $\mathbf{F}_{\mathrm{I}}$ and E are the ionic forces and the energy of interaction at the reference geometry $\mathbf{R}^{\mathrm{ref}}$, respectively. E^{ref} corresponds to the reference dispersion interaction energy. By tuning the height ($\sigma_1 = h_{11}^{(l)}$) and the width (σ_2) of an additional projector [$p_{l1}(r) \propto r^2\exp(-r^2/(2\sigma_2^2))$], P^{disp} is minimized in such a way that the reference location and depth of the interaction energy minimum are reproduced for the calibration system. The choice to augment the ECPs by calibrating only one additional polarization channel for the dispersion forces is not crucial and could easily be extended to other angular momentum channels. For all the DFT calculations presented in this chapter, CPMD [82], a plane wave cutoff of 100 Ry, and the exchange-correlation functional BLYP have been used.

Table 4.1: Calculated static polarizabilities, quadrupole and dipole moments for BLYP calculations without correction (BLYP), with DCACPs (BLYP+DCACPs), and MP2 calculations for comparison. *bz* represents benzene, and $bz-Ar$ the benzene-argon complex. All values are in atomic units.

Method	α_{Ar}	Q_{bz}[1]	$\Delta\alpha_{bz}$[1]	α_{bz-Ar}[1]	μ^{z}_{bz-Ar}
BLYP	12.30	-5.35	39.18	55.0	0.047
BLYP+DCACP	12.31	-5.50	38.45	58.1	0.035
MP2	11.15[2]	-6.46[2]	35.07[3]	59.2[2]	0.037[2]

4.3 Results and discussion

4.3.1 Calibration

As a test case, dispersion corrected atom centered potentials (DCACPs) have been calibrated for carbon and argon. In the case of (aromatic) carbon, the benzene dimer in its parallel sandwich configuration is used as a reference system (as presented in the graph of Fig. 4.1) while for argon, the argon dimer is used (shown in Fig. 4.2). For benzene w_{I} was chosen to be zero in the case of hydrogen and one in the case of carbon, while for argon $w_{\mathrm{I}} = 1$.

The resulting values for σ_1 and σ_2 create a weak long range attractive potential. In the inset of the graph in Fig. 4.1 the applied additional projector for carbon $p_{11}(r)$ is plotted against r. It is interesting to note that the minimum of this attractive potential lies at 3.3 Å which is close to the equilibrium separation. However, the magnitude σ_1 remains so small that e.g. the geometry of an isolated benzene monomer is not distorted (the average changes of the bond lengths are only $\approx$ 0.01 Å). Moreover, electronic quantities of the monomers remain basically unchanged, e.g. the static polarizability (α) of argon or the permanent quadrupole moment Q and the static polarizability anisotropy ($\Delta\alpha = \alpha_{yy} - \alpha_{zz}$) of benzene (Table 4.1).

---

[1] $Q = \langle z^2 - \frac{1}{2}x^2 - \frac{1}{2}y^2 \rangle$, $\Delta\alpha_{bz} = \alpha^{bz}_{zz} - \alpha^{bz}_{yy}$, $\alpha_{bz-Ar} = \alpha^{bz-Ar}_{zz}$

[2] MP2 results from Ref. [96]

[3] MP2 results from Ref. [97]

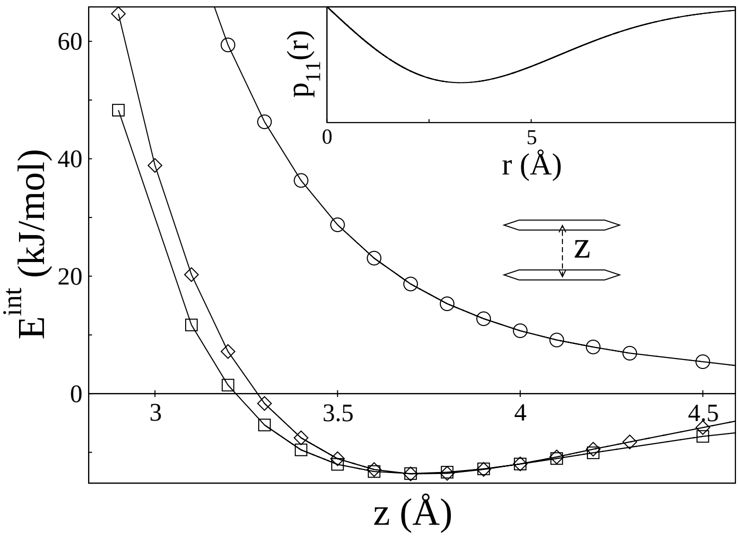

Figure 4.1: Calibration of the DCACP for carbon: potential energy curves of the energy of interaction (E^{int} = E^{dimer}-2$E^{monomer}$) are plotted for the benzene dimer in its sandwich configuration as a function of the distance z. ◯ corresponds to BLYP, ◇ to BLYP + DCACP, and squares to MP2 data from Ref. [98]. In atomic units the calibrated values of the additional p-channel for carbon are $\sigma_1 = -0.00352$ and $\sigma_2 = 3.280$. In the inset the additional p-channel projector $p_{11}(r)$ [Eq. (5.3)] is depicted in arbitrary units as a function of r, the minimum is roughly at 3.3 Å.

4.3.2 Assessing transferability

Using the DCACPs, interaction energies have been computed for a T-shaped benzene dimer configuration and for a slab made of two layers of graphene. The results are presented in Fig. 4.3 and Fig. 4.4 and show an astonishing transferability of the calibrated DCACPs. For the T-shaped benzene dimer the results compare very well to the corresponding MP2 calculations from Ref. [98] which use the same basis set as those which have been used for the calibration in the sandwich configuration. In order to get an idea of the performance of the correction when describing graphite the interaction

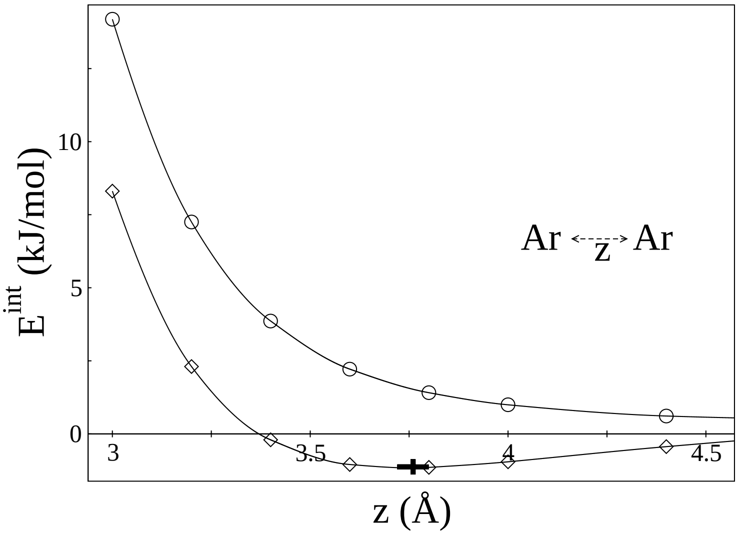

Figure 4.2: Calibration of the DCACP for argon: potential energy curves of the total energy of interaction ($E^{int} = E^{Dimer}$-$2E^{Monomers}$) are plotted as a function of the distance z. ◯ corresponds to BLYP, ◇ to BLYP+DCACPs, the MP2 result [96] for the interlayer distance and energy of interaction is marked by a cross. In atomic units the calibrated values of the additional f-channel for argon are σ_1 = -0.002 and σ_2 = 2.9.

energy of two graphene sheets have been calculated. To this end, 64 atoms have been arranged in a slab made of two layers, and periodic boundary conditions have been applied within the xy plane of the graphite sheets. The system was isolated in the z direction which is normal to the planes. For graphene layers no MP2 data for comparison is available in the literature. However, the calculated equilibrium distance of 3.3 Å and interaction energy of 32 meV/atom are in astonishingly good agreement with the experimental interlayer distance and the experimental energy of interaction between two graphene sheets, 3.35 Å and 35 ± 10 meV/atom [99], respectively. Using the same setup as for the graphene single point calculations, results are presented for 0.7 ps NVT Born-Oppenheimer dynamics at 300 K in Fig. 4.4. They confirm the findings that using

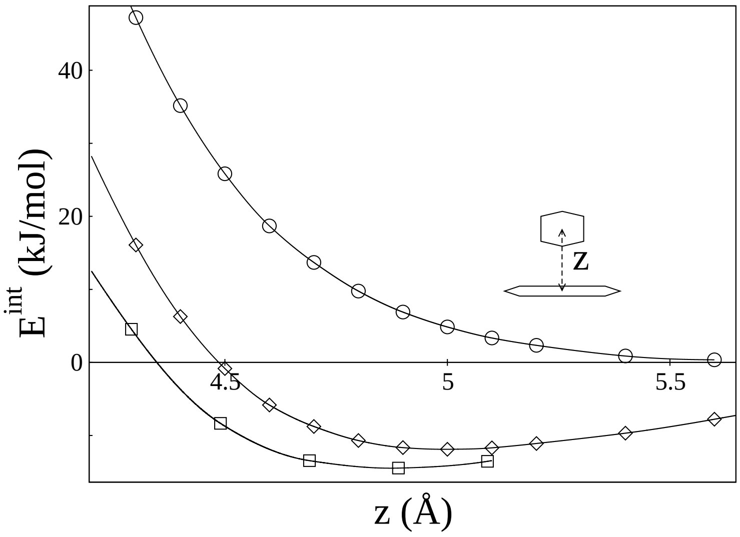

Figure 4.3: Potential energy curves of the total energy of interaction (E^{int} = E^{dimer}- $2E^{monomer}$) are plotted for the benzene dimer in its T-shaped configuration as a function of the distance z. ○ corresponds to BLYP, ◇ to BLYP + DCACP, and the squares to MP2 data from Ref. [98]. Values for σ_1 and σ_2 as they resulted from the calibration in Fig. 4.1.

the upgraded ECPs the average distance between the sheets is ≈ 3.3 Å while using only BLYP the sheets simply dissociate, as expected from the purely repulsive interaction energy curve.

In order to extend the assessment of the transferability to combinations of different atoms, the benzene-argon dimer has been investigated. Without any further tuning of the DCACP parameters, the potential energy curve for the benzene-argon dimer in its C_{6v} symmetry has been computed. The resulting curve is presented in Fig. 4.5 and reproduces the equilibrium distance and interaction energy of corresponding MP2 calculations [96]. Also electronic properties such as the static polarizability (α_{bz-Ar}) due to an electric field parallel to the C_{6v} symmetry axis and the small permanent

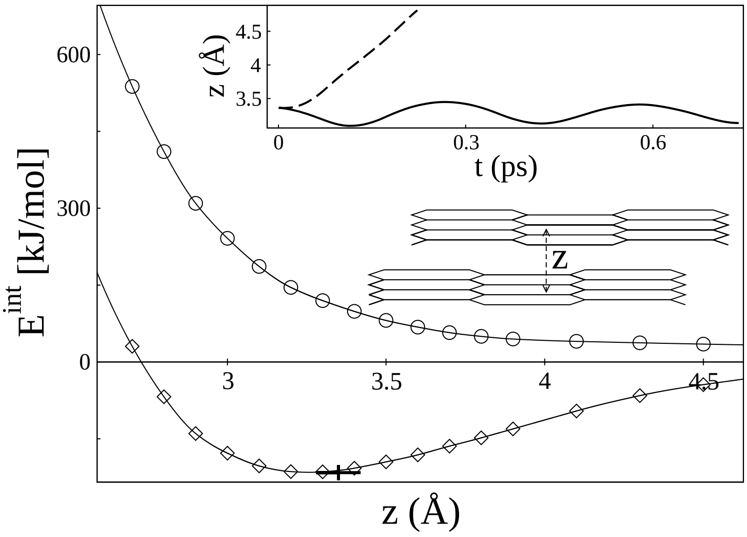

Figure 4.4: Potential energy curves of the energy of interaction (E^{int} = E^{dimer}-2$E^{monomer}$) are plotted for the slab of graphite. ○ corresponds to BLYP, and ◇ to BLYP+DCACPs.The experimental value is marked by a cross [99]. In the inset the averaged interlayer distance z is presented during first principles BO-MD using BLYP (dotted) and BLYP + DCACPs (continuous).

dipole moment (μ^{z}_{bz-Ar}) induced by the mutual polarization of the monomers show good agreement with MP2 predictions (Table 4.1). The inset in the graph of Fig. 4.5 depicts the difference of the electron density when DCACPs are used. The electron density is decreased in the short range regions of the atoms and increased in the outer core regions, mutually polarizing thus each moiety and leading to a small additional electron density overlap. As a result weak bonding is obtained.

As another test case, the H_2-benzene dimer has been studied. The potential energy curve of interaction of the hydrogen molecule approaching the benzene plane along the orthogonal C_{6v} symmetry axis is given in Fig. 4.6. The results upon using the DCACPs for carbon only compare very well with MP2 calculations from Ref. [96].

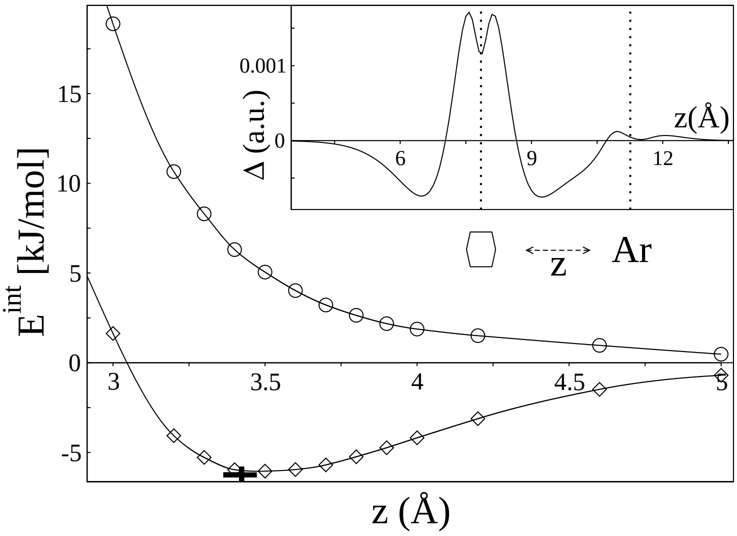

Figure 4.5: For the benzene-argon dimer potential energy curves of the total energy of interaction (E^{int} = E^{dimer}-$\sum E^{monomers}$) are plotted as a function of the distance z. ○ corresponds to BLYP, and ◇ to BLYP+DCACPs. The MP2 result [96] for the intermolecular distance and energy of interaction is marked by a cross. In the inset the C_{6v} symmetry axis z is plotted versus $\Delta = \int dx\, dy\, (n^{norm}(\mathbf{r}) - n^{opt}(\mathbf{r}))$ (the differences between integrated xy planes of the electron density of the benzene-argon dimer at equilibrium distance computed with and without DCACPs). The dotted lines show the position of the moieties: benzene (the molecular plane is perpendicular to z) is at 7.85 Å on the z axis, argon is at 11.26 Å.

All results indicate that no dispersion correction is necessary for the hydrogen atoms, neither being in benzene nor in the H_2 molecule.

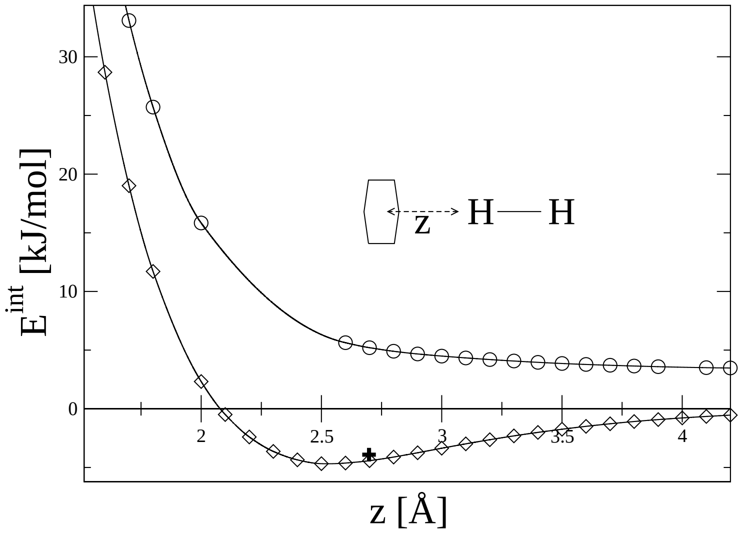

Figure 4.6: For the benzene-H_2 dimer potential energy curves of the total energy of interaction ($E^{int} = E^{dimer} - \sum E^{monomers}$) are plotted as a function of the intermolecular distance z along the orthogonal C_{6v} symmetry axis. ◯ corresponds to BLYP, and ◇ to BLYP+DCACPs. The MP2 result [96] for the intermolecular distance and energy of interaction is marked by a cross. DCACPs are only used for carbon, all hydrogen atoms remain uncorrected.

4.4 Conclusions

All the results obtained in this chapter suggest that it is possible to correct for the lack of electron correlation across low density regions with dispersion-optimized atom based effective potentials. For several reasons this scheme seems to have advantages with respect to the usual empirical corrections. First, the improved static electronic properties (dipole moment, quadrupole moment, and polarizability) indicate that due to the non locality of the ECP projectors, the valence wavefunctions reproduce more of the characteristics of dispersion interactions than a simple additive atom-atom based correction. Secondly, properly calibrated and transferable atomic DCACPs do no longer need any artificial *a priori* assignment of interacting groups or atoms. Thirdly, viewing the additional correcting potential as a small perturbing field in the outer molecular region, it is clear that mutual polarization of moieties is obtained as well as small additional density overlap. Both phenomena are expected to lead to an attraction as well as to be very sensitive to slight modifications in the electronic structure. This implies that the correction might be able to adapt for all kinds of variations in the electronic structure, such as the change of the state of hybridization. Hence, this correction scheme has the potential to be highly transferable.

A possibility has been shown to generally include dispersion forces in all DFT first principles calculations at essentially no additional cost. It is concluded that the scheme to optimize effective atom centered potentials can be used to improve the description of molecular properties within DFT. The potential of the method has been illustrated by means of successfully modeling attractive long range vdW forces within DCACP based GGA DFT calculations.

Chapter 5

Transferability of dispersion corrected atom centered potentials

It is nobler to declare oneself wrong than to insist on being right - especially when one is right.
Friedrich Nietzsche (1844 - 1900), (Thus Spoke Zarathustra)

Abstract

Recently, a novel scheme has been introduced for optimizing atom based nonlocal external potentials within the framework of density functional theory (DFT) in order to systematically improve the description of molecular properties [*Phys. Rev. Lett.*

93, 153004 (2004); *J. Chem. Phys.* **122**, 14113 (2005)]. In this chapter, a small library of dispersion corrected atom centered potentials (DCACP) is presented for the atoms C, Ar, Kr, and Br. To this end, DCACPs are calibrated in order to reproduce the equilibrium distance and binding energy of MP2 potential energy surfaces of the weakly-bonded homo dimers: Ar_2, Kr_2, and $(Br_2)_2$. In all cases studied, using DFT with the generalized gradient approximation functional BLYP, and the DCACPs, the influence of dispersion forces on equilibrium and transition state geometries, interaction energies and transition barriers can be reproduced in good agreement with MP2 calculations and without any significant increase in computational cost. The transferability of the DCACPs to other systems is assessed by addressing various systems: (i) ideal van der Waals clusters of the type Ar_nKr_m ($\forall$ n, m = $\{0,1,2,3,4\}$ and $2 \leq n+m \leq 4$), (ii) the effect of DCACPs on covalent bonds and conformers of the hydrocarbon molecule cyclooctatetraene which features a system of π-bonds, (iii) the competition of simultaneous electrostatic and dispersion forces for the equilibrium structure and transition states of the hydrogen bromide dimer $(HBr)_2$. In all cases, the performance of the DCACPs is remarkably good.

5.1 Introduction

Weak long range dispersion forces have a purely quantum origin: they represent the attractive interaction between self induced instantaneous multipole moments of isolated ground state electron distributions [85]. These forces are of crucial importance in nature because they influence many fundamental inter and intra molecular phenomena such as the interactions between rare gas atoms, surface adsorptions, melting and boiling points, heats of sublimation, hydrophobic interactions, solvation effects, conformational properties of macromolecules (for instance the tertiary and quaternary structures of biomolecules such as proteins or DNA), molecular recognition, the packing of molecular crystals, intercalation of drugs into DNA and π-π stacking effects, to name only a few. Recently, it has been shown that also macroscopic phenomena, such as the adhesion of gecko setae on surfaces, can be attributed solely to dispersion interactions [100–102]. However, while some density functional theory (DFT) exchange-correlation potentials show spurious binding for van der Waals (vdW) complexes, it is not yet generally possible to describe correctly vdW interactions within DFT using the local density approximation (LDA), the generalized gradient approximation (GGA) or even the - on average more accurate - hybrid exchange-correlation functionals [29, 86–88, 95, 103]. In view of the ubiquitous nature of these forces the incorrect description of weak long range interactions constitutes a serious failure of the many conventional approximations to the exact exchange-correlation potential in DFT.

Introduction of non-locality into a “vdW-functional” as proposed in Ref. [90, 104, 105] or by electron density partitioning [92] can abolish this deficiency but usually implies the arbitrary assignment of molecular fragments. Alternatively, Misquitta et al. [93] or Kohn et al. [89] proposed more general schemes which include dispersion in DFT but only at increased computational cost. As a consequence, empirical atom-atom based correction terms have been proposed and assessed [88, 94] using C_6 coefficients in the London C_6/r^6 asymptotic expression for the dispersion energy. Besides the fact that again fragments need to be assigned, these simple empirical corrections suffer from the fact that for each pair of fragments individual damping functions have to be identified to allow for the correct repulsive short-range behavior. Furthermore, preliminary calculations and assessments of appropriate C_6 coefficients are necessary requiring for instance computationally more demanding time dependent DFT calculations [106]. Moreover, the electronic structure remains uncorrected by the use of this pair potential based correction, or, even worse, might be distorted by the artificially restrained geometries.

Recently, effective atom centered potentials have been optimized with respect to molecular references within the framework of first principles electronic structure calculations [63, 107]. The scheme was successfully applied to cure the lack of dispersion forces in standard DFT exchange-correlation functionals. In analogy to the effective core potential (ECP) approach, the functional form of the atom centered potentials was chosen to be identical to the analytic pseudopotential by Goedecker et al. [56, 57] but at a different range. These Gaussian-based norm conserving dual-space pseudopotentials are separable and nonlocal. In the case of ECP generation their parameters are obtained for each atom by iteratively minimizing a penalty functional, which expresses the deviations of ECP-generated Kohn-Sham (KS) valence orbitals from their (relativistic) all-electron counterparts. For the purposes of this chapter, this approach has been generalized to molecules and a wider range of penalties. The functional form of the ECPs is being retained for the following reasons: (i) the analytical form allows a rigorous differential approach for their optimization, (ii) the nonlocal form can inherently cast the nonlocal character of dispersion forces, (iii) no significant additional computational cost emerges upon extension, and (iv) it is user-friendly to include dispersion forces in DFT calculations by simply adding calibrated parameters to an ECP file. Hence, for this approach the molecular point of view is included into the design of an optimized atom centered potential (OACP).

The OACPs obtained in such a way can improve the total Hamiltonian at the specific level of theory - if a suitable molecular reference can be defined for calibration. For DFT as electronic structure method, one can make use of density functional perturbation theory for a gradient based optimization of the OACPs [107]. In particular, in order to remedy the failure of most GGA DFT calculations to describe London dispersion forces, it was proposed to calibrate 'dispersion corrected' atom centered potentials (DCACPs) [63]. Specifically, the extended KS-Hamiltonian reads $\hat{H}^{\mathrm{KS}}_{\mathrm{ext}} = \hat{H}^{\mathrm{KS}} + \sum_{\mathrm{I}} V_{\mathrm{I}}^{\mathrm{SG}_{l+1}}$. Where the additional nonlocal potential $V_{\mathrm{I}}^{\mathrm{SG}_{l+1}}$ centered on every atom I corresponds to an additional angular momentum channel $l+1$ with the same functional form as the ECP by Goedecker et al. [56]. $V_{\mathrm{I}}^{\mathrm{SG}_{l+1}}$ needs to be 'dispersion calibrated' for every atom type with the help of the potential energy surface (PES) of a suitable, typically homo nuclear, vdW complex as a reference system. The interference between the DCACPs and the ordinary ECPs is minimized by the fact that they act at different ranges in space: the ECPs are strongly limited to the atomic core regions of the molecule while the DCACPs act at longer range. Furthermore, in order to describe weakly bonded systems the magnitude of the additional correcting potential can be kept very small.

Here, a small library of DCACPs (for C, Br, Ar, and Kr) is provided, which can be used within BLYP DFT, and their transferability is assessed for a variety of geometries, systems and interaction types. To this end, a simple procedure is followed to minimize a given penalty with respect to a reference. As a reference large basis set MP2 interaction energy curves have been computed for typically homo nuclear supermolecular vdW complexes. In the case of DCACPs, an intuitive functional form has been chosen for the penalty, namely the interaction energy and the ionic forces at equilibrium distance.

In order to assess the transferability other complexes have been computed with BLYP DFT using these calibrated DCACPs without any further tuning. The DFT results are compared to corresponding *ab initio* calculations at the same level of theory as the data used for calibration. The choices of (a) the specific form of the penalty, (b) to use the GGA functional BLYP, and (c) to use MP2/aug-cc-pVTZ calculations as a reference are arbitrary. This combination seems to be reasonable because the penalty is simple and BLYP and MP2 are well established methods. However, it is not claimed that this combination is optimal. The same procedure could equally well be applied in the context of any other penalty, exchange-correlation functional, or arbitrarily exact reference. However, in this chapter, reference calculations at the MP2 level of theory are considered to be a reasonable compromise between accuracy and computational cost. High accuracy methods like coupled cluster theory or SCF response methods (e.g. coupled perturbed Hartree-Fock calculations) are desirable as benchmarks. But unfortunately, for larger systems, theoretical treatments beyond MP2 rapidly become computationally intractable even as references.

DCACPs are calibrated for the atoms Ar, Kr, and Br in the reference systems Ar_2, Kr_2, and $(Br_2)_2$ and the previously introduced carbon DCACP which was calibrated for the benzene dimer (C_6H_6 in its sandwich conformation) [63] is used. The transferability and in particular the scaling of properties with system size were tested systematically by studying the equilibrium structures of all possible hetero and homo nuclear clusters of Ar and Kr dimers, trimers and tetramers. For the tetramers, we also investigate the description of planar transition states (TS) on the PES. The complexes of Ar and Kr have been chosen because interactions between noble gases are solely due to dispersion interactions and their calculation represents thus an ideal benchmark. In order to assess the performance of the DCACPs also for the description of intramolecular London dispersion forces for a system which is dominated by the steric effects of covalent bonds, the apolar organic molecule cyclooctatetraene (COT) (Fig. 5.1) has been chosen. The structure of COT and its conformational changes have been attracting the

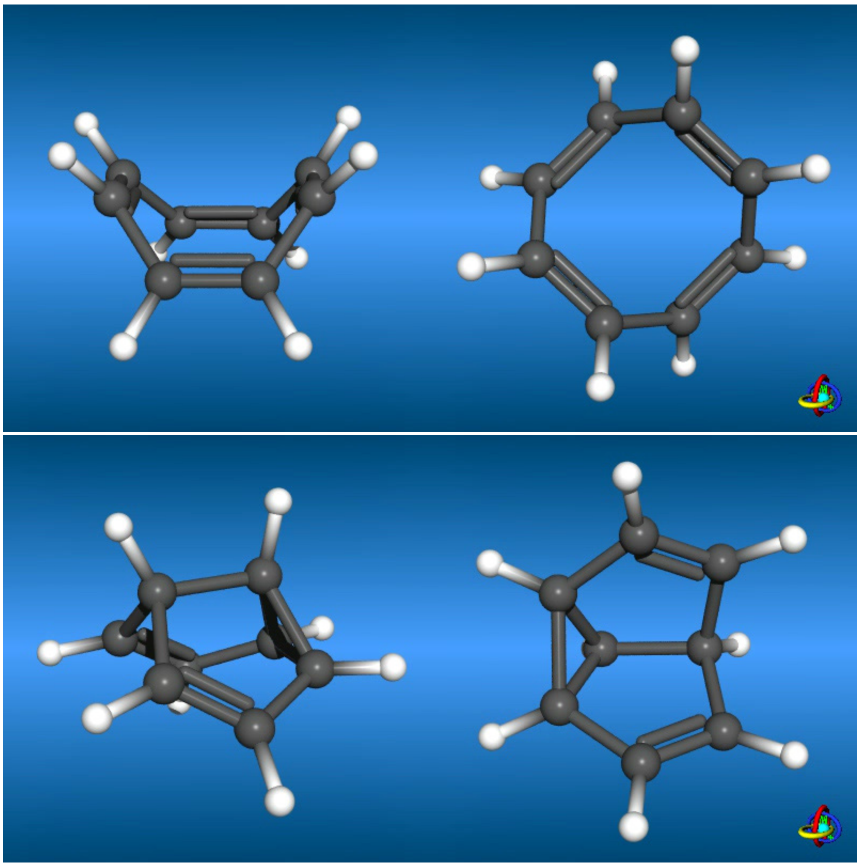

Figure 5.1: Cyclooctatetraene (above), a precursor in the synthesis of semibullvalene (below), an important model system for intramolecular Cope rearrangements. Pictures taken from Ref. [108].

attention of scientists since a first NMR study in 1962 [109, 110]. One can study Hückel rules and aromaticity for COT (COT has not $(4n+2)$ π electrons and is therefore not a Hückel aromat, n being integer positive numbers) [111], it exhibits Jahn-Teller effects, and it is used as a precursor in the synthesis of semibullvalene (see Fig. 5.1) [112] - an exemplary text book classic for intramolecular Cope rearrangements. COT is also a quencher in laser devices [113].

Here it is investigated, if within BLYP DFT the DCACPs can account for a better description of the relative energies of different conformers and if they perturb the covalent bonding.

Finally, a ’mixed’ system is considered in which covalent chemical bonds, strong electrostatic interaction (dipole-dipole), hydrogen bonding, and dispersion effects occur simultaneously. Such a ’mixed’ system allows to test if the approach to include dispersion forces deteriorates in some respect the description of the other predominant interactions. This is of interest because hydrogen bonding and permanent dipole-dipole interactions act in a similar range as London forces. For this purpose, the hydrogen bromide dimer has been chosen as a test case. $(\mathrm{HBr})_2$ is an ideal representative for the simultaneous presence of all these interactions. The equilibrium structure as well as several TSs on the PES are studied.

5.2 Methods and computational details

The basic idea of the discussed approach has been introduced in Refs. [63, 107]. It deals with the iterative minimization of a penalty functional P by variational tuning of adjustable parameters of analytic atom centered effective potentials which are of the same form as Goedecker’s pseudopotentials [56]. The way the penalty functional is designed determines which molecular property will be optimized. It usually penalizes the deviations of a selected physical property, e.g. ionic forces, computed with a given set of values for the ECP parameters (which is denoted by σ_i), with respect to a reference value which can be computed at any level of theory. Thus, the minimization of $P(\{\sigma_i\})$ (with respect to any observable that can be expressed *via* the KS-orbitals of the system) allows to approach as much as possible an arbitrary reference - within the limits of the chosen functional form of the ECP approach.

The analytic pseudopotentials introduced by Goedecker et al. [56, 57] consist of a local part $V^{\mathrm{loc}}(\mathbf{r})$ and of nonlocal parts $V_l^{\mathrm{nl}}(\{\sigma_i\}, \mathbf{r}, \mathbf{r}')$ with specific projectors for each angular momentum channel l:

$$
\begin{aligned}
V^{\mathrm{ECP}}(\mathbf{r},\mathbf{r}') &= V^{(\mathrm{loc})}(\mathbf{r})\delta(\mathbf{r}-\mathbf{r}') + \sum_l V_l^{(\mathrm{nl})}(\mathbf{r},\mathbf{r}') && (5.1)\\
V^{(\mathrm{loc})}(\mathbf{r}) &= \frac{-Z_{\mathrm{ion}}}{r}\mathrm{erf}\left[\frac{r}{r_{\mathrm{loc}}\sqrt{2}}\right] + \exp\left[-\frac{r^2}{2r_{\mathrm{loc}}^2}\right] \times \\
&\quad \left(C_1 + C_2\frac{r^2}{r_{\mathrm{loc}}^2} + C_3\frac{r^4}{r_{\mathrm{loc}}^4} + C_4\frac{r^6}{r_{\mathrm{loc}}^6}\right) && (5.2)\\
V_l^{(\mathrm{nl})}(\mathbf{r},\mathbf{r}') &= \sum_{m=-l}^{+l} Y_{lm}(\hat{\mathbf{r}}) \sum_{j,k=1}^{3} p_{lh}(r) h_{kj}^{(l)} p_{lj}(r') Y_{lm}^*(\hat{\mathbf{r}}'). && (5.3)
\end{aligned}
$$

where $p_{lh}(r) \propto r^{l+2(h-1)}\exp(-r^2/(2r_l^2))$, $r = |\mathbf{r}-\mathbf{R}_\mathrm{I}|$ on the position $\mathbf{R}$ of nucleus I, $\hat{\mathbf{r}}$ is the unit vector in the direction of $\mathbf{r}$, and Y_{lm} denotes a spherical harmonic. $\{r_{\mathrm{loc}}, C_1, C_2, C_3, C_4, h_{kj}^{(l)}, r_l, ...\}$ span the atom specific parameter space $\{\sigma_i\}$, the dimensionality of it being determined by the largest angular momentum of the ECP. In this chapter, the optimization of the DCACPs is chosen to be restricted in all cases to the parameters belonging to a single additional (nonlocal) angular momentum channel. This is an arbitrary choice, which has been successful in a recent study on vdW complexes [63], however, the number of additional angular momenta and their parameters, *i.e.* the space in which P shall be minimized, is optional for the purposes of the optimization. For all the calibrations, the following simple penalty functional is minimized: $P^{\mathrm{disp}}(\mathbf{R}^{\mathrm{ref}})$:

$$
P^{\mathrm{disp}}(\mathbf{R}^{\mathrm{ref}}) = |E^{\mathrm{ref}}(\mathbf{R}^{\mathrm{ref}}) - E(\mathbf{R}^{\mathrm{ref}})|^2 + \sum_{\mathrm{I}}^{N_{\mathrm{ions}}} w_\mathrm{I}\, |\mathbf{F}_\mathrm{I}(\mathbf{R}^{\mathrm{ref}})|^2, \tag{5.4}
$$

by following the penalty derivatives $\{\mathrm{d}P^{\mathrm{disp}}(\mathbf{R}^{\mathrm{ref}})/\mathrm{d}\sigma_i\}$. $E^{\mathrm{ref}}(\mathbf{R}^{\mathrm{ref}})$ is the total potential energy of interaction computed with the reference method at the nuclear configuration $\mathbf{R}^{\mathrm{ref}}$ which corresponds to the equilibrium geometry determined with the reference method (here MP2/aug-cc-pVTZ). $E(\mathbf{R}^{\mathrm{ref}})$ corresponds to the total potential energy of interaction computed with the DFT electronic structure theory (here with the BLYP exchange-correlation potential) for the same nuclear configuration as the reference. $\mathbf{F}_\mathrm{I}(\mathbf{R}^{\mathrm{ref}})$ are the ionic forces within the ECP electronic structure theory acting on the nuclei I, which have to vanish at the reference equilibrium position $\mathbf{R}^{\mathrm{ref}}$. For every calibration, Eq. (6.3) is minimized by iterative variation of the parameters of the additional angular momentum channel. All MP2 calculations have been carried out using the aug-cc-pVTZ basis set [114, 115] as available in GAUSSIAN03 [116]. Sinnokrot et al. have shown for the benzene dimer that using this basis set a realistic estimate of the binding energy due to dispersion can be made [98]. For all MP2 calculations reported here, the counterpoise-correction has been used to account for the basis set superposition error (BSSE). All DFT calculations have been carried out using the program CPMD [82], the xc-functional BLYP [35, 36], and a plane-wave cutoff of 150 Ry in case of the rare gases Ar and Kr, and 100 Ry in case of the COT and the bromine systems: DCACPs have not been been used for any of the hydrogen atoms. In the context of the same reasoning as in chapter 3 pseudopotentials of Ref. [56, 57] have been used for all the calculations even if only LDA pseudopotentials have been available (specifically for the rare gases and for bromine). No BSSE correction is necessary for plane wave calculations because the number of basis functions is not modified upon changing the number of atoms. For all geometry optimizations the residual tolerance for ionic forces has been set to 0.00045 for MP2, or to 0.0005 a.u. for DFT calculations.

5.2.1 Rare gas atoms

DCACPs for argon and krypton have been calibrated by minimizing Eq. (6.3) so that the depth and the location of the minimum of the potential energy curves of the homo nuclear dimers Ar_2 and Kr_2 are reproduced within an accuracy of ≈ 1 J/mol (Fig. 5.3). To reach this accuracy, it turned out to be necessary for Kr to use a 2×2 matrix h^f_{kj} while for Ar, a single h^d_{11} coefficient was sufficient. The results of the calibration are presented in Fig. 5.3. After calibration the geometries of all possible dimers and trimers have been optimized at the BLYP DFT and at the MP2 level of theory. The equilibrium geometries of all the tetramers have only been obtained within DFT. Imposing a planar structure, geometries have also been optimized for all TSs on the PES of the tetramers.

5.2.2 Cyclooctatetraene

For carbon the DCACPs have been used which had been previously calibrated for the benzene dimer [63, 117] with r_p = 3.28, h_{11}^p = -0.0035. The equilibrium geometries of COT in its 'tub-shaped' D_{2d} and in its 'crown-shaped' conformation were optimized using BLYP DFT. In the same way, also the D_{4h} TS geometry for the ring inversion has been obtained by imposing a planar structure. A view of COT in its TS, tub, and crown conformation is given in Fig. 5.2.

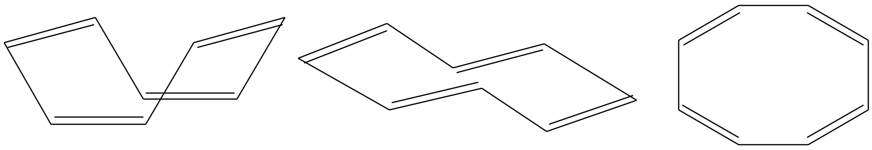

Figure 5.2: Structures of cyclooctatetraene (COT) C_8H_8. Left: the 'tub-shaped' D_{2d} global minimum conformation. Middle: the local minimum 'crown-shaped' conformer. Right: the planar D_{4h} ring inversion transition state.

5.2.3 Bromine compounds

A DCACP for Br has been calibrated by minimizing Eq. (6.3) such that the depth and the location of the minimum of the interaction energy of $(Br_2)_2$ are reproduced. To this end, first the geometry of Br_2 has been optimized using MP2. Keeping the intramolecular distance of the two molecular moieties fixed, the intermolecular distance has been varied. Variation of the distance along a D_{2h}-symmetry axis (all atoms in one plane) results in less binding energy than along a C_{2v}-symmetry axis ("crossed" Br-Br bonds). Therefore the latter has been chosen for calibration purposes. The equilibrium geometry of the $(HBr)_2$ complex has been optimized using MP2 and DFT. In addition three TS structures for the hydrogen-bond isomerization have also been investigated. Their geometries have been taken from Ref. [118].

5.3 Results and discussion

5.3.1 Rare gas atoms

For the homo nuclear dimers Ar_2 and Kr_2 the MP2 PES curves ($E^{int}=E^{Dimer}-2*E^{Monomer}$) as a function of interatomic distance, the initial BLYP DFT curves and the final DCACP BLYP DFT curves are shown in Fig. 5.3. The resulting values for the DCACPs are $r_d = 2.86$, $h_{11}^{d} = -0.002$ for Ar and $r_f = 3.61$, $h_{11}^{f} = -0.0015$, $h_{22}^{f} = 0.004$ for Kr. The MP2 results (-0.98 kJ/mol and -1.42 kJ/mol for Ar_2 and Kr_2, respectively) are in good agreement with corresponding results obtained from recent literature [119]. As expected, the initial BLYP DFT curves show a purely repulsive behavior in both cases. The calibrated DCACP BLYP DFT curves reproduce accurately the minimum of the reference curves, however in the case of Kr three parameters need to be optimized, whereas for Ar two parameters are sufficient. While also the repulsive part of the reference curves is remarkably well reproduced, the characteristic asymptotic $1/r^6$ tail of dispersion interaction is less well described. However, this is not surprising since the $1/r^6$ behavior is at the moment not included into the penalty functional and since the chosen functional form of the DCACPs does not necessarily imply a correct dissociation behavior.

Also the effect of the use of DCACPs on the electronic structure has been investigated for the case of Ar_2. The effect is negligible: upon inclusion of DCACPs, the integrated absolute electron density difference with respect to the MP2 density is reduced by 10^{-6} a.u. [Fig. 5.4].

Using DCACP BLYP DFT, the total energies of interaction for equilibrium geometries of all possible Ar and Kr hetero dimer, trimers, and tetramers correlate very well with MP2 calculations (left hand side of Fig. 5.5) within a root mean square deviation (rmsd) of only 0.41 kJ/mol. Also the interaction energies of the planar TS structures of all tetramers correlate well with corresponding MP2 values (right hand side of Fig. 5.5) with a rmsd of 1.27 kJ/mol, even though the slope of a linear fit is not approaching unity. The scaling for the increasing van der Waals energy for an increasing number of Kr atoms over the number of Ar atoms is well reproduced. There are two possible

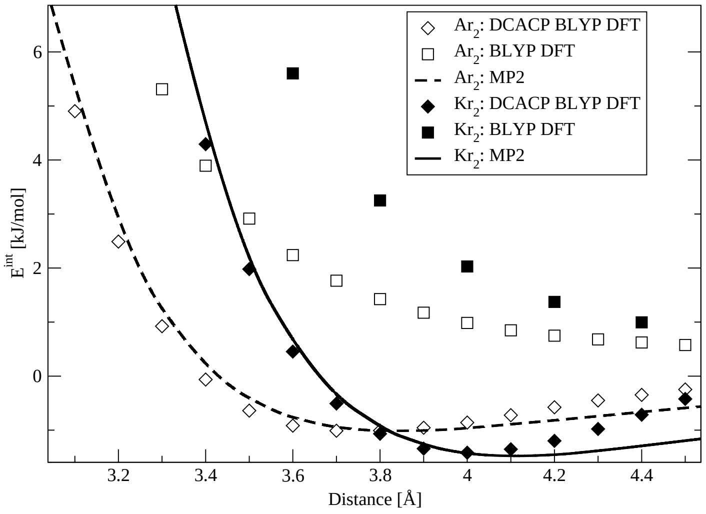

Figure 5.3: Calibration of Ar and Kr for homo nuclear dimers: the total energy of interaction (E^{int}=E^{Dimer}-2*$E^{Monomer}$) as a function of interatomic distance.

planar TSs for the Ar_2Kr_2 tetramer: the 'crossed' and the 'parallel' arrangements, the result for the 'parallel' configuration shows the largest deviation (≈ 0.25 kJ/mol) but is still very accurate with respect to MP2. The slight increase of the rmsd when going from equilibrium structures to TSs might be due to the fact that for the TSs the MP2 energies result from structures which have been only optimized using DCACP BLYP DFT or also due to the general tendency of BLYP to underestimate activation energies.

5.3.2 Cyclooctatetraene

The energy barrier for the conformational change leading to a ring inversion of COT has been determined by computing the energy difference between the conformational global minimum of COT in its 'tub-shaped' D_{2d} conformation and its planar D_{4h} geometry. As presented in Table 5.1, the DCACP BLYP DFT calculations yield a value

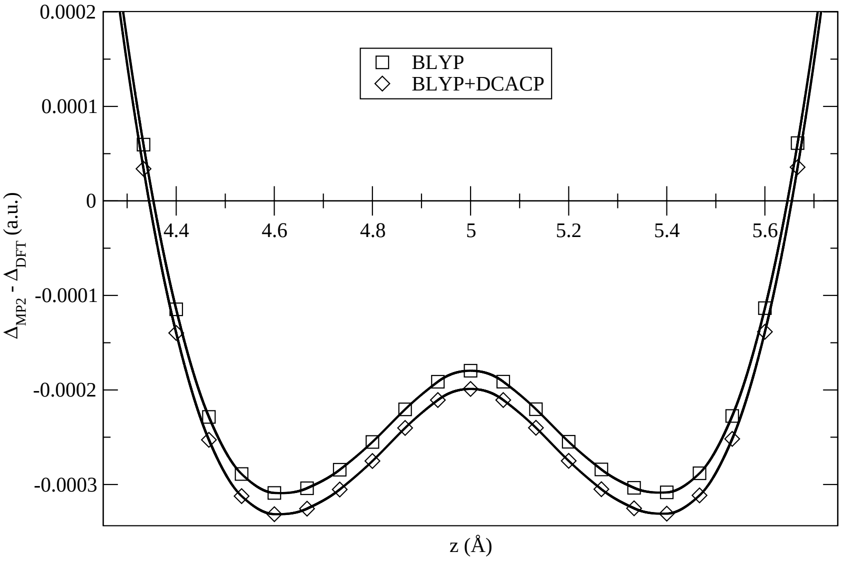

Figure 5.4: Interatomic region of Ar_2: the differences between integrated xy planes of the electron density ($\Delta_{MP2} - \Delta_{DFT} = \int dxdy[n^{MP2}(\mathbf{r}) - n^{DFT}(\mathbf{r})]$) is plotted against z for normal DFT calculations (BLYP) and for dispersion corrected DFT calculations (DCACP). The atoms are at a distance of 3.8 Å, *i.e.* at z = 3.1 and 6.9 Å. The integrated absolute electron density difference with respect to the MP2 density is reduced by 10^{-6} a.u. upon use of the DCACPs.

which is significantly closer to CAS [110, 120] or MP2 [121] estimates taken from literature than the BLYP DFT value. The energetically less favorable 'crown-shaped' conformer has likewise been geometry optimized and its relative total energy is compared to literature values (Table 5.1). The results indicate that the use of DCACPs improves substantially the description of conformational barriers and that the effect of intramolecular dispersion interactions are not negligible for conformational processes. Furthermore, a certain degree of transferability with respect to the presence of aromaticity is demonstrated since opposed to benzene COT does not obey the Hückel rule

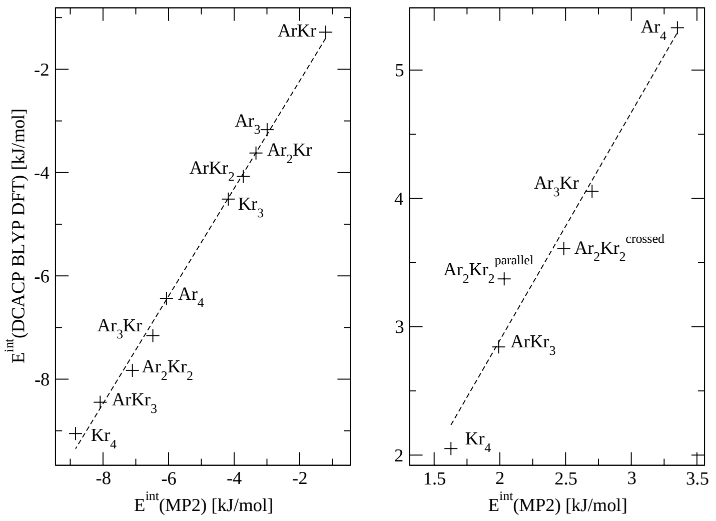

Figure 5.5: Left panel: correlation of the interaction energies for equilibrium structures of Ar and Kr dimers, of trimers, and tetramers (correlation coefficient: 0.998). Right panel: correlation of the interaction energies of planar transition states for Ar and Kr tetramers (correlation coefficient: 0.980). The dotted lines correspond to a linear fit of the data. Note that for the transition states, the slope is not close to 1. The total energy of interaction (E^{int}=E^{Dimer}-2*$E^{Monomer}$) has been obtained within BLYP DFT using DCACPs and within MP2 using the Counterpoise correction. For the dimer and trimers the geometry is optimized within DFT and MP2, for the tetramers the geometry is optimized only using DFT. The MP2 interaction energies of the tetramers have been obtained at the DFT geometry. The root mean square deviation (rmsd = $[1/N\sum_i^N(E_i^{int}(\text{MP2})-E_i^{int}(\text{DFT}))^2]^{1/2}$) of the equilibrium and transition state geometry are 0.41 kJ/mol and 1.27 kJ/mol, respectively.

and is therefore not aromatic. However, for relative energy differences between local geometrical minima on the PES (’tub’-COT, and ’crown’-COT), the dispersion forces seem to cancel and therefore no improvement can be shown with respect to results in the literature.

Table 5.1: Calculated transition barriers for the ring inversion of the 'tub-shaped' cyclooctatetraene (COT) *via* a D_{4h} planar transition state and energy differences between 'tub-shaped' and 'crown-shaped' conformers (TC). Every structure has been geometry optimized, for the transition states a planar geometry has been imposed. All values are in kJ/mol.

System	DFT[1]	DCACP DFT[1]	DFT[2]	CAS[3]	G2[4]	CAS[5]
Barrier	39.3	46.4	48.2	45.6	57.4	45.6
TC	55.3	53.6	-	-	-	58.0

5.3.3 Bromine compounds

Geometry optimization of Br_2 at the MP2/aug-cc-pVTZ level yields an interatomic equilibrium distance of 2.28 Å. The energy of interaction curves before and after the calibration of a DCACP for Br are shown in Fig. 5.6. The intramolecular distance has been kept fixed for the calibration and the calculation of the potential energy curves. In contrast to the calibration of the rare gas atoms, for $(Br_2)_2$ the tail as well as the repulsive part of the reference interaction curve are less well reproduced.

After calibration on $(Br_2)_2$ a set of four different geometries of the HBr-dimer has been studied. Using once BLYP DFT and once DCACP BLYP DFT, the geometry of the equilibrium structure (EQ) of $(HBr)_2$ has been optimized as depicted on the left hand side of Fig. 5.7. Proceeding likewise for the three TSs on the PES of the HBr-dimer, (i) the TS for the exchange of the intramolecular proton as depicted on the right hand side of Fig. 5.7 (TS1) has been obtained. TS1 has been geometry optimized while keeping the Br-Br distance fixed at 4.07 Å and keeping both HBrBr angles fixed at 45 degrees. (ii) The linear [H-Br$\cdots$Br-H] TS has been optimized by keeping the Br-Br distance at 4.02 Å and imposing linearity (TS2). (iii) Another linear TS [Br-H$\cdots$Br-H] has been optimized by keeping the Br-Br distance at 4.33 Å and imposing

---

[1] BLYP DFT

[2] B3LYP DFT results from Ref. [122]

[3] CASSCF results from Ref. [120]

[4] G2(MP2) results from Ref. [121]

[5] CAS results from Ref. [110]

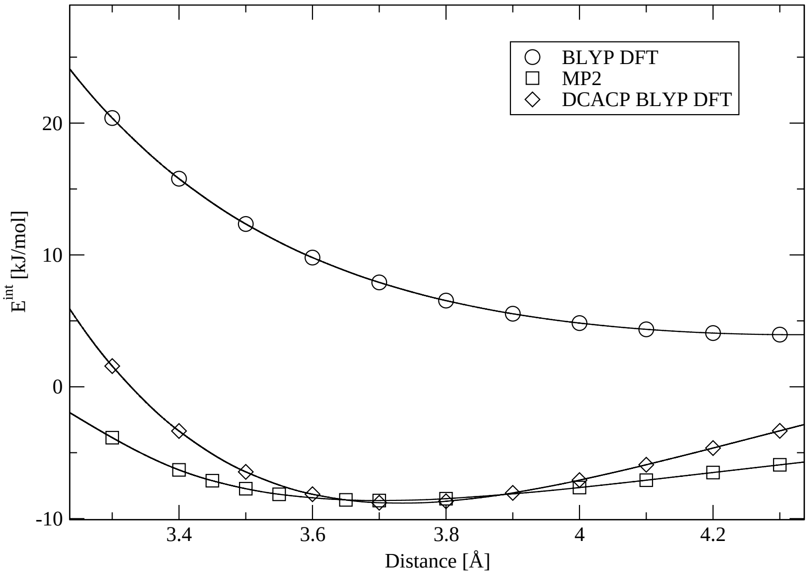

Figure 5.6: Calibration of Br in the $(Br_2)_2$ complex: the total energy of interaction ($E^{int}=E^{Dimer}-2*E^{Monomer}$) as a function of the distance between two Br_2 molecules.

likewise linearity (TS3). The fixed distances between the Br atoms for the TSs were taken from Ref. [118]. For all obtained geometries the corresponding MP2 single point

Figure 5.7: Left: the HBr dimer in its equilibrium geometry (EQ): Br-Br distance at 4.1 Å, H-Br-Br angle is 80 or 10 degree, respectively. Right: the hydrogen exchange transition state with 45 degrees for both H-Br-Br angles (TS1) is presented. Both complexes are planar.

Table 5.2: Deviation of total BLYP DFT energies of interaction from MP2 results. The conformations of EQ, TS1, TS2, and TS3 are explained in the text and in Fig. 5.7. All values are in kJ/mol and correspond to E^{int}_{MP2}-E^{int}_{DFT}.

Structure	EQ	TS1	TS2	TS3
DFT[1]	-4.2	-6.0	-4.3	-4.3
DCACP DFT[2]	-0.3	-0.6	0.5	-1.2

calculations have been carried out for comparison. The deviation of the resulting total interaction energies from MP2 calculations are presented in Table 5.2. While the standard BLYP DFT calculations show a systematic deviation by roughly 4 kJ/mol the DCACP BLYP DFT calculations compare significantly better and do no longer exhibit a systematic deviation. All the MP2 calculations carried out with the DCACP BLYP DFT geometries show more interaction than those carried out with the BLYP DFT optimized structures. As in the case of the tetramers of Ar and Kr, also for $(HBr)_2$ the energy of interaction of the equilibrium structure compares better with MP2 results than the results for the TSs.

5.4 Conclusions

Using the standard GGA functional BLYP, an overview of DFT calculations has been presented for some vdW complexes with and without the dispersion corrected atom centered potentials. The DCACPs have been obtained by calibration with respect to simple homo nuclear weakly-bonded reference systems, and could successfully be applied to other systems without any further changes. Specifically, equilibrium structures and transition states of all rare gas dimers, trimers, and tetramers consisting of Ar and Kr have been described. Furthermore, it could be shown for conformers of COT that the use of DCACPs improves the description of a conformational barrier, while it does not affect the energy difference between local geometrical minima. The calculation of the interaction in the hydrogen bonded hydrogen bromide dimer is improved considerably for the ground state geometry as well as for transition states on the PES. In a recent study [63], an accurate description for argon-benzene, benzene-benzene, and graphite sheets could be shown.

---

[1] MP2 results correspond to BLYP DFT geometry

[2] MP2 results correspond to DCACP BLYP DFT geometry

In summary, the results suggest that dispersion forces can be reliably predicted in a transferable and general fashion within DFT using DCACPs. One can conclude that for many systems of chemical interest the predictive power of GGA DFT can be enforced substantially when using DCACPs while leaving the computational cost constant. Work is in progress to test the DCACPs in combination with other exchange correlation functionals than BLYP, to explicitly include the correct short range repulsive and the asymptotic $1/r^6$ behavior into the penalty functional, to optimize the functional form of the DCACP, and to establish a comprehensive library of DCACPs for every atom type.

Chapter 6

General rational compound design

Ernest Rutherford (1871-1937), Frederick Soddy (1877-1956)

In 1901, Ernest Rutherford and Frederick Soddy discovered that radioactivity was a sign of fundamental changes within elements, and it was Soddy who quickly made the connection between this and the ancient search for the philosopher's stone (Soddy had studied alchemy extensively as a hobby). At the moment of realization that their radioactive thorium was converting itself into radium, bit by bit, Soddy later recalled that he shouted out: "Rutherford, this is transmutation!" Rutherford snapped back, "For Mike's sake, Soddy, don't call it transmutation. They'll have our heads off as alchemists." [123].

Abstract

A variational particle number approach for general rational compound design (GRCD) is presented. Within first order perturbation theory, an expression for GRCD is obtained in terms of minimization of a suitably defined penalty functional using molecular chemical potentials as gradients. The method is applied to the design of a non-peptidic inhibitor for XIAP proteins which are over-expressed in cancer cells. Starting with a highly potent peptidic inhibitor, from first principle electronic structure calculations a non-peptidic and stable structure is derived which exhibits an estimated binding of the same order of magnitude as the initial structure.

6.1 Introduction

The design of optimized compounds which exhibit desired molecular properties is a central goal of many product-oriented theoretical research fields in material sciences, chemistry, and pharmacy. However, even *in silico* a systematic screening of chemical space, *i.e.* the huge molecular space spanned by all the possible combinations and configurations of electrons and nuclei, for interesting properties is beyond any capacity [24]. Compound design efforts try to establish a mapping of a given initial molecular system (defined by its Hamiltonian $\hat{H}$) to the observable of interest (O). If this mapping is successful, it is then assumed that key variables can be identified which span a smaller subspace to which the chemical space can be reduced. I.e. once the information of how to modify $\hat{H}$ in such a way that its observable approaches the target observable O_0 corresponding to the desired molecular property is obtained, the initial mapping (on the left in Eq. 6.1) can be inverted (to the right):

$$\left(\hat{H} \mapsto O\right) \quad \leftrightarrow \quad \left(O_0 \mapsto \hat{H}_0\right). \tag{6.1}$$

Therefore one tries to identify an optimal system $\hat{H}_{\text{opt}}$ simply *via* $O_0 \approx O_{\text{opt}} \mapsto \hat{H}_{\text{opt}}$. Within traditional rational drug design for instance, the binding of a given drug to a protein is often studied in much detail in order to gain knowledge of how the structure $\hat{H}$ of the drug needs to be modified in order to to increase its binding affinity. Thus, the underlying interest in a given Hamiltonian is often not due to the system *per se*, but due to its interesting properties and how they can be improved by tuning $\hat{H}$ in its chemical space.

Even though there is a large variety of approaches to solve this mapping problem ranging from empirical-statistical quantitative structure property relationships (QSPR) to classical force field and semiempirical calculations [124], only for the energetic approaches a rational inversion of the mapping can be attempted within a physical framework. The analytical expression for the potential energy in empirical force fields and the fact that the free energy is an equation of state has motivated much research connecting different molecules reversibly through a coupling parameter, commonly called λ. Thermodynamic integration and other approaches to relative free energies have been successfully carried out ever since Kirkwood's seminal paper on 'λ-space' in 1935 [125–129]. However, to declare λ a dynamical variable, including it in a statistical mechanics scheme, and using it for compound design has been implemented only recently [130, 131]. Despite these substantial efforts to access the free energy surface space spanned by different molecules, due to the empirical and classical nature of the potential energy function, chemical space is greatly restricted for these approaches. Namely to regions where electronic structure effects do not occur and also to regions for which force fields could have been already established. This implies hence, that these methods are less appropriate for compound design.

Thus, the predictive power of first principles calculations is being exploited to explore the full chemical space for $\hat{H}$ in order to generally establish $\hat{H} \mapsto O$. Using quantum mechanics it should therefore be possible to optimize deterministically $\hat{H}$ anywhere in chemical space and thereby also to carry out *de novo* compound design in the sense of Refs. [13, 132, 133]. However, the wide spread use of QSPR approaches endorses that also the currently employed first principles methods are still too heuristic in tackling this problem. Consequently, even a detailed and accurate understanding on the left hand expression in Eq. 6.1 does not yet necessarily lead to an inversion of the mapping.

Here, the effort is undertaken to address this problem with a non heuristic formulation for a *general* rational compound design (GRCD). The presented approach inverts the mapping in Eq. 6.1 using standard density functional theory (DFT) [20, 26, 30] within a grand-canonical ensemble (GCE) notation. Namely Eq. (6.1) will be iteratively evaluated. For demonstration the GRCD approach is applied to the design of a non-peptidic inhibitor of the anti-cancer target human XIAP (X-Chromosome linked inhibitor-of-apoptosis-proteins).

XIAPs regulate the delicate balance between cell proliferation and apoptosis (programmed cell death) [134, 135] by reversely binding to apoptosis proteins caspases [136, 137]. XIAP activity can be mediated by the binding of the first four N-terminal residues of SMAC (second mitochondrial-derived activator of caspases) [138], or other peptides containing similar N-terminal sequences. This apoptotic homeostasis is, however, strongly affected by the over-expression of the XIAPs in cancer cells. Based on SMAC potent peptidic inhibitors have been devised. However, as small oligo-peptides, the latter are not suitable as drug candidates since *in vivo* they would be rapidly cleaved by proteases. No non-peptidic XIAP inhibitors have been proposed, up to date. The gain of control of the XIAP activity *via* non-peptidic inhibitor design constitutes therefore an important anti-cancer strategy.

6.2 Methods and computational details

Within DFT and using the Born-Oppenheimer approximation for the adiabatic separation of the nuclear and the electronic wavefunction, any ground state observable O is a functional of the electron density $n(\mathbf{r})$. The latter is, according to the first Hohenberg-Kohn theorem [20], for a fixed number of electrons ($N_e = \int d^3r\, n$) in a one-to-one relationship to the external potential v. For an unperturbed system, v is a simple functional of the nuclear charge distribution $Z(\mathbf{r})$,

$$v[Z] = -\int d^3r' \, \frac{Z(\mathbf{r}')}{|\mathbf{r}-\mathbf{r}'|}. \tag{6.2}$$

In the classical limit $Z(\mathbf{r}) = Z_{\mathrm{I}}\delta(\mathbf{r}-\mathbf{R}_{\mathrm{I}})$. $Z_{\mathbf{I}}$ is the number of protons at $\mathbf{r} = \mathbf{R}_{\mathrm{I}}$, *i.e.* the atomic number of atom I. The total number of protons is hence, in analogy to the electrons, $N_p = \int d^3r\, Z$. Therefore, instead of $n(\mathbf{r})$, also the combination of fixed $Z(\mathbf{r})$ and N_e can be used as an argument, $O(N_e, [Z(\mathbf{r})])$.

In analogy to the variational optimization of atom centered potentials for molecular properties [63, 107], this allows to define an exact expression for general rational compound design *via* a penalty functional P which is to be minimized by variations of N_e and Z,

$$\min_{N_e,Z} P(N_e,[Z]) \quad = \quad \min_{N_e,Z} \left|O(N_e,[Z]) - O_0\right|. \tag{6.3}$$

$P(N_e,[Z])$ penalizes deviations of $O(N_e,[Z])$ from a desired reference property O_0. If one considers $O(N_e,[Z])$ to be the GCE energy functional $E(N_e,[Z])$, the system $\hat{H}$ to be in contact with an electron and proton particle reservoir, and $O_0 = E_0 \leq E(N_e,[Z])$, then Eq. (6.3) reduces to the zero temperature GCE variational theorem [27]. The electronic GCE energy $E(N_e,[Z])$ is obtained from the stationary principle for atoms and molecules at a fixed Z [139]: $\delta\{E(N_e,[Z])$ - $\mu_e N_e\} = 0$. Where

$$E(N_e,[Z]) \quad = \quad \int d^3r\, n(\mathbf{r})v(\mathbf{r}) + F_{GC}[n(\mathbf{r})] \tag{6.4}$$

$$\quad = \quad E_{ext}(N_e,[Z]) + F_{GC}[n(\mathbf{r})] \tag{6.5}$$

(see Eq. (2.3) and following). $F_{GC}[n(\mathbf{r})]$ is the universal, only implicitly dependent on Z, GCE ground-state functional while μ_e is a Lagrange multiplier attached to the constraint that $N_e = \int d^3r\, n(\mathbf{r})$, the electronic chemical potential

$$\mu_e \quad = \quad \frac{\delta E(N_e,[Z])}{\delta n(\mathbf{r})} = \frac{\partial E(N_e,[Z])}{\partial N_e}. \tag{6.6}$$

μ_e is of central importance in DFT and is greatly exploited within conceptual DFT, as recently reviewed in Ref. [7]. After minimization of $E(N_e,[Z])$ with respect to n, the total potential energy of a system can also be written as a functional of Z:

$$E^{tot}(N_e,[Z]) \quad = \quad E(N_e,[Z]) + \frac{1}{2}\int d^3r d^3r' \frac{Z(\mathbf{r})Z(\mathbf{r}')}{|\mathbf{r}-\mathbf{r}'|}. \tag{6.7}$$

$$\quad = \quad E_{ext}(N_e,[Z]) + F_{GC}[n] + E^{ion}[Z]. \tag{6.8}$$

Now, in analogy to the electronic chemical potential, a chemical potential μ_n is introduced which measures the tendency of the molecule to vary its ionic structure Z. Unlike μ_e, this *nuclear* chemical potential is not a constant for each molecule but a (local) function of space because of the discrete nature of the ionic charge distribution, allowing for many local (conformational) energy minima for the same N_e,

$$\begin{aligned}
\mu_n(\mathbf{r}) &= \frac{\delta E^{tot}}{\delta Z(\mathbf{r})}, && (6.9)\\
&= -\int d^3r' \left(\frac{\delta E_{ext}(N_e,[Z])}{\delta v(\mathbf{r}')} \frac{\delta v(\mathbf{r}')}{\delta Z(\mathbf{r})} + \frac{\delta E_{ext}(N_e,[Z])}{\delta n(\mathbf{r}')} \frac{\delta n(\mathbf{r}')}{\delta Z(\mathbf{r})} \right) \\
&\quad + \frac{\delta F_{GC}[n]}{\delta Z(\mathbf{r})} + \frac{\delta E^{ion}}{\delta Z(\mathbf{r})}, && (6.10)\\
&= -\int d^3r' \left(n(\mathbf{r}') \frac{\delta v(\mathbf{r}')}{\delta Z(\mathbf{r})} + v(\mathbf{r}') \frac{\delta n(\mathbf{r}')}{\delta Z(\mathbf{r})} \right) \\
&\quad + \frac{\delta F_{GC}[n]}{\delta Z(\mathbf{r})} + \int d^3r' \frac{Z(\mathbf{r}')}{|\mathbf{r}-\mathbf{r}'|}, && (6.11)\\
&= -\int d^3r' \left(\frac{n(\mathbf{r}')}{|\mathbf{r}-\mathbf{r}'|} + v(\mathbf{r}') n^{(1)}(\mathbf{r},\mathbf{r}') \right) \\
&\quad + \frac{\delta F_{GC}[n]}{\delta Z(\mathbf{r})} + \int d^3r' \frac{Z(\mathbf{r}')}{|\mathbf{r}-\mathbf{r}'|}, && (6.12)
\end{aligned}$$

where $n^{(1)}(\mathbf{r},\mathbf{r}')$ denotes the derivative $\delta n(\mathbf{r}')/\delta Z(\mathbf{r})$ and represents the linear change in the electronic structure $n(\mathbf{r}')$ of the system being induced by a local variation of the ionic charge distribution $Z(\mathbf{r}) \mapsto Z(\mathbf{r}) + dZ$,

$$n^{(1)}(\mathbf{r},\mathbf{r}') = \sum_{i=1}^{N} [\phi_i^{*(0)}(\mathbf{r}')\phi_i^{(1)}(\mathbf{r},\mathbf{r}') + \phi_i^{*(1)}(\mathbf{r},\mathbf{r}')\phi_i^{(0)}(\mathbf{r}')]. \tag{6.13}$$

This perturbed density can be computed within CPMD [44] using the density functional perturbation module [43] and the perturbation Hamiltonian given in the appendix or Ref. [107]. $\delta F_{GC}[n]/\delta Z(\mathbf{r})$ consists of the functional derivatives of the Coulomb energy, of the KS expression for the kinetic energy of the electrons, and of the exchange-correlation energy with respect to Z. However, for a discrete ionic charge distribution and within first order perturbation theory (*i.e.* assuming the density to be independent of Z), the derivative of Eq. (6.12) is simply the electrostatic field probed by a positive charge at $\mathbf{r}$:

$$\mu_n(\mathbf{r}) \approx -\int d^3r' \frac{n(\mathbf{r}')}{|\mathbf{r}-\mathbf{r}'|} + \sum_{\mathrm{I}} \frac{Z_{\mathrm{I}}}{|\mathbf{r}-\mathbf{R}_{\mathrm{I}}|}. \tag{6.14}$$

The derivative of the energy with respect to changes in atomic number was already presented within first order perturbation theory (or in analogy to the Hellmann-Feynman theorem) by Wilson and later by Parr and coworkers [140–142]. However, here we wish to consider the explicit molecular response upon an infinitesimal small variation of the nuclear charge distribution everywhere in space, which goes beyond the usual expression for the molecular response upon a variation in the external potential, namely $\delta E/\delta v = n$.

For pseudopotential DFT calculations, the nuclear chemical potential at $\mathbf{r} = \mathbf{R_I}$ in Eq. (6.12) can not be approximated by eq. (6.14) but can be obtained within first order perturbation theory

$$\mu_n(\mathbf{r} = \mathbf{R_I}) \approx E^{(1)}_{\mathbf{I}} = \langle \Psi^{(0)} | \hat{H}'_{\mathbf{I}} | \Psi^{(0)} \rangle, \tag{6.15}$$

$\Psi^{(0)}$ is the unperturbed and normalized wavefunction. The perturbation Hamiltonian is the same as in the appendix and Ref. [107], namely the derivative of the analytical pseudopotentials of Goedecker et al. [56] with respect to all their parameters $\{\sigma_i\}$:

$$\hat{H}'_{\mathbf{I}} = \sum_j c_j \frac{\partial V^{PP}_{\mathbf{I}}(\mathbf{R_I}, \{\sigma_i\})}{\partial_{\sigma_j}}. \tag{6.16}$$

Here, $\{c_j\ (\in \{1, -1\})\}$ determine the composition of μ_n in terms of derivatives of the energy with respect to the σ_j parameters. However, for the purpose of the chemical potential, the perturbation Hamiltonian of the appendix needs to be extended by the derivative with respect to the atomic number ($\sigma_0 = Z_{\mathbf{I}}$),

$$\frac{\partial V^{PP}_{\mathbf{I}}(\mathbf{R_I}, \{\sigma_i\})}{\partial \sigma_0} = -\frac{1}{|\mathbf{r} - \mathbf{R_I}|} \mathrm{erf}\left[\frac{|\mathbf{r} - \mathbf{R_I}|}{\sigma_1 \sqrt{2}}\right]. \tag{6.17}$$

Note that because of the orbital dependence of the non-local terms in the pseudopotential, Eq. (6.15) not simply equals $\int d^3r\, n(\mathbf{r}) \hat{H}'_{\mathbf{I}}$. $\mu_n(\mathbf{r} = \mathbf{R_I})$ can hence be approximated by the sum of the first order perturbations of the energy induced by an infinitesimal variation $\sigma_j \mapsto \sigma_j + d\sigma_j$ of the j^{th} pseudopotential parameter σ_j. Eq. (6.15) has been implemented into CPMD [44].

Since atomic numbers are simply classical point charges within conventional BO-DFT, it is intuitively easier to consider them as non-integers than in the case of electrons. The validity of DFT when extended to the unphysical regime of pure electronic states involving non-integer occupation numbers has been subject to much controversial discussions since the seminal papers of Janak [143] and Perdew et al. [139, 144, 145], but has recently been well established by several authors [146, 147] and even efficient algorithms for the optimization of occupation numbers have already been devised [148]. Hence, there are several approximations to the electronic chemical potential using KS-eigenvalues [7].

6.3 Results and discussion

6.3.1 Atoms

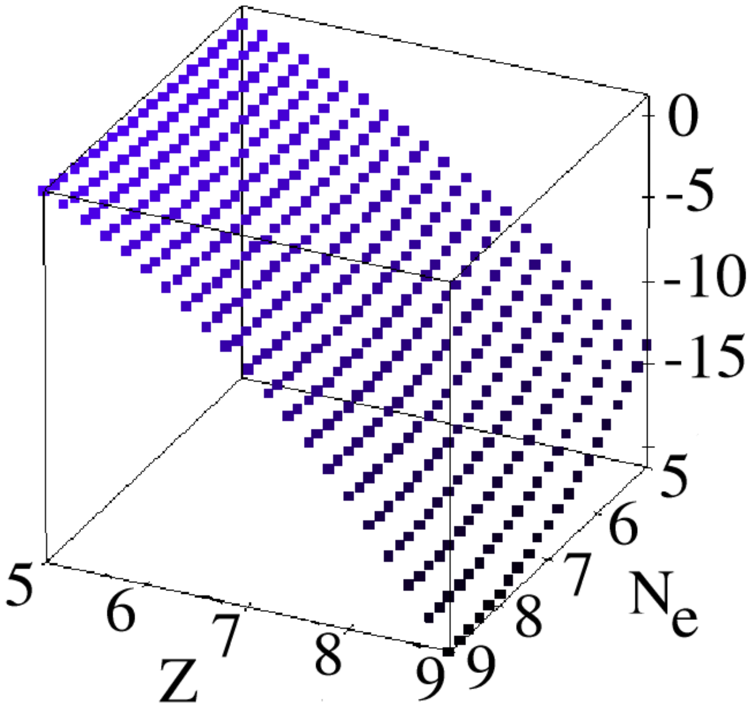

Figure 6.1: Two dimensional total atomic potential energy surface [a. u.] [149] as a function of the number of electrons N_e and the atomic number $Z(\mathbf{r} = \mathbf{R_I})$. Only fractional independent changes of 0.2 are considered for electrons and atomic number, ranging from boron (N_e = 5, Z = 5) up to fluorine (N_e = 9, Z = 9). The total potential energy of boron ($E^{tot}(N_e = 5, Z_\mathbf{I} = 5)$) is set to zero, and all other values refer to it.

To illustrate the variation in the number of electrons and protons in atoms, atomic total potential energies $E(N_e, [Z(\mathbf{r} = \mathbf{R_I})])$ have been computed [149] for fractional number of particles (Fig. 6.1). The derivative discontinuity at integer values of N_e, as it would be expected for the exact yet unknown KS-potential [139, 145], is not reproduced by the employed generalized gradient approximation to the exchange-correlation functional [149]. However, the typical convex shape of the isoprotonic curves is reproduced. The isoelectronic curves show a concave behavior, in agreement with Ref. [142]. In the zero temperature limit the slope of the $E(N_e, Z)$ surface in Fig. 6.1 corresponds hence to linear combinations of $\mu_n(\mathbf{r} = \mathbf{R})$ and μ_e. Using Fig. 6.1, one can show that the set of $\{c_j\}$ parameters in Eq. (6.16) for j = 0,...,5 is $\{c_j\}$ = $\{$1,1,-1,-1,-1,-1$\}$ (when considering $\mu_n(\mathbf{R})$ for second row elements).

6.3.2 Molecules

In order to investigate fractional atomic numbers in molecules, the following globally isoelectronic and isoprotonic transformation has been studied by varying the number of hydrogen nuclei as well as the atomic number in the molecules: $CH_4 \rightarrow NH_3 \rightarrow H_2O \rightarrow HF$. Total energies of geometry optimized systems are given for all coupling parameter λ values in Fig. 6.3. A smooth and continuously decreasing energy profile is observed for the complete transformation, the expected tendency of a decreased total potential energy for an increased atomic number of the heavy atom is obtained.

For molecules, μ_e and $\mu_n(\mathbf{r})$ contain in principle all the ground state chemistry. Within a GCE they represent the respective response of a given system in contact with a particle reservoir upon number variation of its electronic or its ionic structure. The higher derivatives of these chemical potentials can be used to define reactivity response functions [7]. For ground state systems, further features of μ_n can be established: (i) $\mu_n(\mathbf{r} \neq \mathbf{R_I})$ is related to the proton affinity of a system at $\mathbf{r}$ for the given geometry $\{\mathbf{R_I}\}$. As an illustration, a projection of $\mu_n(\mathbf{r} \neq \mathbf{R_I})$ (according to Eq. (6.15)) onto the molecular plane of formic acid is presented in Fig. 6.2. As intuition would suggest, the proton affinity is largest close to the oxygen atoms. (ii) $\mu_n(\mathbf{r} = \mathbf{R_{I=H}})$ measures a vertical acidity, *i.e.* the tendency of the molecule to lose the proton, or the tendency to act as a hydrogen bond donor. (iii) All $\mu_n(\mathbf{r} = \mathbf{R_I})$ are cusps. They measure the

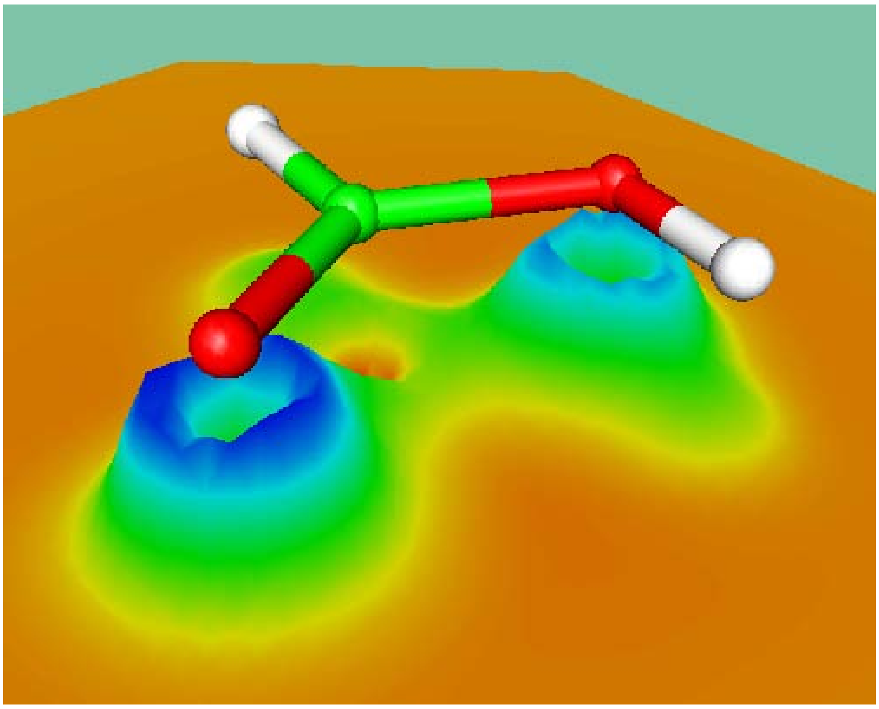

Figure 6.2: Three dimensional projection of the electrostatic potential (= $\mu_n(\mathbf{r})$ within the first order approximation of Eq. (6.14)) onto the molecular plane of formic acid.

transmutational tendency for each atom **I** in a molecule. Since intranuclear interactions are not considered, this quantity represents an unphysical but not meaningless tendency. It is suggested to call $\mu_n(\mathbf{r} = \mathbf{R_I})$ an *alchemical* potential. (iv) Note that pseudopotential and valence electron density calculations have been used and that hence the results at $\mathbf{r} \approx \mathbf{R_I}$ are not representative. As mentioned above they can be obtained within order perturbation theory by Eq. (6.15).

Fig. 6.3 is an example for smooth transmutational variations in the ionic structure at a constant global number of protons and electrons in the molecule. Only a linear combination of the alchemical potentials of the annihilated hydrogens and of the transmuted heavy atom can give the gradient of the curve in Fig. 6.3.

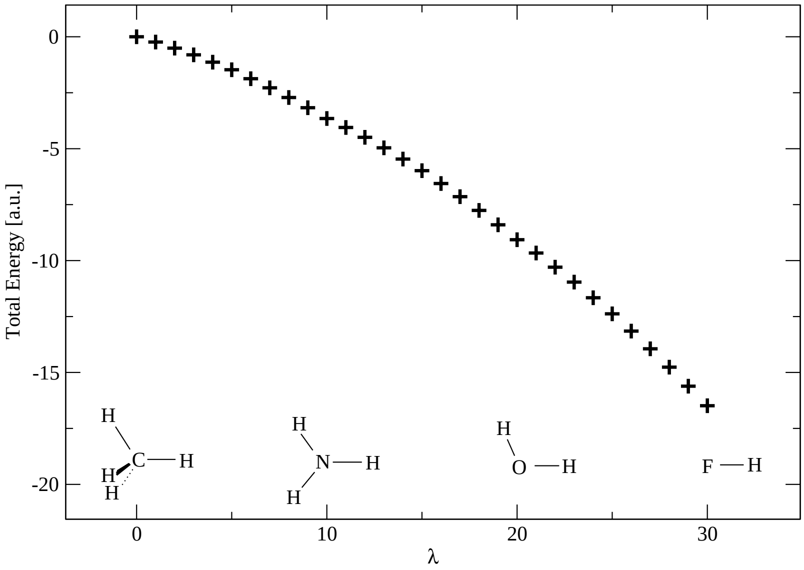

Figure 6.3: Total molecular potential energy [a. u.] [149] for coupling parameter λ transforming CH_4 (λ = 0) → NH_3 (λ = 10) → H_2O (λ = 20) → HF (λ = 30). λ corresponds to the projected annihilation of the hydrogen pseudopotentials and the simultaneous transmutation of the heavy atom pseudopotentials. Geometries are optimized for every λ. All energies refer to CH_4.

6.3.3 Compound design

As a model system for the design of a compound, the formic acid dimer has been chosen. The carboxy group of formic acid offers a simultaneous hydrogen bond acceptor and donor. By using the alchemical potential on the two oxygens of one moiety, predictions have been obtained of how these two atoms need to be transmutated in order to maximize the energy of interaction ($E^{int} = E^{complex} - \sum E^{monomers}$) of the complex. Assuming isoelectronic transformations and for the ions only an increase or a decrease by 1 in the atomic number, 2^3 complexes are possible. These structures are depicted in Fig. 6.4. In order to measure exclusively the effect on the electronic Hamiltonian,

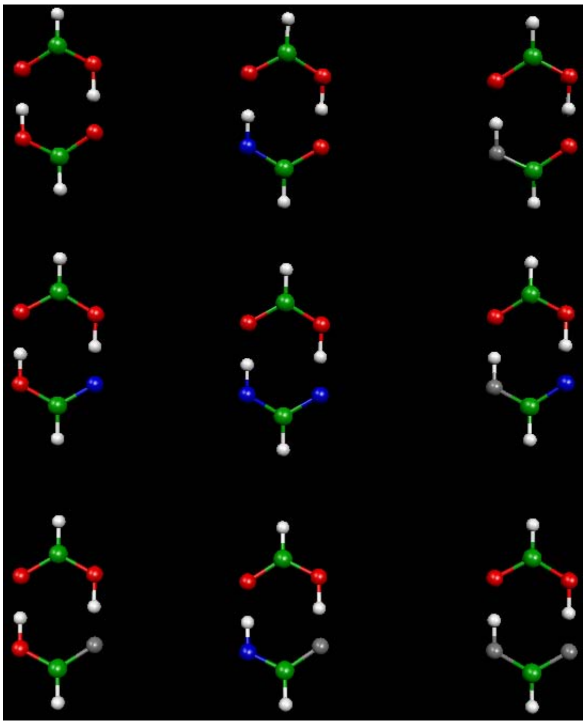

Figure 6.4: All possible formic acid dimers for transmutations of the oxygen atoms of one moiety for Δ Z = 1,0,-1. The number of electrons N_e is constant (36 valence electrons), and the total charge is N_e-$\sum_\mathbf{I} Z_\mathbf{I}$. Green represents carbon, white hydrogen, red oxygen, blue nitrogen, and grey fluorine atoms. Alchemical derivatives for the oxygens and energy of interactions for all mutants are given in table 6.1.

the geometry is only optimized for the formic acid dimer (first row, first column) and kept fixed for all the mutants. Table 6.1 gives the energies of interaction as well as the alchemical potentials of the energy of interaction. For all the dimers, the energy of interaction is predicted to increase upon increasing the atomic number. $|\mu_{al}|$ is always smaller for the alcohol than for the carbonyl oxygen, indicating a higher sensibility of the energy of interaction for variations in Z in the latter atom. This phenomenon can be rationalized by the fact that the electron density surrounding the carbonyl oxygen is decaying faster than the density surrounding the alcohol oxygen. Because of the faster decay, the interaction of the carbonyl density with the ionic core will be larger than for

Table 6.1: Total potential energies of interaction (E) and alchemical potentials for its change: for the left (μ^l_{al}) and the right (μ^r_{al}) oxygen of the lower moiety of all the formic acid complexes depicted in Fig. 6.4. Negative values for μ_{al} correspond to a predicted gain in energy of interaction upon increase of Z. The ordering corresponds to Fig. 6.4. All values are in atomic units.

row	E	μ^l_{al}	μ^r_{al}	E	μ^l_{al}	μ^r_{al}	E	μ^l_{al}	μ^r_{al}
1	-0.027	-2.9	-3.2	-0.018	-2.9	-3.2	-0.061	-2.9	-3.3
2	-0.043	-2.8	-3.2	-0.015	-2.9	-3.2	-0.057	-2.7	-3.2
3	-0.015	-3.0	-3.4	+0.012	-2.9	-3.3	-0.080	-3.1	-3.5

the alcohol oxygen, leading also to a higher sensitivity, *i.e.* alchemichal potential.

Starting from the combination oxygen, oxygen (O,O), the derivatives suggest to go to fluorine for both atoms (F,F). And indeed, the (F,F) species exhibits the largest energy of interaction for all the dimers. Considering (N,O) the alchemical potential would suggest that upon change to (N,F) the energy of interaction would increase which is not the case however. Thus, the potential energy surface is not necessarily as steadily increasing as it is suggested when regarding the example of the CH_4 → .. → HF transformation depicted in Fig. 6.3. Indeed there is little reason to believe that a penalty functional surface spanned by the number of particles should be generally smooth and simple to optimize.

6.3.4 A non-peptidic inhibitor for XIAP

When applying GRCD in the form of Eq. 6.3 to inhibitor design, one starts from a suitable initial structure. In the case of XIAP, effective tetrapeptidic inhibitors have been identified *in vitro* through combinatorial screening of the amino acid positions 1, 2 and 4 of the AVPI [see Fig. 6.5(a)] sequence (the first four residues of SMAC) [150]. Although the alternative ARPF [see Fig. 6.5(b)] sequence presents a high affinity (IC_{50} sub nano molar concentration [150]), such sequences would be easily cleaved *in vivo* by proteases.

To this end, one searches a suitable non-peptidic and inhibiting structure, *i.e.* sub-

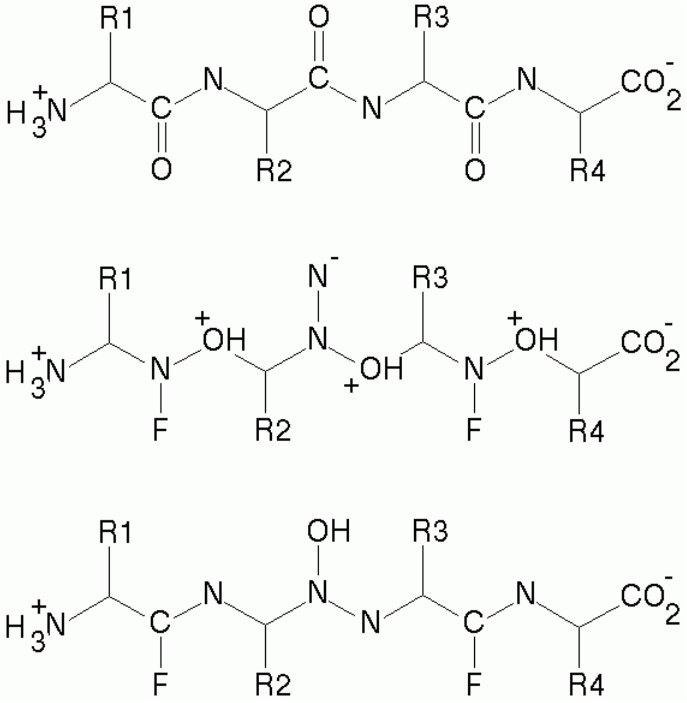

Figure 6.5: Topological sketches of the inhibitor structures. Upper panel: peptidic [(a) AVPI: R1 = Ala, R2 = Val, R3 = Pro, R4 = Ile, (b) ARPF: R1 = Ala, R2 = Arg, R3 = Pro, R4 = Phe], middle panel: first guess non-peptidic ARPF [(c)], and lower panel: final guess non-peptidic ARPF [(d) np-ARPF]. Only the terminals and the peptidic atoms are specified. Hydrogens attached to carbon are omitted for the sake of clarity.

strate, $\hat{H}_{opt}$ that maximizes as observable O the energy of interaction, $E^{\mathrm{int}} = E^{\mathrm{com}}$-$E^{\mathrm{inh}}$-$E^{\mathrm{prot}}$, where E^{com} represents the total potential energy of the complex of the inhibitor bond to the protein, and the E^{prot} and E^{inh} correspond to the energies of the isolated protein and the inhibitor, respectively. A more comprehensive study would need to include here the contribution due to the energy of solvation. However, since only small structural changes are carried out within this study and since the binding affinity needs only to be determined relative to the peptidic inhibitor, here the effect of solvation is neglected. The functional derivative, which can be used for gradient based minimization of the penalty, with respect to variation in the positive charge distribution of the inhibitor (Z^{inh}) is:

$$\frac{\delta P}{\delta Z} = \frac{\delta E^{\text{com}}}{\delta Z^{\text{inh}}} - \frac{\delta E^{\text{inh}}}{\delta Z^{\text{inh}}}. \tag{6.18}$$

For the design of a non-peptidic inhibitor derived from the ARPF-XIAP inhibitor, only independent transmutations are considered for the nine second row atoms ($\mathbf{I}$ = 1,...,9) constituting the three peptide bonds which need to be altered (Fig. 6.5). I.e., Eq. (6.18) reduces to variations only at the positions of these atoms,

$$\begin{aligned} \delta P/\delta Z &= \sum_{\mathbf{I}=1}^{9} \left(\frac{\delta E^{\text{com}}}{\delta Z_{\mathbf{I}}} - \frac{\delta E^{\text{inh}}}{\delta Z_{\mathbf{I}}} \right) && (6.19) \\ &= \sum_{\mathbf{I}=1}^{9} \left(\mu_n^{\text{com}}(\mathbf{R_I}) - \mu_n^{\text{inh}}(\mathbf{R_I}) \right). && (6.20) \end{aligned}$$

At a later stage, one would also be interested in following the complete μ also at $\mathbf{r} \neq \mathbf{R_I}$ in order to grow or shrink the compound. However, assessing the performance of such an approach is beyond the scope of the present study.

In order to be able to compute and follow the 9 alchemical potentials, 5 ns standard classical molecular dynamics simulation of the human XIAP have been conducted in order to equilibrate the enzyme-inhibitor complexes for AVPI [Fig. 6.5(a)] and ARPF [Fig. 6.5(b)] [151]. For GRCD, out of a snapshot of the equilibrated XIAP-ARPF complex, an isolated cluster has been computed with DFT [149]. This cluster consists out of the inhibitor and all residues of XIAP within 5 Å distance of the peptidic atoms, being saturated with hydrogen bonds.

Starting from the highly potent peptide ARPF [Fig. 6.5(b)], the 9 peptidic atoms have been transmutated according to their alchemical derivatives [Eq. (6.15)] in particle space [Eq. (6.18)]. I.e. the atomic number of all these atoms has been increased or decreased according to their alchemical derivative of the compound design penalty. Allowing changes in $Z_{\mathbf{I}}$ of ± 1, out of 3^9 possible structures one is proposed. This obtained new non-peptidic model compound [Fig. 6.5(c)] exhibits a drastically enhanced binding affinity corresponding to an increase in the interaction energy of roughly 50 kcal/mol. However, DFT calculations show that it is unstable as a monomer in gas phase. An iterative procedure following the $\{\mu_n(\mathbf{R_I})\}$ only for one atom per peptide bond, combined with saturation with hydrogen atoms, and conservation of charge re-

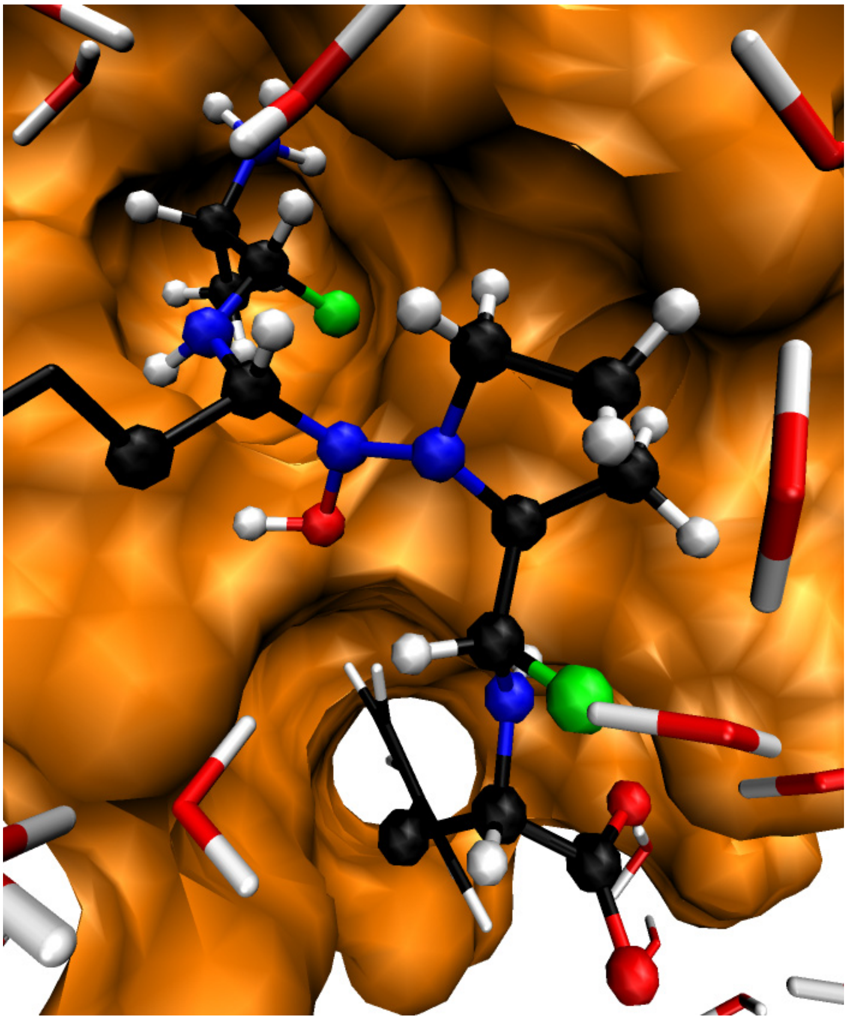

Figure 6.6: QM/MM [152] optimized geometry of the proposed non-peptidic inhibitor np-ARPF [Fig. 6.5(d)] solvated in the XIAP binding pocket. Using the alchemical potential atoms of the three peptide bonds of the ARPF [Fig. 6.5(b)] have been modified by transmutation to O, C, N, and F (represented respectively by red, black, blue, or green spheres).

sulted into another stable non-peptidic inhibitor compound: np-ARPF [Fig. 6.5(d) and Fig. 6.6].

The geometries of the full AVPI, ARPF and np-ARPF-protein complexes have been optimized within a QM/MM scheme [152], the inhibitor structures have constituted the QM region, the protein and the solvent the MM region. With respect to the QM/MM equilibrated AVPI-XIAP complex, the ARPF and np-ARPF-XIAP (Fig. 6.6) complexes yield, respectively, averaged interaction energies of -18.9 and -18.5 kcal/mol. Since only hydrogen atoms have been used to satisfy the valency of the modified peptide bonds, the entropic contributions to the macroscopic binding affinity to XIAP for ARPF and np-ARPF are expected to be comparable, *i.e.* the IC_{50} of the np-ARPF is likewise expected to be in the sub nano molar range.

6.4 Conclusions

In conclusion, GCE DFT calculations have been extended to molecules by the chemical potential for nuclei $\mu_n(\mathbf{r})$. For $\mathbf{r} = \mathbf{R_I}$, it is proposed to call this quantity the *alchemical potential*. It measures the tendency of a system to transmutate a given atom **I**. As it could be shown for the model system of the formic acid dimer, for GRCD purposes, the gradient based optimization of a penalty can be non-trivial because the penalty spanned in particle space is expected to be rather rough. However, with the help of QM/MM calculations combined with stability testing, the suggested general rational compound design scheme has been successfully applied to the first principle design of a new non-peptidic XIAP inhibitor with an expected binding affinity comparable to a highly potent tetra-peptidic inhibitor. Overall, the results suggest that GRCD can easily be extended and applied to other compound design problems exploring chemical space in a more rational manner than with the conventional screening methods.

Stronger variations of the compound shape, other geometries and finite temperature effects, and a thorough inclusion of additional constraints remain to be assessed. Positive results for these issues would promise relief from the necessarily heuristic approaches within conventional rational compound design.

Chapter 7

Conclusions

Don’t worry about people stealing your ideas. If your ideas are any good, you’ll have to ram them down people’s throats.
Howard Aiken (1900-1973)

In this thesis, atom centered potentials for an improved description or for the design of molecules within density functional theory (DFT) are assessed.

The fundamental idea of this thesis is introduced in chapter 3 in the form of a simple gradient based optimization of a general penalty functional in the space of parameters defining atom centered potentials. In particular, the density functional perturbation theory module of Ref. [43] in conjunction with the perturbation Hamiltonian given in the appendix can be exploited [107]. Examples and test cases are given for the electron density and energetic properties for the systems acetic acid and water. As an ultimate application of an improvement of the description, the inclusion of London dispersion forces into the GGA functional BLYP is tackled in chapter 4. The transferability of the resulting dispersion corrected atom centered potentials (DCACPs) is assessed for a large variety of molecular complexes, such as the benzene dimer, rare gas clusters, or the hydrogen bromide dimer in chapter 5. However, establishing and assessing a library of DCACPs for all atoms in the periodic table is clearly beyond the scope of this thesis and remains subject to further studies. The same is true for using the same scheme to address other properties than the London dispersion forces.

The formulation of a penalty for molecular properties of chapter 3 is extended in chapter 6 to compound design by inclusion of the atomic number in the parameter space. Following the gradient implies hence transmutational changes. The gradient of the energy with respect to this extended set of parameters turns out to have also a physical meaning being closely related to conceptual DFT [7], it measures the local tendency of a molecule to vary its ionic structure. It is hence proposed to name this gradient the nuclear chemical potential. For the purposes of the compound design addressed in chapter 6 the nuclear chemical potential is computed only within first order perturbation theory. As a test case, the chemical space is screened for the formic acid dimer in order to predict the compound which yields maximal energy of interaction. Within QM/MM the scheme is then successfully applied to the drug design of a non-peptidic inhibitor which is of potential use for anti-cancer therapy. Other applications of this compound design are subject to current research efforts as well as the realization of the electronic and nuclear chemical potentials as *ab initio* forces which could be used for sampling in λ space as it is already implemented for empirical forcefield approaches [130, 131].

In summary, the results presented in this thesis allow to draw several conclusions:

1. Using a pragmatic, that is in this case a molecular, approach to design atom centered correcting potentials, it is possible to improve the accuracy of DFT.
2. Atom centered corrections which have the form of an effective potential are especially useful. This can be rationalized by seeing the OACPs as a correcting

link between the geometrical constraints on the atoms (due to the reference) and the electronic structure which in return generates ionic forces and thereby the molecular geometry. However, one has to be careful when defining appropriate and sufficiently general penalty functionals for optimization.

3. The transferability of OACP has been assessed in some depth for the correction of London dispersion forces. The DCACPs show a remarkable transferability to other regions in phase and chemical space. This promises to enable us to generally remedy the lack of these forces for first principles simulations at finite temperature in a user friendly manner.

4. A nuclear chemical potential $\mu_n(\mathbf{r})$ for molecules has been presented within DFT. It measures the tendency of the system to vary its ionic structure at a given point in real space and is therefore a local property.

5. At the position $\mathbf{R_I}$ of the ions $\mathbf{I}$ of the system, the nuclear chemical potential measures the *transmutational* tendency of an atom to vary its atomic number. $\mu_n(\mathbf{r} = \mathbf{R_I})$ is called an *alchemical* potential.

6. Gradients of a property penalty with respect to the ionic structure or the number of electrons can be defined using the electronic and the nuclear chemical potential. This allows to explore efficiently and more rationally the penalty hypersurfaces spanned in chemical space. The approach has been successfully used for the design of a non-peptidic inhibitor of XIAP.

Bibliography

[1] W.H.E. Schwarz, D. Andrae, S.R. Arnold, J. Heidberg, H. Hellmann jr., J. Hinze, A. Karachalios, M.A. Kovner, P.C. Schmidt, and L. Zülicke. *Bunsen-Magazin*, 2:60, 1999.

[2] H. Hellmann. *Quantum Chemistry*. ONTI Moscow and Leningrad, 1937.

[3] P. Ragué Schleyer, N. Allinger, T. Clark, J. Gasteiger, P.A. Kollman, H.F. Schaefer III., and P.R. Schreiner, editors. *Encyclopedia of Computational Chemistry*. John Wiley and Sons, 1998.

[4] M. Quack. *Angew. Chem. Int. Ed.*, 41:4619, 2002.

[5] S. Park, F. Khalili-Araghi, E. Tajkhorshid, and K. Schulten. *J. Chem. Phys.*, 119:3559, 2003.

[6] A. Laio and M. Parrinello. *Proc. Natl Acad. Sci. USA*, 99:12562, 2002.

[7] P. Geerlings, F. De Proft, and W. Langenaeker. *Chem. Rev.*, 103:1793, 2003.

[8] A.R. Leach. *Molecular Modelling*. Addison Wesley Longman Limited, 1998.

[9] `http://en.wikipedia.org/wiki/Accuracy`.

[10] M. Grüning, O. V. Gritsenko, and E. J. Baerends. *J. Phys. Chem. A*, 108:4459, 2004.

[11] A. Lüchow and J. B. Anderson. Monte carlo methods in electronic structures for large systems. *Annu. Rev. Phys. Chem.*, 51:501, 2000.

[12] *Medicinal Quantum Chemistry*, volume 88 of *Methods and Principles in Medicinal Chemistry, Series Editors: R. Mannhold, H. Kubiny, G. Folkers*. Wiley-VCH, Weinheim, Germany, 2003.

[13] G. H. Jóhannesson, T. Bligaard, A. V. Ruban, H. L. Skriver, K. W. Jacobsen, and J. K. Nørskov. *Phys. Rev. Lett.*, 88:255506, 2002.

[14] F. Maseras and A. Lledos, editors. *Computational Modeling of Homogeneous Catalysis*. Kluwer Academic Publisher Dordrecht/Boston/London, 2002.

[15] `ISI Web of knowledge, http://isiknowledge.com/`.

[16] `http://www.top500.org`.

[17] `http://www.intel.com/research/silicon/mooreslaw.htm`.

[18] `http://www.thocp.net/hardware/supercomputers.htm`.

[19] D. M. York, T. Lee, and W. Yang. *Phys. Rev. Lett.*, 80:5011, 1998.

[20] P. Hohenberg and W. Kohn. *Phys. Rev.*, 136:B864, 1964.

[21] E. Runge and E. K. U. Gross. *Phys. Rev. Lett.*, 52:997, 1984.

[22] R. Car and M. Parrinello. A combined approach to DFT and molecular dynamics. *Phys. Rev. Lett.*, 55:2471, 1985.

[23] J. B. Krieger, Y. Li, and G. J. Iafrate. *Phys. Rev. A*, 45:101, 1992.

[24] P. Kirkpatrick and C. Ellis. *Nature*, 432:823, 2004.

[25] N. Argaman and G. Makov. *Am. J. Phys.*, 68:69, 2000.

[26] W. Kohn, A. D. Becke, and R. G. Parr. *J. Phys. Chem.*, 100:12974, 1996.

[27] R. G. Parr and W. Yang. *Density functional theory of atoms and molecules*. Oxford Science Publications, 1989.

[28] R. M. Dreizler and E.K.U. Gross. *Density Functional Theory*. Springer Verlag, 1990.

[29] W. Koch and M. C. Holthausen. *A Chemist's Guide to Density Functional Theory*. Wiley-VCH, 2002.

[30] W. Kohn and L. J. Sham. *Phys. Rev.*, 140:A1133, 1965.

[31] J. C. Slater. A simplification of the hartree-fock method. *Phys. Rev.*, 81:385, 1951.

[32] F. Bloch. The electron theory of ferromagnetism and electrical conductivity. *Z. Phys.*, 57:545, 1929.

[33] P. A. M. Dirac. Note on exchange phenomena in the thomas atom. *Proc. Camb. Phil. Soc.*, 26:376, 1930.

[34] D. M. Ceperley and B. J. Alder. *Phys. Rev. Lett.*, 45:566, 1980.

[35] A. D. Becke. *Phys. Rev. A*, 38:3098, 1988.

[36] C. Lee, W. Yang, and R. G. Parr. *Phys. Rev. B*, 37:785–789, 1988.

[37] R. Colle and D. Salvetti. *Theor. Chim. Acta*, 37:329, 1975.

[38] P. J. Stevens, F. J. Devlin, C. F. Chabalowski, and M. J. Frisch. *J. Phys. Chem.*, 98:11623, 1993.

[39] Warren E. Pickett. Pseudopotential methods in condensed matter applications. *Comp. Phys. Rep.*, 9:115–198, 1989.

[40] M. Dolg. In J. Grotendorst, editor, *Modern Methods and Algorithms of Quantum Chemistry*, volume 3, page 507. John von Neumann Institute for Computing, Jülich, NIC Series, 2000.

[41] P. Pulay. *Mol. Phys.*, 229, 1969.

[42] W. H. Press, S. A. Teukoldky, W. T. Vetterling, and B. P. Flannery. *Numerical recipes*. Cambridge University Press, second edition edition, 1992.

[43] A. Putrino, D. Sebastiani, and M. Parrinello. Generalized variational density functional perturbation theory. *J. Chem. Phys.*, 113:7102, 2000.

[44] Jurg Hutter et al. Computer code CPMD, version 3.8. Copyright IBM Corp. and MPI-FKF Stuttgart 1990-2003, `http://www.cpmd.org`.

[45] D. Marx and J. Hutter. *Ab Initio* molecular dynamics: Theory and implementation. *Modern Methods and Alogorithms of Quantum Chemistry*, 1:301, 2000. `http://www.fz-juelich.de/wsqc/proceedings/`.

[46] A. Laio, J. VandeVondele, and U. Rothlisberger. A hamiltonian electrostatic coupling scheme for hybrid car-parrinello molecular dynamics simulations. *J. Chem. Phys.*, 116:6941, 2002.

[47] H. Hellmann. *J. Chem. Phys.*, 3:61, 1935.

[48] H. Hellmann. *J. Chem. Phys.*, 4:324, 1936.

[49] U. von Barth and C. D. Gelatt. *Phys. Rev. B*, 21:2222, 1980.

[50] J. C. Phillips and L. Kleinman. *Phys. Rev.*, 116:287, 1959.

[51] J. D. Weeks and S. A. Rice. *J. Chem. Phys.*, 49:2741, 1968.

[52] V. Heine and D. Weaire. *Solid State Physics*, 24:249, 1970.

[53] D. R. Hamann, M. Schluter, and C. Chiang. Norm-conserving pseudopotentials. *Phys. Rev. Lett.*, 43:1494, 1979.

[54] G. B. Bachelet, D. R. Hamann, and M. Schluter. *Phys. Rev. B*, 26:4199, 1982.

[55] P. A. Christiansen, Y. S. Lee, and K. S Pitzer. *J. Chem. Phys.*, 71:4445, 1979.

[56] S. Goedecker, M. Teter, and J. Hutter. *Phys. Rev. B*, 54:1703, 1996.

[57] C. Hartwigsen, S. Goedecker, and J. Hutter. *Phys. Rev. B*, 58:3641, 1998.

[58] R. T. Sharp and G. K. Horton. *Phys. Rev.*, 90:317, 1953.

[59] A. Görling and M. Levy. *Phys. Rev. A*, 50:196, 1994.

[60] L. Fritsche and J. M. Yuan. *Phys. Rev. A*, 57:3425, 1998.

[61] R. Colle and R. K. Nesbet. *J. Phys. B*, 34:2475, 2001.

[62] W. Yang and Q. Wu. *Phys. Rev. Lett.*, 89:143002, 2002.

[63] O. A. von Lilienfeld, I. Tavernelli, U. Rothlisberger, and D. Sebastiani. Optimization of effective atom centered potentials for london dispersion forces in density functional theory. *Phys. Rev. Lett.*, 93:153004, 2004.

[64] O. A. von Lilienfeld, I. Tavernelli, U. Rothlisberger, and D. Sebastiani. Performance of optimized atom centered potentials for weakly bonded systems using density functional theory. *Phys. Rev. B*, 2005. accepted.

[65] Q. Zhao and R. G. Parr. *Phys. Rev. A*, 46:2337, 1992.

[66] Q. Zhao and R. G. Parr. *J. Chem. Phys.*, 98:543, 1993.

[67] Q. Zhao, R. C. Morrison, and R. G. Parr. *Phys. Rev. A*, 50:2138, 1994.

[68] A. D. Becke. *J. Chem. Phys.*, 98:5648–5652, 1993.

[69] A. Warshel. In *Computer Modeling of Reactions in Enzymes*. J. Wiley, New York, 1991.

[70] ACS. In J. Gao and M. A. Thompson, editors, *Combined Quantum Mechanical and Molecular Mechanical Methods*. American Chemical Society, Washington DC, 1999.

[71] N. Reuter, A. Dejaegere, B. Maigret, and M. Karplus. *J. Phys. Chem. A*, 104:1720, 2000.

[72] D. Bakowies and W. Thiel. *J. Phys. Chem.*, 100:10580, 1996.

[73] Yingkai Zhang, Tai-Sung Lee, and Weitao Yang. *J. Phys. Chem.*, 110:46–54, 1999.

[74] F. Bessac, F. Alary, Y. Carissan, J. L. Heully, J. P. Daudey, and R. Poteau. *J. Mol. Struct. (THEOCHEM)*, 632:43, 2003.

[75] M. Sulpizi, U. Rothlisberger, A. Laio, A. Cattaneo, and P. Carloni. *Biophys. J.*, 82:359, 2002.

[76] G. A. DiLabio, M. M. Hurley, and P. A. Christiansen. *J. Chem. Phys.*, 116:9578, 2002.

[77] A. Warshel and M. Levitt. *J. Mol. Biol.*, 103:227, 1976.

[78] G. Monard, M. Loos, V. Théry, K. Baka, and J.-L. Rivail. *Int. J. Quantum Chem.*, 58:153, 1996.

[79] T. A. Wesolowski and A. Warshel. *J. Phys. Chem.*, 97:8050, 1993.

[80] L. A. Curtiss, P. C. Redfern, K. Raghavachari, and J. A. Pople. *J. Chem. Phys.*, 109:42, 1998.

[81] B. G. Johnson, C. A. Gonzales, P. M. W. Gill, and J. A. Pople. *Chem. Phys. Lett.*, 221:100, 1994.

[82] Jurg Hutter, D. Marx, P. Focher, M. Tuckerman, W. Andreoni, A. Curioni, E. Fois, U. Rothlisberger, P. Giannozzi, T. Deutsch, A. Alavi, D. Sebastiani, A. Laio, J. VandeVondele, A. Seitsonen, S. Billeter, and M. Parrinello. Computer code CPMD, version 3.8. Copyright IBM Corp. and MPI-FKF Stuttgart 1990-2003, `http://www.cpmd.org`.

[83] G. Martyna and M. Tuckerman. *J. Chem. Phys.*, 110:2810, 1999.

[84] C. I. Bayly, P. Cieplak, W. D. Cornell, and P. A. Kollman. A well-behaved electrostatic potential based method using charge restraints for determining atom-centered charges: The resp model. *J. Phys. Chem.*, 97:10269, 1993.

[85] D. P. Craig and T. Thirunamachandran. In *Molecular Quantum Electrodynamics*. Dover Publications, Inc., Mineola, New York, 1998.

[86] S. Kristyán and P. Pulay. *Chem. Phys. Lett.*, 229:175, 1994.

[87] J. M. Pérez-Jordá and A. D. Becke. *Chem. Phys. Lett.*, 233:134, 1995.

[88] E. J. Meijer and Michiel Sprik. *J. Chem. Phys.*, 105:8684, 1996.

[89] W. Kohn, Y. Meir, and D. E. Makarov. *Phys. Rev. Lett.*, 80:4153, 1998.

[90] H. Rydberg, B. I. Lundqvist, D. C. Langreth, and M. Dion. *Phys. Rev. B*, 62:6997–7006, 2000.

[91] H. Rydberg, M. Dion, N. Jacobsen, E. Schröder, P. Hyldgaard, S. I. Simak, D. C. Langreth, and B. I. Lundqvist. *Phys. Rev. Lett.*, 91:126402, 2003.

[92] Tomasz A. Wesolowski and F. Tran. *J. Chem. Phys.*, 118:2072–2080, 2003.

[93] A. J. Misquitta, B. Jeziorski, and K. Szalewicz. *Phys. Rev. Lett.*, 91:33201–, 2003.

[94] R. LeSar. *J. Phys. Chem.*, 88:4272–4278, 1984.

[95] X. Wu, M. C. Vargas, S. Nayak, V. Lotrich, and G. Scoles. *J. Chem. Phys.*, 115:8748, 2001.

[96] W. Klopper, H. P. Lüthi, Th. Brupbacher, and A. Bauder. *J. Chem. Phys.*, 101:9747, 1994.

[97] H. Soscún, J. Hernández, R. Escobar, C. Toro-Mendoza, Y. Alvarado, and A. Hinchliffe. *Int. J. Quantum Chem.*, 90:497, 2002.

[98] M. O. Sinnokrot, E. F. Valeev, and C. D. Sherrill. *J. Am. Chem. Soc.*, 124:10887–10893, 2002.

[99] L. X. Benedict, N. G. Chopra, M. L. Cohen, A. Zettl, S. G. Louie, and V. H. Crespi. Microscopic determination of the interlayer binding energy in graphite. *Chem. Phys. Lett.*, 286:490, 1998.

[100] K. Autumn, M. Sitti, Y. A. Liang, A. M. Peattie, W. R. Hansen, S. Sponberg, T. W. Kenny, R. Fearing, J. N. Israelachvili, and R. J. Full. *Proc. Natl Acad. Sci. USA*, 99:12252, 2002.

[101] K. Autumn, Y. A. Liang, S. T. Hsieh, W. Zesch, W. P. Chan, T. W. Kenny, R. Fearing, and R. J. Full. *Nature*, 405:681, 2000.

[102] C. Gay and L. Leibler. *Phys. Rev. Lett.*, 82:936, 1999.

[103] T. van Mourik and R. J. Gdanitz. *J. Chem. Phys.*, 116:9620, 2002.

[104] Y. Andersson, D. C. Langreth, and B. I. Lundqvist. *Phys. Rev. Lett.*, 76:102–105, 1996.

[105] E. Hult, Y. Andersson, and B. I. Lundqvist. *Phys. Rev. Lett.*, 77:2029–2032, 1996.

[106] S. J. A. van Gisbergen, J. G. Snijders, and E. J. Baerends. *J. Chem. Phys.*, 103:9347, 1995.

[107] O. A. von Lilienfeld, I. Tavernelli, U. Rothlisberger, and D. Sebastiani. Variational optimization of effective atom centered potentials for molecular properties. *J. Chem. Phys.*, 122:14113, 2005.

[108] `http://caramel.oc.chemie.tu-darmstadt.de/lemmi/movies1.html`.

[109] F. a. L. Anet. *J. Am. Chem. Soc.*, 84:671, 1962.

[110] J. L. Andrés, O. Castano, A. Morreale, R. Palmeiro, and R. Gomperts. *J. Chem. Phys.*, 108:203, 1998.

[111] M. J. S. Dewar, A. Harget, and E. Haselbach. *J. Am. Chem. Soc.*, 91:7521, 1969.

[112] H. E. Zimmerman and H. Iwamura. *J. Am. Chem. Soc.*, 92:2015, 1970.

[113] R. P. Frueholz and A. Kuppermann. *J. Chem. Phys.*, 69:3614, 1978.

[114] T. H. Dunning and Jr. *J. Chem. Phys.*, 90:1007, 1989.

[115] K. A. Peterson, D. E. Woon, T. H. Dunning, and Jr. *J. Chem. Phys.*, 100:7410, 1994.

[116] M. J. Frisch, G. W. Trucks, H. B. Schlegel, G. E. Scuseria, M. A. Robb, J. R. Cheeseman, J. A. Montgomery, Jr., T. Vreven, K. N. Kudin, J. C. Burant, J. M. Millam, S. S. Iyengar, J. Tomasi, V. Barone, B. Mennucci, M. Cossi, G. Scalmani, N. Rega, G. A. Petersson, H. Nakatsuji, M. Hada, M. Ehara, K. Toyota,

R. Fukuda, J. Hasegawa, M. Ishida, T. Nakajima, Y. Honda, O. Kitao, H. Nakai, M. Klene, X. Li, J. E. Knox, H. P. Hratchian, J. B. Cross, C. Adamo, J. Jaramillo, R. Gomperst, R. E. Stratmann, O. Yazyev, A. J. Austin, R. Cammi, C. Pomelli, J. W. Ochterski, P. Y. Ayala, K. Morokuma, G. A. Voth, P. Salvador, J. J. Dannenberg, V. G. Zakrzewski, J. B. Foresman, J. V. Ortiz, Q. Cui, A. G. Baboul, S. Clifford, J. Cioslowski, B. B. Stefanov, G. Liu, A. Liashenko, P. Piskorz, I. Komaromi, R. L. Martin, D. J. Fox, T. Keith, M. A. Al-Laham, C. Y. Peng, A. Nanayakkara, M. Challacombe, P. M. W. Gill, B. Johnson, W. Chen, M. W. Wong, C. Gonzalez, J. A. Pople, Gaussian, Inc., and Pittsburgh PA. Computer code Gaussian 03, Revision A.1, 2003.

[117] In our previous study [63], we have erroneously indicated that we have added a d-channel to the ECP of carbon and a f-channel to the ECP of argon. In fact, we added a p-channel to carbon and a d-channel to argon.

[118] J. Castillo-Chará, A. L. McIntosh, Z. Wang, R. R. Lucchese, and J. W. Bevan. *J. Chem. Phys.*, 120:10426, 2004.

[119] P. Slavicek, R. Kalus, P. Paska, I. Odvarkova, P. Hobza, and A. Malijevsky. *J. Chem. Phys.*, 119:2102, 2003.

[120] O. Castano, R. Palmeiro, L. M. Frutos, and J. Luisandrés. *J. Comp. Chem.*, 23:732, 2002.

[121] T. M. Miller, A. A. Viggiano, and A. E. S. Miller. *J. Phys. Chem. A*, 106:10200, 2002.

[122] D. H. Paik, D. Yang, I. Lee, and A. H. Zewail. *Angew. Chem. Int. Ed.*, 43:2830, 2004.

[123] `http://en.wikipedia.org/wiki/Philosopher%27s_stone`.

[124] D. C. Young. *Computational Chemistry*. Wiley interscience, 2001.

[125] J. G. Kirkwood. *J. Chem. Phys.*, 3:300, 1935.

[126] D. A. Pearlman and B. Govinda Rao. *Encyclopedia of Computational Chemistry*, volume 2. John Wiley and Sons, 1998. editor = P. Ragué Schleyer and N. Allinger and T. Clark and J. Gasteiger and P.A. Kollman and H.F. Schaefer III. and P.R. Schreiner.

[127] W. L. Jorgensen. *Encyclopedia of Computational Chemistry*, volume 2. John Wiley and Sons, 1998.

[128] A. E. Mark. *Encyclopedia of Computational Chemistry*, volume 2. John Wiley and Sons, 1998.

[129] T. P. Straatsma. *Encyclopedia of Computational Chemistry*, volume 2. John Wiley and Sons, 1998.

[130] B. Tidor. *J. Phys. Chem.*, 97:1069, 1993.

[131] X. Kong and C. L. Brooks III. *J. Chem. Phys.*, 105:2414, 1996.

[132] C. Wolverton and A. Zunger. *Phys. Rev. Lett.*, 81:606, 1998.

[133] A. Franceschetti and A. Zunger. *Nature*, 402:60, 1999.

[134] S. W. Fesik. *Cell*, 103:273, 2000.

[135] D. R. Green. *Cell*, 102:1, 2000.

[136] Y. Shi. *Nat. Struct. Biol.*, 8:394, 2001.

[137] S. Piana and U. Rothlisberger. *Proteins*, 55:932, 2004.

[138] S. Srinivasula, R. Hegde, A. Saleh, P. Datta, E. Shiozaki, J. Chai, R.-A. Lee, P. D. Robbins, T. Fernandes-Alnemri, Y. Shi, and E. S. Alnemri. *Nature*, 410:112, 2001.

[139] J. P. Perdew, R. G. Parr, M. Levy, and J. L. Balduz. *Phys. Rev. Lett.*, 49:1691, 1982.

[140] E. B. Wilson, Jr. *J. Chem. Phys.*, 36:2232, 1961.

[141] P. Politzer and R. G. Parr. *J. Chem. Phys.*, 61:4258, 1974.

[142] R. G. Parr, R. A. Donnelly, M. Levy, and W. E. Palke. *J. Chem. Phys.*, 68:3801, 1978.

[143] J. F. Janak. *Phys. Rev. B*, 18:7165, 1978.

[144] J. Perdew and A. Zunger. *Phys. Rev. B*, 23:5048, 1981.

[145] J. P. Perdew and M. Levy. *Phys. Rev. Lett.*, 51:1884, 1983.

[146] M. E. Casida. *Phys. Rev. B*, 59:4694, 1999.

[147] A. Tachibana and R. G. Parr. *Int. J. Quantum Chem.*, 41:527, 1992.

[148] E. Cancès, K. N. Kudin, G. E. Scuseria, and G. Turinici. *J. Chem. Phys.*, 118:5364, 2003.

[149] All DFT calculations have been carried out using Becke's exchange potential [35] and the correlation potential of Lee, Yang and Perdew [36] (BLYP) in the planewave code CPMD [44] as well as pseudopotentials from Goedecker et al. [56], and a wavefunction cutoff of 100 Ry.

[150] R. A. Kipp, M. A. Case, A. D. Wist, C. M. Cresson, M. Carrell, E. Griner, A. Wiita, P. A. Albiniak, J. Chai, Y. Shi, M. F. Semmelhack, and G. L. McLendon. *Biochem.*, 41:7344, 2002.

[151] Starting from the SMAC-XIAP complex NMR averaged structure (protein data bank (PDB) code 1G3F) the AVPI and the ARPF have been modeled in the active site. The system is constituted by the BIR3 domain of human XIAP (94 residues), Zn^{2+} and having either AVPI and 2 Na^{+} or ARPF and 1 Na^{+} ion as inhibitors. A periodic water box of 6.6^3 nm^3 with a total of 9077 or 9073 water molecules has been used. MD runs have been carried out together with extensions of the GROMOS96 43A1 force field [153] and SPC water model in the NPT (T = 300 K, P = 1 bar) ensemble for 5 ns ($\Delta t = 2$ fs). Temperature and pressure have been kept constant by coupling to a heat, respectively, pressure

bath. Longe range electrostatic interactions have been handled using the particle mesh Ewald method. Atomic coordinates have been saved every 1 ps.

[152] Low temperature hybrid quantum mechanics [149]/molecular mechanics (QM/MM) [46] Born-Oppenheimer molecular dynamics has been carried out in order to optimize the geometry for the full AVPI, ARPF and npARPF-protein complexes. The QM region has been represented by the main chain of the inhibitor structure. Two inhibitor side chains (Arg and Phe), the protein and the water solvent have constituted the MM region [151].

[153] W. F. van Gunsteren et al. *Biomolecular Simulation: The GROMOS96 Manual and User Guide*. vdf Hochschulverlag AG, ETH Zurich, 1996.

[154] O. A. von Lilienfeld, R. Lins, and U. Rothlisberger. Variational particle number approach for rational compound design. 2005. Submitted.

List of Figures

1.1 A survey over the number of scientific publications containing 'density functional theory' (cross) in their title or 'chemical space' (plus) in their text [15]. 7

1.2 Cray Research-CRAY I vector architecture designed in 1976 by Seymour Cray [18] 8

3.1 LEFT to RIGHT: Isosurfaces of some occupied KS-orbitals of the full acetic acid (lower row) and of the link atom acetic acid (upper row). . 33

3.2 History of the minimization of the density penalty as a function of σ_1 of oxygen in water and acetic acid and of carbon in acetic acid. 35

3.3 The labeling of the atoms in acetic acid for table 3.3. 36

4.1 Calibration of the DCACP for carbon: potential energy curves of the energy of interaction ($E^{int} = E^{dimer}$-$2E^{monomer}$) are plotted for the benzene dimer in its sandwich configuration as a function of the distance z. ◯ corresponds to BLYP, ⋄ to BLYP + DCACP, and squares to MP2 data from Ref. [98]. In atomic units the calibrated values of the additional p-channel for carbon are $\sigma_1 = -0.00352$ and $\sigma_2 = 3.280$. In the inset the additional p-channel projector $p_{11}(r)$ [Eq. (5.3)] is depicted in arbitrary units as a function of r, the minimum is roughly at 3.3 Å. . 47

4.2 Calibration of the DCACP for argon: potential energy curves of the total energy of interaction (E^{int} = E^{Dimer}-2$E^{Monomers}$) are plotted as a function of the distance z. ○ corresponds to BLYP, ◇ to BLYP+DCACPs, the MP2 result [96] for the interlayer distance and energy of interaction is marked by a cross. In atomic units the calibrated values of the additional f-channel for argon are σ_1 = -0.002 and σ_2 = 2.9. 48

4.3 Potential energy curves of the total energy of interaction (E^{int} = E^{dimer}-2$E^{monomer}$) are plotted for the benzene dimer in its T-shaped configuration as a function of the distance z. ○ corresponds to BLYP, ◇ to BLYP + DCACP, and the squares to MP2 data from Ref. [98]. Values for σ_1 and σ_2 as they resulted from the calibration in Fig. 4.1. 49

4.4 Potential energy curves of the energy of interaction (E^{int} = E^{dimer}-2$E^{monomer}$) are plotted for the slab of graphite. ○ corresponds to BLYP, and ◇ to BLYP+DCACPs.The experimental value is marked by a cross [99]. In the inset the averaged interlayer distance z is presented during first principles BO-MD using BLYP (dotted) and BLYP + DCACPs (continuous). 50

4.5 For the benzene-argon dimer potential energy curves of the total energy of interaction (E^{int} = E^{dimer}-$\sum E^{monomers}$) are plotted as a function of the distance z. ○ corresponds to BLYP, and ◇ to BLYP+DCACPs. The MP2 result [96] for the intermolecular distance and energy of interaction is marked by a cross. In the inset the C_{6v} symmetry axis z is plotted versus $\Delta = \int dx\, dy\, (n^{norm}(\mathbf{r}) - n^{opt}(\mathbf{r}))$ (the differences between integrated xy planes of the electron density of the benzene-argon dimer at equilibrium distance computed with and without DCACPs). The dotted lines show the position of the moieties: benzene (the molecular plane is perpendicular to z) is at 7.85 Å on the z axis, argon is at 11.26 Å. . 51

4.6 For the benzene-H_2 dimer potential energy curves of the total energy of interaction (E^{int} = E^{dimer}-$\sum E^{monomers}$) are plotted as a function of the intermolecular distance z along the orthogonal C_{6v} symmetry axis. ◯ corresponds to BLYP, and ◇ to BLYP+DCACPs. The MP2 result [96] for the intermolecular distance and energy of interaction is marked by a cross. DCACPs are only used for carbon, all hydrogen atoms remain uncorrected. 52

5.1 Cyclooctatetraene (above), a precursor in the synthesis of semibullvalene (below), an important model system for intramolecular Cope rearrangements. Pictures taken from Ref. [108]. 60

5.2 Structures of cyclooctatetraene (COT) C_8H_8. Left: the 'tub-shaped' D_{2d} global minimum conformation. Middle: the local minimum 'crown-shaped' conformer. Right: the planar D_{4h} ring inversion transition state. 64

5.3 Calibration of Ar and Kr for homo nuclear dimers: the total energy of interaction (E^{int}=E^{Dimer}-2*$E^{Monomer}$) as a function of interatomic distance. 66

5.4 Interatomic region of Ar_2: the differences between integrated xy planes of the electron density ($\Delta_{\mathrm{MP2}} - \Delta_{\mathrm{DFT}} = \int dxdy[n^{\mathrm{MP2}}(\mathbf{r}) - n^{\mathrm{DFT}}(\mathbf{r})]$) is plotted against z for normal DFT calculations (BLYP) and for dispersion corrected DFT calculations (DCACP). The atoms are at a distance of 3.8 Å, *i.e.* at z = 3.1 and 6.9 Å. The integrated absolute electron density difference with respect to the MP2 density is reduced by 10^{-6} a.u. upon use of the DCACPs. 67

5.5 Left panel: correlation of the interaction energies for equilibrium structures of Ar and Kr dimers, of trimers, and tetramers (correlation coefficient: 0.998). Right panel: correlation of the interaction energies of planar transition states for Ar and Kr tetramers (correlation coefficient: 0.980). The dotted lines correspond to a linear fit of the data. Note that for the transition states, the slope is not close to 1. The total energy of interaction (E^{int}=E^{Dimer}-2*$E^{Monomer}$) has been obtained within BLYP DFT using DCACPs and within MP2 using the Counterpoise correction. For the dimer and trimers the geometry is optimized within DFT and MP2, for the tetramers the geometry is optimized only using DFT. The MP2 interaction energies of the tetramers have been obtained at the DFT geometry. The root mean square deviation (rmsd = $[1/N\sum_i^N(\mathrm{E}_i^{int}(\mathrm{MP2})-\mathrm{E}_i^{int}(\mathrm{DFT}))^2]^{1/2}$) of the equilibrium and transition state geometry are 0.41 kJ/mol and 1.27 kJ/mol, respectively. . . 68

5.6 Calibration of Br in the $(Br_2)_2$ complex: the total energy of interaction (E^{int}=E^{Dimer}-2*$E^{Monomer}$) as a function of the distance between two Br_2 molecules. 70

5.7 Left: the HBr dimer in its equilibrium geometry (EQ): Br-Br distance at 4.1 Å, H-Br-Br angle is 80 or 10 degree, respectively. Right: the hydrogen exchange transition state with 45 degrees for both H-Br-Br angles (TS1) is presented. Both complexes are planar. 70

6.1 Two dimensional total atomic potential energy surface [a. u.] [149] as a function of the number of electrons N_e and the atomic number $Z(\mathbf{r} = \mathbf{R_I})$. Only fractional independent changes of 0.2 are considered for electrons and atomic number, ranging from boron (N_e = 5, Z = 5) up to fluorine (N_e = 9, Z = 9). The total potential energy of boron ($E^{tot}(N_e = 5, Z_\mathbf{I} = 5)$) is set to zero, and all other values refer to it. 80

6.2 Three dimensional projection of the electrostatic potential (= $\mu_n(\mathbf{r})$ within the first order approximation of Eq. (6.14)) onto the molecular plane of formic acid. 82

6.3 Total molecular potential energy [a. u.] [149] for coupling parameter λ transforming CH_4 ($\lambda = 0$) → NH_3 ($\lambda = 10$) → H_2O ($\lambda = 20$) → HF ($\lambda = 30$). λ corresponds to the projected annihilation of the hydrogen pseudopotentials and the simultaneous transmutation of the heavy atom pseudopotentials. Geometries are optimized for every λ. All energies refer to CH_4. 83

6.4 All possible formic acid dimers for transmutations of the oxygen atoms of one moiety for Δ Z = 1,0,-1. The number of electrons N_e is constant (36 valence electrons), and the total charge is N_e-$\sum_{\mathbf{I}} Z_{\mathbf{I}}$. Green represents carbon, white hydrogen, red oxygen, blue nitrogen, and grey fluorine atoms. Alchemical derivatives for the oxygens and energy of interactions for all mutants are given in table 6.1. 84

6.5 Topological sketches of the inhibitor structures. Upper panel: peptidic [(a) AVPI: R1 = Ala, R2 = Val, R3 = Pro, R4 = Ile, (b) ARPF: R1 = Ala, R2 = Arg, R3 = Pro, R4 = Phe], middle panel: first guess non-peptidic ARPF [(c)], and lower panel: final guess non-peptidic ARPF [(d) np-ARPF]. Only the terminals and the peptidic atoms are specified. Hydrogens attached to carbon are omitted for the sake of clarity. . . . 86

6.6 QM/MM [152] optimized geometry of the proposed non-peptidic inhibitor np-ARPF [Fig. 6.5(d)] solvated in the XIAP binding pocket. Using the alchemical potential atoms of the three peptide bonds of the ARPF [Fig. 6.5(b)] have been modified by transmutation to O, C, N, and F (represented respectively by red, black, blue, or green spheres). 88

List of Tables

3.1 Calculated total permanent dipole moments $|\mu|$ for geometrically fixed R-CO_2H. R = CH_3 corresponds to full QM acetic acid, D^{opt} is a link OACP replacing the CH_3 group, H indicates hydrogen capping, D^{con} is an empirically optimized monovalent link carbon atom which reproduces a H_3C-CH_3 bond length [75], and F corresponds to fluorine capping. All values are in Debye. 32

3.2 Deviation Δ with respect to the B3LYP results for calculated total dipole moments $|\mu|$, RESP charges q^{RESP}, bond lengths $d_{\text{O-H}}$ and angles for water. Dipole moments are in Debye, charges are in atomic units, and angles are in degrees. 36

3.3 Deviation Δ with respect to the B3LYP results for calculated RESP charges q^{RESP} for acetic acid: $H_3C^{(5)}C^{(4)}O^{(3)}O^{(2)}H^{(1)}$ (precise labeling in Fig. 3.3). All values are in atomic units. 36

3.4 Deviation Δ with respect to the B3LYP results for calculated dipole moment along the molecular axis (μ_z) and the O-H bond length $d_{\text{O-H}}$ for acetic acid. Dipole moments are in Debye, distances are in atomic units. 37

3.5 Bond lengths d for acetic acid $H_3C^{(5)}C^{(4)}O^{(3)}O^{(2)}H^{(1)}$ (precise labeling in Fig. 3.3) in Å. 38

3.6 Proton affinities for water (wat) and acetic acid (acac) at fixed geometry being optimized for the protonated species. For acetic acid, also the deprotonated species has been optimized (acac-geo). All values are in a.u.. 38

4.1 Calculated static polarizabilities, quadrupole and dipole moments for BLYP calculations without correction (BLYP), with DCACPs (BLYP+DCACPs), and MP2 calculations for comparison. *bz* represents benzene, and $bz - Ar$ the benzene-argon complex. All values are in atomic units. . . 46

5.1 Calculated transition barriers for the ring inversion of the 'tub-shaped' cyclooctatetraene (COT) *via* a D_{4h} planar transition state and energy differences between 'tub-shaped' and 'crown-shaped' conformers (TC). Every structure has been geometry optimized, for the transition states a planar geometry has been imposed. All values are in kJ/mol. 69

5.2 Deviation of total BLYP DFT energies of interaction from MP2 results. The conformations of EQ, TS1, TS2, and TS3 are explained in the text and in Fig. 5.7. All values are in kJ/mol and correspond to E^{int}_{MP2}-E^{int}_{DFT}. 71

6.1 Total potential energies of interaction (E) and alchemical potentials for its change: for the left (μ^{l}_{al}) and the right (μ^{r}_{al}) oxygen of the lower moiety of all the formic acid complexes depicted in Fig. 6.4. Negative values for μ_{al} correspond to a predicted gain in energy of interaction upon increase of Z. The ordering corresponds to Fig. 6.4. All values are in atomic units. 85

Appendix: Perturbation Hamiltonian

Here, we give the explicit separable form of the perturbation Hamiltonian in Eq. (3.4) for a given Goedecker pseudopotential [56] V^{ECP} of maximal angular momentum l = s. $\hat{H}'_j$ is the analytic derivative of the real space form of the analytic nonlocal and separable pseudopotential in Eq. (5.2-5.3) with respect to the j^{th} parameter σ_j. The parameters $\{\sigma_j\}$ are defined in the following order: $\{r_{\mathrm{loc}}, C_1, C_2, r_s, h_{s11}\}$. $\hat{H}'|\phi(\mathbf{r})\rangle$ = $\sum_j \hat{H}'_j|\phi(\mathbf{r})\rangle$ = $\sum_j \partial_{\sigma_j} V^{\mathrm{ECP}}|\phi(\mathbf{r})\rangle$, where the individual components are given by:

$$\frac{\partial}{\partial\sigma_1}V^{(\mathrm{loc})}(\mathbf{r})\phi(\mathbf{r}) = \left(\frac{Z_{ion}\sqrt{2}}{\sqrt{\pi}\sigma_1^2} + \frac{r^2\sigma_3}{\sigma_1^3}\left(\frac{r^2}{\sigma_1^2} - 2\right)\right)\exp[-\frac{r^2}{2\sigma_1^2}]\phi(\mathbf{r}), \tag{7.1}$$

$$\frac{\partial}{\partial\sigma_2}V^{(\mathrm{loc})}(\mathbf{r})\phi(\mathbf{r}) = \exp[-\frac{r^2}{2\sigma_1^2}]\phi(\mathbf{r}), \tag{7.2}$$

$$\frac{\partial}{\partial\sigma_3}V^{(\mathrm{loc})}(\mathbf{r})\phi(\mathbf{r}) = \frac{r^2}{\sigma_1^2}\exp[-\frac{r^2}{2\sigma_1^2}]\phi(\mathbf{r}), \tag{7.3}$$

$$\frac{\partial}{\partial\sigma_4}V_l^{(\mathrm{nl})}(\mathbf{r},\mathbf{r}')\phi(\mathbf{r}) = \frac{\partial}{\partial\sigma_4}\int d\mathbf{r}'\, V_l^{(\mathrm{nl})}(\mathbf{r},\mathbf{r}')\phi(\mathbf{r}') \tag{7.4}$$

$$= \left(\frac{1}{\pi^{3/2}\sigma_5^3}\int d\mathbf{r}'\, \exp[-\frac{r'^2}{2\sigma_5^2}]\phi(\mathbf{r}')\right)\exp[-\frac{r^2}{2\sigma_5^2}], \tag{7.5}$$

$$\frac{\partial}{\partial\sigma_5}V_l^{(\mathrm{nl})}(\mathbf{r},\mathbf{r}')\phi(\mathbf{r}) = \frac{\partial}{\partial\sigma_5}\int d\mathbf{r}'\, V_l^{(\mathrm{nl})}(\mathbf{r},\mathbf{r}')\phi(\mathbf{r}') \tag{7.6}$$

$$\begin{aligned} &= \left(\left(\frac{\sigma_4 r^2}{\sigma_5^6\pi^{3/2}} - \frac{3\sigma_4}{\sigma_5^4\pi^{3/2}}\right)\int d\mathbf{r}'\exp[-\frac{r'^2}{2\sigma_5^2}]\phi(\mathbf{r}')\right. \\ &+ \left.\frac{\sigma_4}{\sigma_5^6\pi^{3/2}}\int d\mathbf{r}' r'\exp[-\frac{r'^2}{2\sigma_5^2}]\phi(\mathbf{r}')\right)\exp[-\frac{r^2}{2\sigma_5^2}]. \end{aligned} \tag{7.7}$$

$r = |\mathbf{r} - \mathbf{R}_\mathrm{I}|$ on the position $\mathbf{R}_\mathrm{I}$ of nucleus I. $\phi(\mathbf{r})$ is a KS-orbital.

Publications

The following manuscripts emerging from this thesis have already been published, accepted, or submitted.

1. ’Optimization of effective atom centered potentials for London dispersion forces in density functional theory’ by O.A. von Lilienfeld, I. Tavernelli, U. Rothlisberger, and D. Sebastiani. *Phys. Rev. Lett.* **93**, 153004 (2004).
2. ’Variational optimization of effective atom centered potentials for molecular properties’ by O.A. von Lilienfeld, I. Tavernelli, U. Rothlisberger, and D. Sebastiani. *J. Chem. Phys.* **122**, 14113 (2005).
3. ’Performance of optimized atom centered potentials for weakly bonded systems using density functional theory’ by O.A. von Lilienfeld, I. Tavernelli, U. Rothlisberger, and D. Sebastiani. *Phys. Rev. B.*, in press (2005).
4. ’Variational particle number approach for rational compound design’ by O.A. von Lilienfeld, R. D. Lins, and U. Rothlisberger. Submitted (2005).
5. ’Study of weakly bonded carbon compounds using dispersion corrected density functional theory’ by E. Tapavicza, I. Lin, O. A. von Lilienfeld, I. Tavernelli, M. Coutinho, and U. Rothlisberger. Submitted (2005).

The following manuscripts involving research results described in this thesis are in preparation.

1. ’An automatic procedure for the generation of QM/MM boundaries’, O.A. von Lilienfeld, I. Tavernelli, and U. Rothlisberger.
2. ’Relative free energies from first principle alchemical changes’, O.A. von Lilienfeld and U. Rothlisberger.
3. ’Hydrogen absorption on carbon nanotubes using dispersion corrected density functional theory’, I. Lin, I. Tavernelli, O.A. von Lilienfeld, and U. Rothlisberger.
4. ’A library of dispersion corrected atom centered potentials for several exchange-correlation functionals in density functional theory’, I. Lin, C. Felsenheimer, M. Coutinho, O.A. von Lilienfeld, I. Tavernelli, and U. Rothlisberger.
5. ’The role of π-π stacking for intercalating DNA-drugs’, I. Lin, C. Felsenheimer, M. Coutinho, I. Tavernelli, O.A. von Lilienfeld, and U. Rothlisberger.
6. ’An *ab initio* molecular dynamics study of van der Waals liquids’, I. Lin, M. Coutinho, I. Tavernelli, O.A. von Lilienfeld, and U. Rothlisberger.
7. ’QM/MM calculations of DHFR - a comparative study’, I. Lin, O.A. von Lilienfeld, L. Guidoni, P. Cummins, I. Tavernelli, J. Gready, and U. Rothlisberger.
8. ’Non-equilibrium dynamics and alchemical variations for relative free energies’, M. Cuendet, O.A. von Lilienfeld, and U. Rothlisberger.

Acknowledgment

First of all, I am deeply indebted and grateful to my supervisor Prof. Dr. Ursula Röthlisberger. I received all the freedom and confidence I dreamed of in order to independently study, investigate, and enjoy what are to me the most fascinating, fundamental, and relevant topics of the microscopic world. She was always present when needed, showed a nearly irrational trust and patience in my results, and never made me feel like being an investment. Consequently, this thesis could profit from individual independence and much freedom for research. I thank her for all the discussions and valuable opinions concerning not only science but also many other topics. Her open-mindedness, her positive and humorous thinking, and the always present Topas have always been greatly enjoyable.

I am also specially indebted to Dr. Joost VandeVondele with whom I started working on pseudopotentials already in the year 2000. The discussions and the work with him have inspired me to invest more and deeper thinking into the physical meaning of pseudopotentials and the representation of nuclei in electronic structure calculations. Our studies on the transformation of H_2O into H_2S in order to compute free energies of solvation are still to be finished. Joost introduced me to the world of scripting and open source. When working with him I became aware of the intellectual fun which can be found in programming for theoretical chemistry and which I had been searching in vain in other branches of chemistry. I also realized that maybe one of the most motivating and inspiring facts in computational sciences is that the finding of the answers to important questions is usually more limited by one's own imagination than by the absence of tools/machines/chemicals/preknowledge etc.

Special thanks go also to Dr. Daniel Sebastiani who helped me a lot to see the physicist's point of view of many problems, who taught me a great deal on coding and how to identify physical, technical, or political difficulties. Furthermore, I am indebted to him for making me aware of the importance of scientific publications and for showing me how to write them.

A lot of what I learned about physics during my PhD-studies comes from Dr. Ivano Tavernelli. He was not only a very sympathetic office mate but also an essential help in calming me down when I popped up with yet another breakthrough-Rocket-science idea and in making me see the physically important parts of many concepts. His kind interest in all my activities and his unpretentious attitude towards life have been most encouraging and motivating for me.

I particularly appreciated the broad introduction to opera, solid state physics and surface science, and Finnish female psychology generously provided by Dr. Ari Seit-

sonen. Ari has always been at disposal when difficult physical questions occurred and has been a great help in reading and discussing my articles, specifically Ref. [154].

Then, there are the many people with whom I worked, discussed, and enjoyed my time in Zürich or Lausanne: Pascal Baillod, Dennis Bucher, Prof. Paolo Carloni, Dr. Mauricio Coutinho and Fabiola, Michel Cuendet, Christian Gossens and Anja, Dipl. Chem. EPFL Samuele Giani, Dr. Leonardo Guidoni and Silvia and Giovanni, Dr. Håkan Hugosson, Dr. Alessandro Laio, I-chun Lin, Dr. Roberto Lins and Theresa Soarez, Dr. Patrick Maurer, Dr. Massimo Mella, Dipl. Chem. EPFL Marc-Etienne Moret, Dr. Stefano Piana and Cristiana and their child, Dr. Ute Röhrig and Daniele, Dr. Maria-Lore Sulpizi and Gianni and Priscilla. I thank the people from Canberra, Australia, Dr. Jill Gready, Dr. Peter Cummins, and Alex and Julia Zelensky for all their time and efforts. Apart from the above mentioned persons, I also enjoyed discussions with Dr. Tomasz A. Wesolowski, Prof. Jürg Hutter, Prof. Michiel Sprik, Prof. Michele Parrinello, Prof. P. Geerlings. I have to thank especially MariaCarola Colombo who was able to stand my presence in our common apartment for two years and with whom I had a great time. Special thanks go to Matteo Guglielmi and Enrico Tapavicza with whom I enjoyed many scientific and non scientific events.

Many thanks go to Karin Pasche who has always been a great and kind help in reducing the nuisance of organizing travels, visits, administration problems and formal issues. Likewise I greatly acknowledge the help of Patrick Favre for printing posters, fixing power cables, and commenting on the installation of 'our' first SUSE-based workstation cluster in Lausanne.

I acknowledge very much the many workshops, conferences, and schools I could attend during my PhD-studies. There, I had the occasion to meet with many others being more or less in my situation: Jochen Blumberger, Atsushi Urakawa, Patricia Sillas, Eneritz Muguruza, Margherita Marsili, Andrea Floris, Attilio Vittorio Vargiu, Alvaro Rodriguez, Eleonora Luppi, Fanny Masson, and Wojciech Welnic.

Many thanks go also to the Zürich gang, *i.e.* Philipp Kurz, whom I have been knowing since our undergraduate studies at Leipzig University in 1996, Michèle C. Erat, Roland K. O. Sigel, Eva Freisinger, Stefanie Senkel, Camille Felsenheimer, who even joined the group recently, and Thomas Bosgiraud.

Special thanks go to Leonie von Brasch, Oda von Breitenstein, Céline Delacroix, Guillaume Fichet, Julius von Grote, Julia Heister, Hans-Christoph von Hirschheydt, Charlotte Leclerc, Pierre Lefranc, Estelle Marandon, Alexandra Meurant, Lidia Verges, and Laurence Philbé and Pierre Wetzel for their friendship during these years. I also have to thank the sweet Annamaria Petrozza for her wonderful support from Cambridgeshire while writing up this thesis.

I am grateful to my god child Fidelia von der Bussche, and her family for the patience with which I was honored to be treated. Visiting them represented always to me a wonderful way to 'recover' from the world of my PhD-life.

Finally and most importantly, I sincerely thank my family, *i.e.* my parents Olga and Hermann for their continuous support and interest they have shown in my studies, and my sisters Marie, Sophie, and Anna, and their respective partners Ansgar, André, and Harry for the many nice, relaxing and exciting moments we spent together during the last years.

Epilogue

Nur mit flinkem Stift umschrieben,
Angetuscht mit leichten Tönen,
Kaum ein Umriss ist geblieben
All des farbenkräftig Schönen.

Und vorbei noch schattenhafter
Wird euch die Staffage gleiten,
Ein im Schlendern aufgeraffter
Haufe schlichter Menschlichkeiten.

Doch des Malers Bild - gleich jenen
Schwindet's bald ins Ungewisse.
Sollten sich unsterblich wähnen
Eines Schattens Schattenrisse?

Paul Heyse
(1830-1914)

And I gave my heart to know wisdom, and to know madness and folly:
I perceived that this also is vexation of spirit.

Ecclesiastes

Curriculum Vitae

Otto Anatole von Lilienfeld-Toal,
born December 16 1976.

January 2002 - February 2005: PhD-studies with Prof. Ursula Röthlisberger, EPFL, Switzerland.

October 2001 - December 2001: Experimental studies on noninvasive blood sugar measurements with Prof. Markus Sigrist, ETHZ, Switzerland.

April 2001 - July 2001: Diploma thesis with Prof. Martin Quack at ETHZ, Switzerland, and Prof. Nicholas Handy at Cambridge University, United Kingdom.

October 1999 - October 2001: Advanced undergraduate studies in chemistry, ETHZ, Switzerland.

October 1998 - October 1999: Advanced undergraduate studies in chemistry, ECPM in Strasbourg, France.

October 1996 - July 1998: Undergraduate studies in chemistry, Universität Leipzig, Germany.

October 1983 - July 1996: School in Bonn, Bad Nauheim, and Gelnhausen, Germany.

Lausanne, March 2005